Journal of Nanomaterials

# Applications of Nanobiomaterials in Tissue Repair 2021

Lead Guest Editor: Xiaoming Li
Guest Editors: Hui-Qi Xie, Nicholas Dunne, and Katerina E. Aifantis

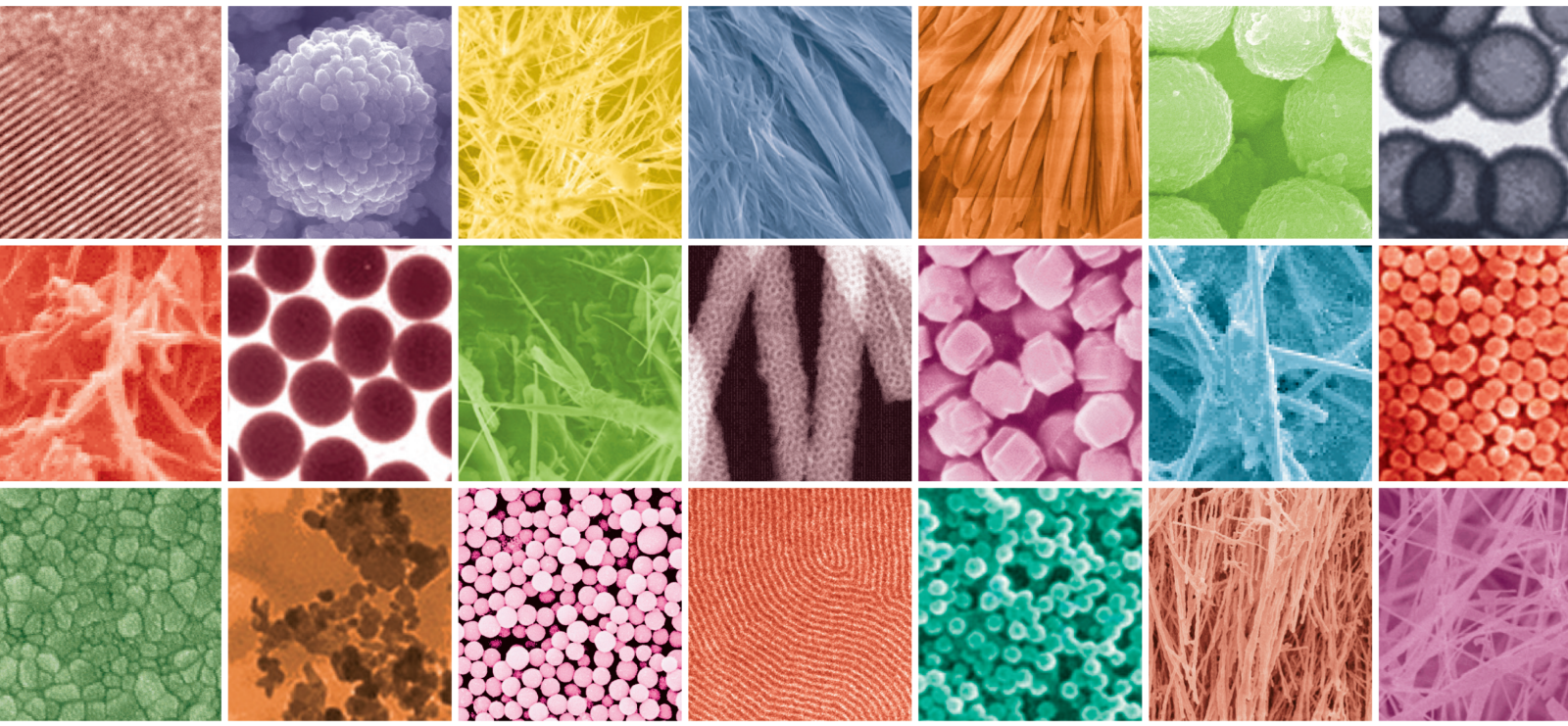

# Applications of Nanobiomaterials in Tissue Repair 2021

Journal of Nanomaterials

# Applications of Nanobiomaterials in Tissue Repair 2021

Lead Guest Editor: Xiaoming Li
Guest Editors: Hui-Qi Xie, Nicholas Dunne, and Katerina E. Aifantis

# Contents

**Valorization of Waste Chicken Feathers: Fabrication and Characterization of Novel Keratin Nanofiber Conduits for Potential Application in Peripheral Nerve Regeneration**
Mduduzi Khumalo, Bruce Sithole, Tamrat Tesfaye, and Prabashni Lekha
Research Article (10 pages), Article ID 7080278, Volume 2022 (2022)

**Nanoparticle-Based Drug Delivery System—A Target Strategy for Osteoarthritis Treatment**
Keda Liu, Dianjian Zhang, and Wei Wang
Review Article (15 pages), Article ID 4064983, Volume 2021 (2021)

**Synthesis and Application of Iron Oxide Nanoparticles in Bone Tissue Repair**
Da Lu, Xueqing Wu, Wei Wang, Chenghao Ma, Baoqing Pei, and Shuqin Wu
Review Article (14 pages), Article ID 3762490, Volume 2021 (2021)

**Repair of Osteoporotic Bone Defects Using Adipose-Derived Stromal Cells and Umbilical Vein Endothelial Cells Seeded in Chitosan/Nanohydroxyapatite-P24 Nanocomposite Scaffolds**
Yifei Fang, Yong Gong, Zhijian Yang, and Yan Chen
Research Article (11 pages), Article ID 6237130, Volume 2021 (2021)

**The Use of Fullerene C60 to Preserve Testicular Tissue after Cryopreservation**
Nataliia Volkova, Mariia Yukhta, and Anatoliy Goltsev
Research Article (8 pages), Article ID 6696733, Volume 2021 (2021)

Hindawi
Journal of Nanomaterials
Volume 2022, Article ID 7080278, 10 pages
https://doi.org/10.1155/2022/7080278

*Research Article*

# Valorization of Waste Chicken Feathers: Fabrication and Characterization of Novel Keratin Nanofiber Conduits for Potential Application in Peripheral Nerve Regeneration

**Mduduzi Khumalo**,[1,2] **Bruce Sithole**,[1,2] **Tamrat Tesfaye**,[1,2,3] **and Prabashni Lekha**[2]

[1]*University of KwaZulu-Natal, Discipline of Chemical Engineering, Durban, South Africa*
[2]*Biorefinery Industry Development Facility, Chemical Cluster, Council for Scientific and Industrial Research, Durban, South Africa*
[3]*Ethiopian Institute of Textile and Fashion Technology, Bahir Dar University, Bahir Dar, Ethiopia*

Correspondence should be addressed to Mduduzi Khumalo; mdukhumalo@hotmail.com

Received 8 June 2021; Revised 13 December 2021; Accepted 8 January 2022; Published 28 January 2022

Academic Editor: Xiaoming Li



Flexible, porous, biocompatible, and biodegradable tubular keratin nanofibers were fabricated as nerve regeneration conduits. Keratin was extracted from waste chicken feathers and then blended with polyvinyl alcohol and transformed into nanofiber conduits by electrospinning. The nanofiber conduits had average diameters that ranged from 170 to 234 nm. The nanofibers' average diameter decreased when the keratin content was increased. In contrast, the range of nanofiber diameter distribution narrowed, suggesting that as nanofibers became thin, their numbers increased, thus reducing the interfacial spaces between them. The analysis confirmed the presence of keratin protein in nanofibers, guaranteeing biocompatibility and biodegradation. TGA showed that keratin improved the thermal stability and hydrophilicity of the nanofibers.

## 1. Introduction

The peripheral nervous system (PNS) is an integral part of the nervous system that enables the body to move muscles and feel normal sensations. Its primary function is to connect the central nervous system (CNS) to tissues and organs [1]. The role of PNS is made possible by central nervous system basic units, called neurons, which are composed of, among others, the bundles of axons that form electric-cable-like peripheral nerves. Unlike CNS protected by the skull and vertebrae, the PNS is exposed to injuries that can either be neuropraxia, axonotmesis, or neurotmesis, where neuropraxia is the least severe, while neurotmesis is the most severe nerve injury [2]. The complicated anatomy of the nerve bundle makes nerve repair difficult, leading to the most unsuccessful treatments. Peripheral nerve injuries remain a challenge for both clinically and basic research despite the advancements that have been made in this field [3]. Current repair methods include end-to-end repair, grafts, and synthetic conduits. While end-to-end suturing, extending, and reconnecting the distal stump to the proximal stump are the simplest and preferred nerve repair method, its success is limited to the gap size and the proximal nerve's availability stump. Furthermore, it is also limited to the amount of tension induced during stump extension over a nerve gap; if it exceeds the optimal level, the repair process results in partial nerve recovery. The treatment may be done by donating the nerve from the other part of the body, autograft. The autograft is advantageous in eliminating or minimizing immunological rejection and is considered the reference standard for closing the nerve gap [4]. However, the balance of functionality between the donor and recipient tissue or organ must be established. This balance limits the treatment if there is a substantial loss of nervous tissue that may require multiple small grafts. Another form of nerve donation treatment is an allograft, whereby the nerve tissue is harvested from the donor of the same species. Even though this process increases nerve tissue availability, it also introduces the chances of disease transmission and immunological response [1, 5].

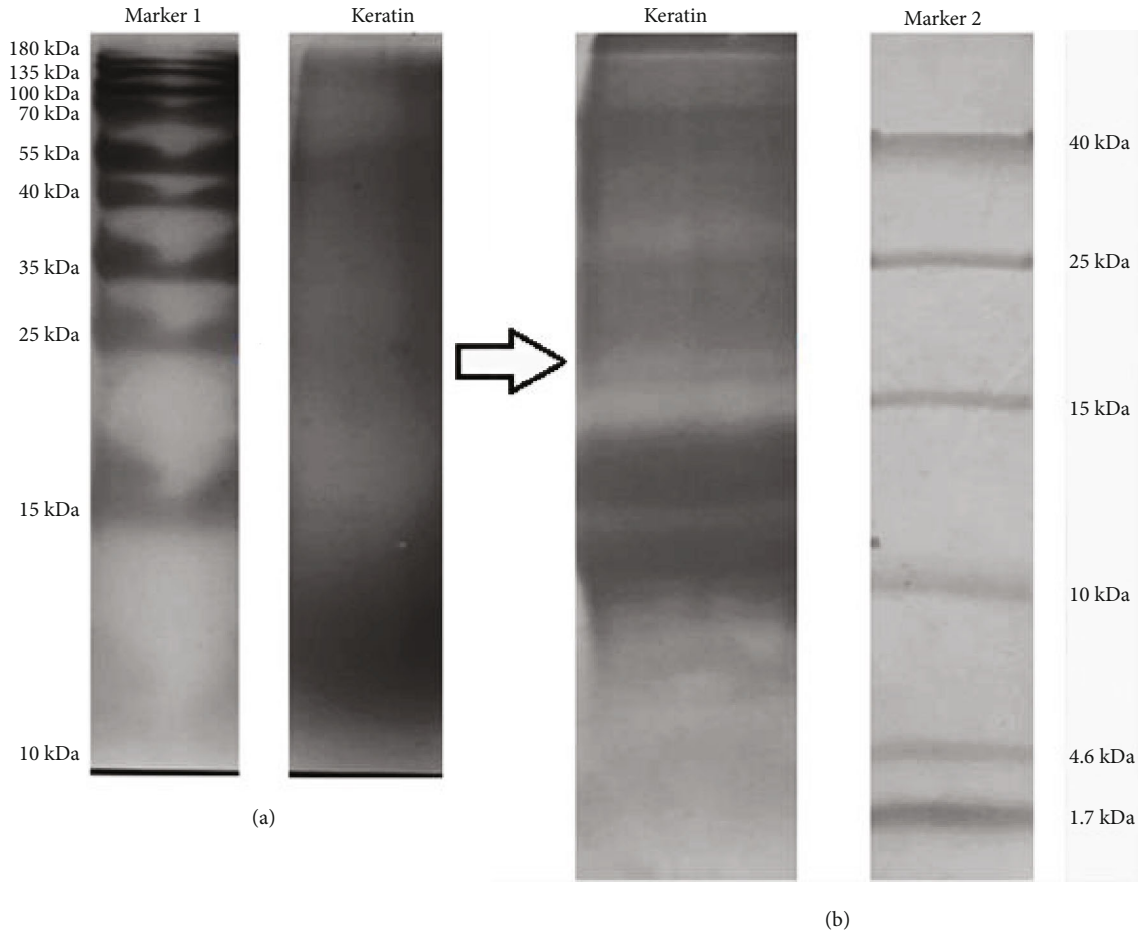


Figure 1: SDS-PAGE gels of extracted keratin protein: glycine gel (a) and tricine gel (b).

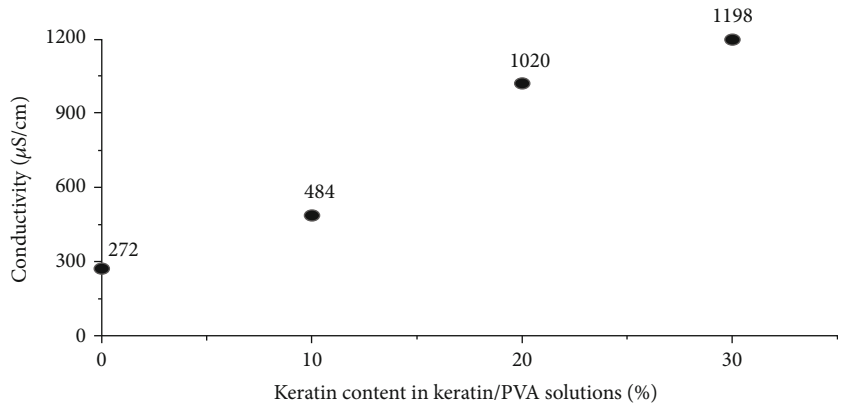


Figure 2: Conductivity of keratin/PVA solutions of different keratin and polyvinyl alcohol ratios.

Therefore, synthetic nerve conduits are favoured for the nerve regeneration process because of their flexibility in mimicking the natural nervous tissue. However, the current commercially available conduits are rigid and inflexible and may cause cell loss due to their lack of physiological properties required during nervous tissue movement [6]. The conduit must be biocompatible, biodegradable, porous, bioresorbable, and mechanically strong [7].

Biocompatible synthetic polymers suit most nerve conduits' fundamental requirements because of their adequate mechanical strength, ductility, and physiochemical compatibility, especially electrospun nanofiber scaffolds [8–10]. Nanofibers have attracted attention for their application as nerve conduits due to their softness, flexibility, high porosity, high surface area to volume ratio, and nanoscale diameter [11, 12]. Research has shown that nanofiber scaffolds

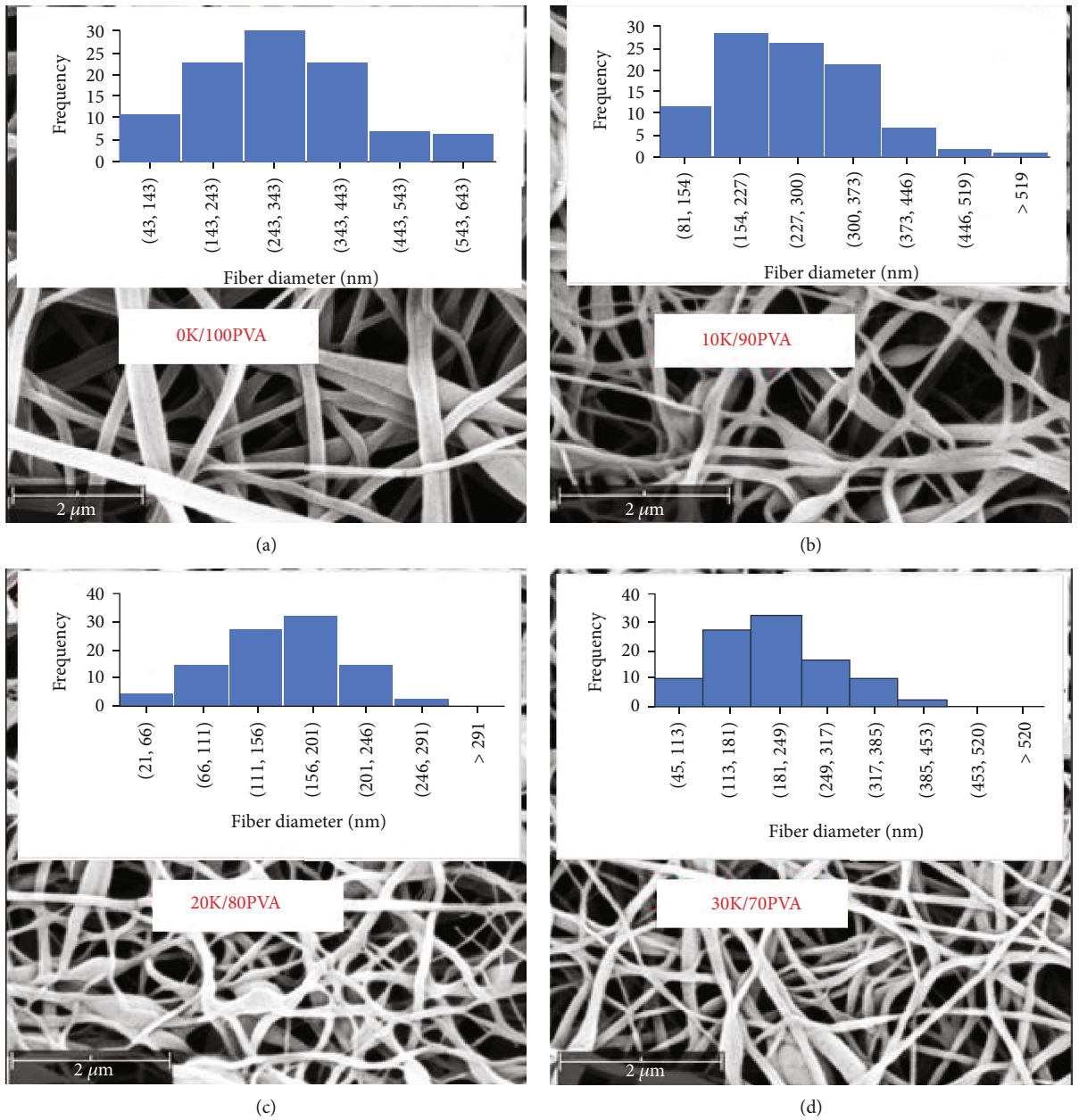


Figure 3: SEM images and distributions of nanofiber diameters of the keratin/polyvinyl alcohol system: (a) 0% keratin/100% PVA, (b) 10% K/90% PVA, (c) 20% K/80% PVA, and (d) 30% K/70% PVA.

support cellular ingrowth due to their ability to mimic the native tissue or organ [13, 14]. Nanofibers can be electrospun into tubular forms that are flexible and soft to allow easy suturing of the distal and proximal stump during nerve repair. Furthermore, their porous nanostructure substrate for cell attachment allows nutrient exchange [5].

While biocompatible polymers have been used to fabricate electrospun nanofiber conduits [15], there is still a need for biodegradable polymers derived from natural resources to increase biocompatibility and lower immunological rejection. Among other synthetic polymers, polyvinyl alcohol (PVA) has been used in biomedical applications, including nerve repair treatment, due to its physical and chemical properties. Polyvinyl alcohol is FDA approved for clinical use in humans, and it has good electrospinnability to form nontoxic nanofibers with large pore sizes. However, cell adhesion for cell growth and biocompatibility need improvement [16, 17]. Consequently, keratin has been used with PVA to increase scaffold biocompatibility. As a biodegradable fibrous protein, keratin can act as an extracellular matrix and promote biocompatibility to minimize immunological rejection. This protein has attracted interest from both scientific and industrial communities due to its exceptional properties and abundance. Interest includes investigating keratin application in the biomedical field. Feng et al. [18] developed keratin films to treat the corneal epithelial wound. It was then concluded that the keratin films were promising alternatives to the amniotic membrane for ocular

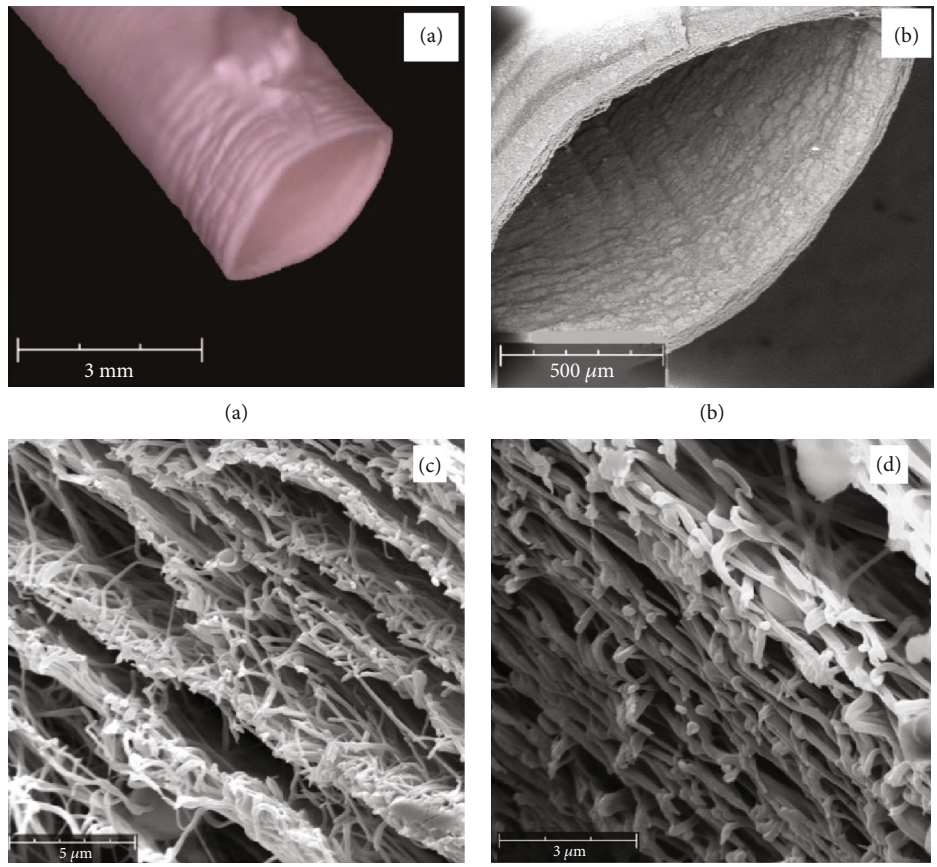


Figure 4: SEM images of keratin nanofibers: (a) tubular structure and (b) the outer and inner surfaces of the tube; (c, d) cross-sections of individual nanofibers, 0% K/100% PVA and 10% K/90% PVA nanofibers, respectively.

surface reconstruction; the films support proliferation, migration, adhesion, and differentiation of human corneal epithelial cells. The protein can also be used to exfoliate molybdenum disulphide ($MoS_2$) to achieve high-quality dispersion of nanolayered $MoS_2$ with a high yield of about 56%. The produced nanolayered sheet has a long shelf-life and improved electrical conductivity [19]. In another study, the effect of transglutaminase on wool keratin films showed a decrease in elongation at break and an increase in tensile strength, thus improving film stability while conserving drug release rate [20]. Further investigation by Ajay Sharma et al. [21] showed that keratin hydrogels could be used as a scaffold for pulp-dentine regeneration since keratin enhanced odontoblast cell behaviour. Choi et al. [22] developed keratin-based nanofibers with high optical transmittance of 88% at 600 nm with improved mechanical properties. Guo et al. [16] used oxidative hair keratin nanoparticles to coat PVA nanofibers for nerve repair, whereby large pore size enhanced neural cell viability and proliferation. Sierpinski et al. [23] produced a biomedical hair-keratin gel and concluded that it promotes vigorous nerve regeneration response by activating Schwann cells. Keratin inclusion facilitates the treatment result comparable to the gold standard conduit, the autograft. Similar results were observed with the application of hydrogel conduit filled with hair keratin for nerve regeneration, in which results were also comparable to the gold standard for nerve repair [24].

Therefore, the current study is aimed at fabricating and characterizing the seamless nanofiber conduit of polyvinyl alcohol and chicken feather keratin to apply in nerve regeneration.

## 2. Methodology and Materials

White chicken feathers were collected from the chicken meat processing plant RCL Foods at Hammarsdale, South Africa. Analytical grade sodium bisulphite, sodium hydroxide, sodium dodecyl sulphate, urea, and polyvinyl alcohol were purchased from Sigma-Aldrich, South Africa. The fabrication of seamless nanofiber conduits was done using Nano Spinner NE200 from Inovenso. The main instruments that were used for analysis were Fourier transform infrared spectroscopy (FTIR), Simultaneous Thermographic Analyzer (STA) 6000, and Carbon, Hydrogen, Nitrogen, Sulphur, and Oxygen (CHNS/O) Analyzer (Series II 2400) from PerkinElmer. Experiments, including keratin extraction, fabricating nanofibers and characterizations such as CHNS, were carried in triplicate, while the sample size of diameter measurements of nanofibers was 100.

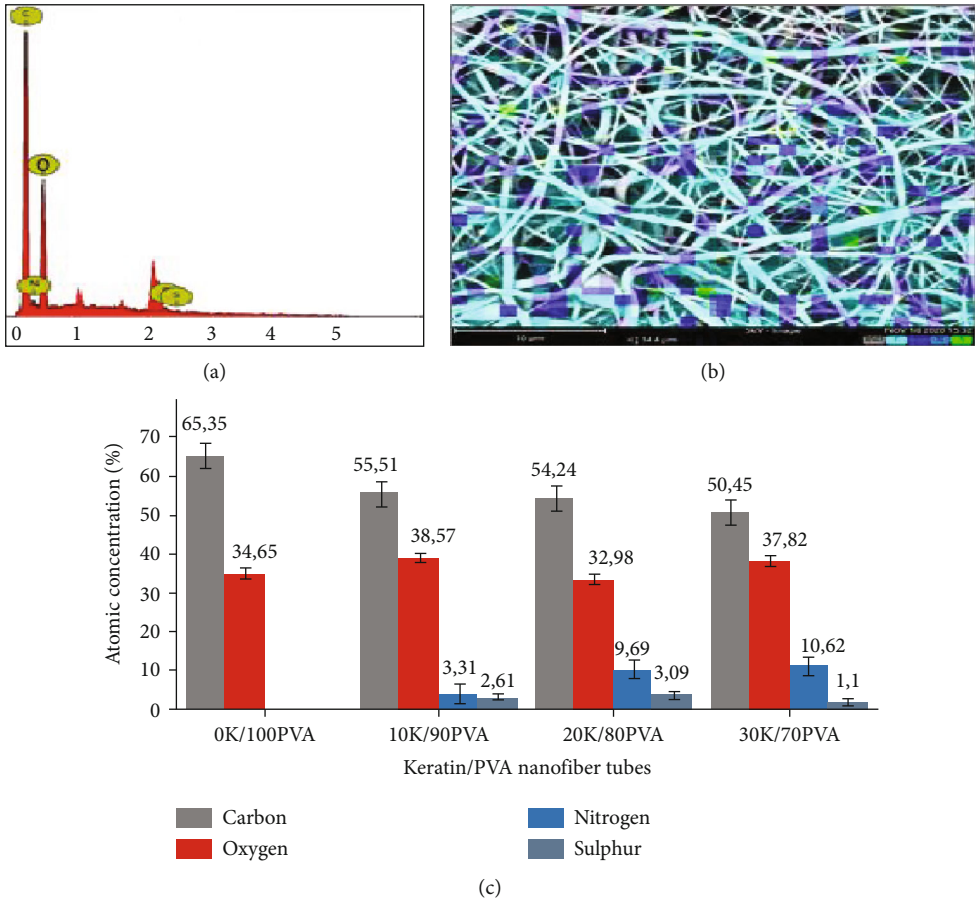


Figure 5: Energy-dispersive X-ray (EDX) results of keratin/PVA nanofiber tubes: (a) EDX spectrum of elements, (b) element mapping, and (c) atomic concentration of nanofibers.

Table 1: Conductivity of different keratin/PVA solutions and average diameters of relevant nanofibers.

| Keratin/PVA | Conductivity (mS/cm) | Average diameter ± Std.dev (nm) | Average pore size ± Std.dev (nm) |
|---|---|---|---|
| 0%/100% | 272 | 234 ± 87 | 0.3 ± 0.081 |
| 10%/90% | 484 | 212 ± 63 | 0.09 ± 0.029 |
| 20%/80% | 1020 | 196 ± 37 | 0.07 ± 0.012 |
| 30%/70% | 1198 | 170 ± 50 | 0.04 ± 0.004 |

*2.1. Pretreatment of Chicken Feathers.* Wet chicken feathers were rinsed with water at 60°C to remove excess blood while manually removing other meat by-products and then autoclaved at a temperature of 121°C and pressure 120 kPa for 30 minutes. After that, they were soaked in 0.5%*v*/*v*sodium hypochlorite for 24 hours before rinsing with water and dried at 25°C.

*2.2. Extraction and Analysis of Chicken Feather Keratin.* Cleaned-disinfected chicken feathers were ground in a milling machine to increase the dissolution rate during the extraction process. They were then soaked in 99% ethanol for 24 hours to remove fatty materials and rinsed with water before drying at 50°C for three days. Fifteen grams of dry and degreased chicken feathers was deep in a solution of 0.23 M sodium bisulphite, 0.07 M sodium dodecyl sulphate, and 1.5 M urea. The reaction mixture was shaken on a linear platform shaker for homogeneous distribution of all mixture components in a container and then heated in a 90°C oil bath. After cooking, the mixture was centrifuged at 9000 rpm for 15 minutes and filtered to separate the insoluble materials and supernatants. The filtrate obtained was dialyzed in distilled water using cellulose membrane dialysis tubes (MWCO 3.5 kDa) for five days. The keratin solution was lyophilized to obtain keratin powder, sealed, and stored in a cold room at 4°C.

*2.3. Preparation for Electrospinning Solutions.* Solutions of various ratios of 0/100 to 30/70 of keratin/polyvinyl alcohol (K/PVA), at a constant concentration of 12 wt%, were

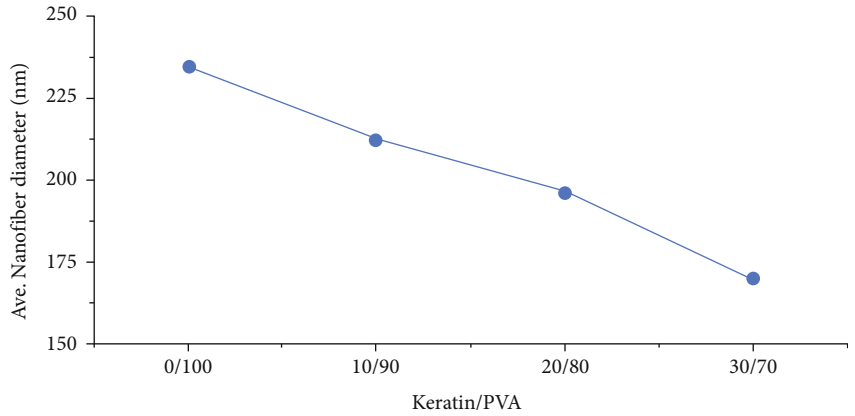


Figure 6: Graph of the effect of keratin content on average diameters of keratin/PVA nanofibers.

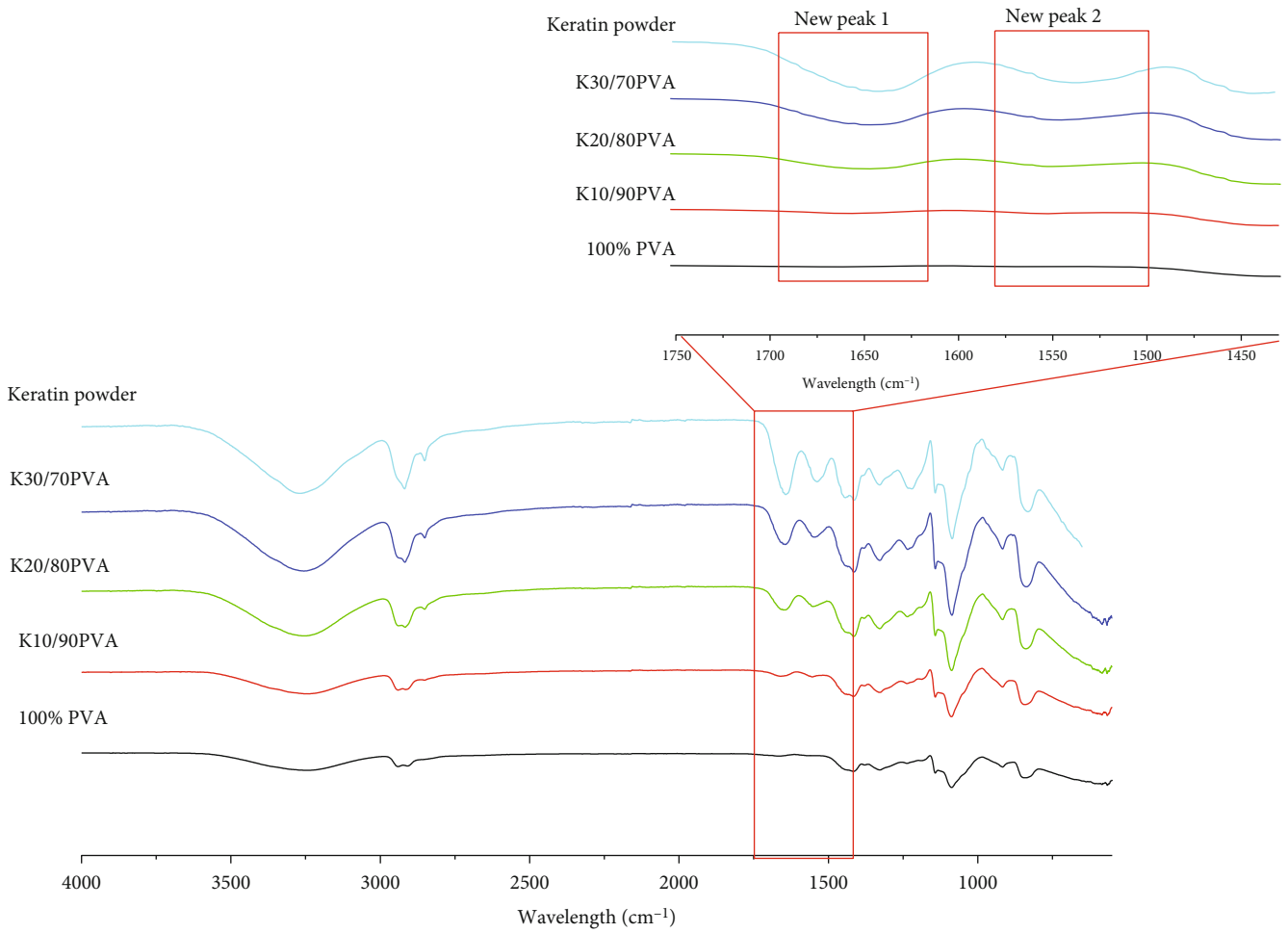


Figure 7: FTIR spectra of chicken feather keratin, PVA nanofibers, keratin/PVA nanofibers, and a zoomed-in subgraph of new peaks.

prepared by initially dissolving chicken feather keratin in deionized water, stirred at 50°C while adding about two drops of 1 M NaOH, and then cooled to room temperature. Polyvinyl alcohol was slowly added into the solution while stirring and further stirred for 30 minutes; the temperature increased to 80°C for 2 hours before cooling to room temperature. The conductivity of the solutions was measured using Metrohm 914 pH/conductometer, and the average of three measurements per solution was recorded. The solutions were then ready for electrospinning.

*2.4. Fabrication of Seamless Nanofiber Conduits.* Each electrospinning solution was placed in a 10 ml polyurethane (PU) syringe; the syringe was then connected by a tube to

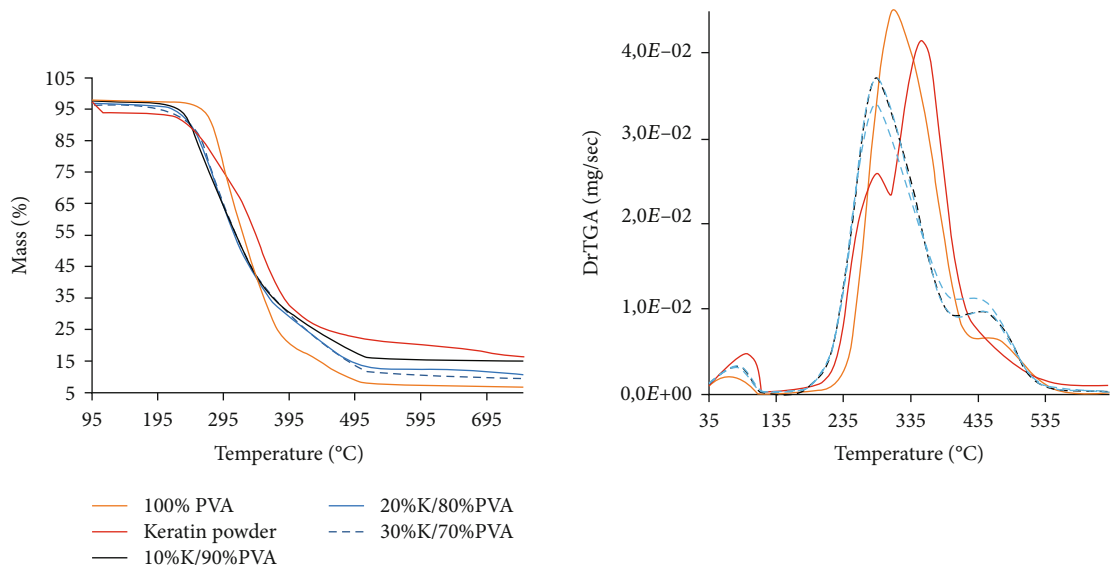


Figure 8: Thermogravimetric analysis and TGA derivative of keratin/PVA nanofibers.

Table 2: Quantity of mass loss of keratin/PVA nanofibers at 100°C and 400°C.

| | Mass loss (%) | |
|---|---|---|
| Sample | $T_{100\circ C}$ | $T_{400\circ C}$ |
| 100% PVA | 2.59 | 80.39 |
| 10% K/90%P VA | 2.49 | 70.11 |
| 20% K/80% PVA | 3.27 | 71.51 |
| 30% K/70% PVA | 3.77 | 70.91 |
| Keratin powder | 3.98 | 68.11 |

a nanospinner nozzle of 0.8 mm inside diameter. The electrospinning parameters were set to 30 kV, 20 cm nozzle-collector distance, 3 ml/hour feed rate, and a collector rotation speed of 52 cm/s.

*2.5. Characterization of Nanofiber Conduits*

*2.5.1. Fourier Transform Infrared Spectroscopy (FTIR).* Functional groups of the keratin, polyvinyl alcohol, and nanofibers were analyzed using Fourier transform infrared spectroscopy (Frontier Universal model, from PerkinElmer) in an attenuated total reflection mode (ATR). Each sample was scanned four times at a wavenumber range of 550–4000 $cm^{-1}$ with a resolution of 4 $cm^{-1}$.

*2.5.2. CHNS Analysis for Crude Protein Content in Nanofibers.* Protein content in nanofibers was done using a CHNS/O analyzer, which determines the content of carbon, hydrogen, nitrogen, and sulphur in the sample. After that, the protein content is calculated by multiplying the nitrogen content by a crude protein conversion factor of 6.25 [25].

*2.5.3. Scanning Electron Microscopy (SEM).* Scanning electron microscopy was used to determine morphological properties of nanofiber conduits such as shape, diameter, porosity, smoothness, and beads. Samples were set up on a metal stub using a sticky carbon disc; they were then gold-coated using a sputter coater before being placed in the ZEISS LEO 1450 Scanning Electron Microscope for imaging. Image-Pro Plus software was then used to analyze the diameters of 100 nanofibers.

*2.5.4. Thermal Gravimetric Analysis.* Thermophysical properties were investigated using a thermal gravimetric analyzer at a heating rate of 30°C/min from 30 to 600°C.

## 3. Results and Discussions

*3.1. Extraction and Characterization of Keratin.* White chicken feathers were obtained after pretreatment. The increased whiteness index of feathers was due to removing brown-yellow oil and fats. The index further advanced after degreasing with ethanol. After that, a mixture of an aqueous solution and chicken feather particles was recovered after 4 hours of cooking. The final purification steps resulted in light brown supernatant and keratin powder after filtration and freeze-drying, respectively. Figure 1 contains the extracted keratin molecular weight's sodium dodecyl sulphate polyacrylamide gel electrophoresis (SDS-PAGE) analysis.

It shows that the extracted keratin has molecular weights that range from about 3 kDa to approximately 60 kDa, whereas the broad, intense band between 10 and 15 kDa indicates that multiple monomers have a molecular weight of 10-15 kDa range [26].

FTIR's functional groups' qualitative analysis confirmed the presence of polypeptide amides, namely, amide A, amide B, amide I, amide II, and amide III represented by the absorbance peaks at 3280.79 $mc^{-1}$, 2919.88 $mc^{-1}$, 1633.74 $mc^{-1}$, 1532.24 $mc^{-1}$, and 1212.05 $mc^{-1}$, respectively [27]. Furthermore, the extracted keratin elemental analysis showed that this keratin has 5.02% sulphur, 46.64% carbon, 10.82% nitrogen, 7.72% hydrogen, and 29.74% other elements,

including oxygen. The extract is composed of 67.63% protein, calculated from the nitrogen percentage in the hydrolysate.

*3.2. Preparation and Characterization of Keratin/PVA Nanofibers.* The prepared electrospinning solutions of various ratios of keratin and PVA, from 00/100 to 30/70, were homogeneous and had a pH of 8 at 24.1°C. The graph in Figure 2 shows the effect of keratin content in the electrospinning solution.

The conductivity of electrospinning solutions increased with an increase in keratin content. The increase in conductivity may be due to polar amino acids in keratin. The morphology of keratin/PVA nanofibers with different keratin contents from 0% to 30% is shown in Figure 3. All nanofibers were cylindrical and became thinner as keratin content was increased. As keratin content increases, the conductivity of the spinning solution increases.

The increase in conductivity increases the polymer jet's electrical charge, increases the electric field force, and results in thinner jets and nanofibers and smaller fiber diameters. In addition to greater electric field strength, increasing conductivity decreases the solution's viscosity, resulting in smaller nanofiber's average diameters. However, there was no noticeable change in the individual nanofibers' cross-sectional shape from 100%bPVA to 90% PVA nanofibers, as shown in Figure 4.

Figure 3 also shows histograms of nanofiber diameters to indicate the diameter distributions that narrow as keratin content increases. Energy-dispersive X-ray (EDX) results, shown in Figure 5, indicate that keratin/PVA nanofibers are mainly composed of carbon, oxygen, nitrogen, and sulphur.

The element mapping of EDX showed that all the atoms were evenly distributed throughout the nanofibers' materials. The significant amounts of nitrogen and sulphur indicated the presence of keratin proteins. There was a noticeable increase in nitrogen percentage as keratin content increased in nanofibers. The conductivity and average diameters of nanofibers are tabulated in Table 1 and shown in Figure 6.

Furthermore, in Figure 5(b), SEM image analysis shows atoms evenly distributed throughout the nanofiber tubes. The average pore sizes decreased from 0.09 to 0.04 pm, decreasing with increased keratin content. This effect can also be attributed to the keratin conductivity effect; high conductivity within the polymer jet causes the jet to split into thinner jets due to the greater repulsive force, resulting in a higher number of fibers per unit area, thus reducing the number of fibers per unit pore size.

The FTIR spectra of PVA nanofibers, keratin powder, and keratin/PVA nanofibers are shown in Figure 7. Keratin spectrum was used as a reference spectrum for keratin/PVA nanofiber spectra. The keratin spectrum exhibited peaks of different amides of keratin protein. A peak at 3282.56 $cm^{-1}$ is N-H stretching of amide A and possible Fermi resonance from the overtone of amide I [28], C-N bending of amide B (2919.88 $cm^{-1}$), CO stretching of amide I (1633.74 $cm^{-1}$), C-N stretching and N-H bending of amide II (1532.24 $cm^{-1}$), amide III's CO stretching (1200 $cm^{-1}$), C-H bending of amide IV (623 $cm^{-1}$), and S-O stretching of cysteine-sulphonate (1212.05 $cm^{-1}$) and disulphide bonds at 550 $cm^{-1}$ [16, 29]. Some PVA spectrum peaks include -OH stretching peak at 3100 $cm^{-1}$, -CHO stretching at 2950 $cm^{-1}$, and CO stretching at 2900 $cm^{-1}$. The addition of keratin into PVA increased the intensity of amides A and B; this can be attributed to the interaction of the $-NH_2$ group of keratin and -OH group of PVA, resulting in hydrogen bond formation.

The increased amount of keratin corresponds with two new peaks related to PVA, at 1642.26 $cm^{-1}$ and 1547.21 $cm^{-1}$. These peaks shift to shorter wavelengths as keratin content increases. The changes in the intensities of peaks, forming new ones and shifting to shorter wavelengths, confirm keratin in the nanofibers and suggest the chemical interactions between keratin and PVA. This chemical reaction between the PVA and keratin functional group minimizes the interaction between keratin macromolecules and increases the keratin's electrospinnability; the amide-carbonyl interaction further prevents phase separation of keratin and PVA in blended spinning solution [30].

TG analysis in Figure 8 shows the mass-loss curves and their derivatives to indicate polyvinyl alcohol nanofibers' thermal behaviour, keratin, and keratin-PVA nanofibers. These graphs show three major mass-loss events for nanofibers and keratin. The first event at just below 100°C was attributed to water evaporation. The mass loss, shown in Table 2, resulted in a mass reduction of 2.59% for 100% PVA nanofibers and 2.49% to 3.98% for 10% to 30% keratin nanofibers and keratin.

The increasing trend of water mass with the increase in PVA keratin content indicates keratin nanofibers' hydrophilicity. The second and significant mass loss occurred between 190°C and 400°C. This was attributed to the degradation of alpha-helix and peptide bonds of amino acid residues [31].

The onset temperature of PVA nanofibers, 190°C, was higher than that of keratin and keratin/PVA nanofibers at 160°C. However, increasing keratin content showed no further effect on the onset temperature of keratin/PVA nanofibers. Nevertheless, PVA nanofibers and keratin showed a high degradation rate, with PVA nanofibers having the highest rate. Both PVA nanofibers and keratin exhibited a high degradation rate than their blend nanofibers. The third mass loss event occurred between 405°C and 490°C; this loss was due to the degradation of the previous mass loss event's by-products. Keratin had a high amount of residuals than PVA, indicating better stability, while the ash content of keratin/PVA nanofibers fell between keratin and PVA.

## 4. Conclusion

Keratin/PVA nanofiber tubes were successfully fabricated without longitudinal seams. The addition of polyvinyl alcohol improved keratin's electrospinnability by interrupting keratin macromolecules' interaction and forming hydrogen bonds. On the other hand, keratin advanced the thermal stability of PVA nanofibers. Keratin nanofibers have a smaller

diameter than keratin-free PVA nanofibers, increasing their surface area. The diameter of the nanofibers decreases when keratin content increases, suggesting the limit in electrospinnability of PVA/keratin blend due to keratin content. When used as nerve conduits, these permeable tubes will provide transportation of nutrients and metabolic waste; they will serve as a barrier that prevents other tissues into the regeneration area. Small diameters increase cell proliferation, cell spreading, and differentiation of neural stem cells while decreasing cell aggregation levels. The keratin-based nanofiber tubes are potential nerve regeneration frames as they mimic the extracellular matrix of the natural fibrous structure of neural tissue. They enhance electrophysiological recovery and axon density. Future investigations on the keratin/PVA nanofiber tubes will include in vitro and in vivo experiments.

## Data Availability

The supporting data to the findings of this work will be available on request.

## Conflicts of Interest

The authors declare that they have no conflicts of interest.

## Acknowledgments

Acknowledgements for project funding and laboratory facilities are given to the Council for Scientific and Industrial Research-Biorefinery Industry Development Facility (CSIR-BIDF), the Department of Science and Technology, and the University of KwaZulu-Natal. The first authors would also like to acknowledge Miss Nomthandazo Hadebe for helping with TGA.

## References

[1] M. C. Dodla, M. Alvarado-Velez, V. J. Mukhatyar, and R. V. Bellamkonda, "Chapter 69- peripheral nerve regeneration," in *Principles of Regenerative Medicine (Third Edition)*, A. Atala, R. Lanza, A. G. Mikos, and R. Nerem, Eds., pp. 1223–1236, Academic Press, Boston, 2019.

[2] J. Moskow, B. Ferrigno, N. Mistry et al., "Review: bioengineering approach for the repair and regeneration of peripheral nerve," *Bioactive Materials*, vol. 4, no. 1, pp. 107–113, 2019.

[3] X. Zhan, M. Gao, Y. Jiang et al., "Nanofiber scaffolds facilitate functional regeneration of peripheral nerve injury," *Nanomedicine: Nanotechnology, Biology and Medicine*, vol. 9, no. 3, pp. 305–315, 2013.

[4] N. Sinis, A. Kraus, D. Drakotos et al., "Bioartificial reconstruction of peripheral nerves using the rat median nerve model," *Annals of Anatomy-Anatomischer Anzeiger*, vol. 193, no. 4, pp. 341–346, 2011.

[5] S. Panseri, C. Cunha, J. Lowery et al., "Electrospun micro- and nanofiber tubes for functional nervous regeneration in sciatic nerve transections," *BMC Biotechnology*, vol. 8, no. 1, p. 39, 2008.

[6] R. Murphy, A. Faroni, J. Wong, and A. Reid, "Protocol for a phase I trial of a novel synthetic polymer nerve conduit 'Polynerve' in participants with sensory digital nerve injury (UMANC)," *F1000Research*, vol. 8, 2019.

[7] R. Tevlin, A. McArdle, D. Atashroo et al., "Biomaterials for craniofacial bone engineering," *Journal of Dental Research*, vol. 93, no. 12, pp. 1187–1195, 2014.

[8] J. Xue, T. Wu, Y. Dai, and Y. Xia, "Electrospinning and electrospun nanofibers: methods, materials, and applications," *Chemical Reviews*, vol. 119, no. 8, pp. 5298–5415, 2019.

[9] P. Zarrintaj, E. Zangene, S. Manouchehri et al., "Conductive biomaterials as nerve conduits: recent advances and future challenges," *Applied Materials Today*, vol. 20, article 100784, 2020.

[10] B. Sowmya, A. B. Hemavathi, and P. K. Panda, "Poly (ε-caprolactone)-based electrospun nano-featured substrate for tissue engineering applications: a review," *Progress in Biomaterials*, vol. 10, no. 2, pp. 91–117, 2021.

[11] X. Zhang, W. Qu, D. Li et al., "Functional polymer-based nerve guide conduits to promote peripheral nerve regeneration," *Advanced Materials Interfaces*, vol. 7, no. 14, p. 2000225, 2020.

[12] S. L. Porter, S. M. Coulter, S. Pentlavalli, and G. Laverty, "Pharmaceutical formulation and characterization of dipeptide nanotubes for drug delivery applications," *Macromolecular Bioscience*, vol. 20, no. 7, p. 2000115, 2020.

[13] H. Yoshimoto, Y. M. Shin, H. Terai, and J. P. Vacanti, "A biodegradable nanofiber scaffold by electrospinning and its potential for bone tissue engineering," *Biomaterials*, vol. 24, no. 12, pp. 2077–2082, 2003.

[14] K. Kim and J. P. Fisher, "Nanoparticle technology in bone tissue engineering," *Journal of Drug Targeting*, vol. 15, no. 4, pp. 241–252, 2007.

[15] C. M. Agrawal and R. B. Ray, "Biodegradable polymeric scaffolds for musculoskeletal tissue engineering," *Journal of Biomedical Materials Research*, vol. 55, no. 2, pp. 141–150, 2001.

[16] T. Guo, X. Yang, J. Deng, L. Zhu, B. Wang, and S. Hao, "Keratin nanoparticles-coating electrospun PVA nanofibers for potential neural tissue applications," *Journal of Materials Science: Materials in Medicine*, vol. 30, no. 1, p. 9, 2018.

[17] X. Wang, T. Yucel, Q. Lu, X. Hu, and D. L. Kaplan, "Silk nanospheres and microspheres from silk/pva blend films for drug delivery," *Biomaterials*, vol. 31, no. 6, pp. 1025–1035, 2010.

[18] Y. Feng, M. Borrelli, T. Meyer-ter-Vehn, S. Reichl, S. Schrader, and G. Geerling, "Epithelial wound healing on keratin film, amniotic membrane and polystyrene in vitro," *Current Eye Research*, vol. 39, no. 6, pp. 561–570, 2014.

[19] V. Agarwal, N. Varghese, S. Dasgupta, A. K. Sood, and K. Chatterjee, "Engineering a 3D $MoS_2$ foam using keratin exfoliated nanosheets," *Chemical Engineering Journal*, vol. 374, pp. 254–262, 2019.

[20] L. Cui, J. Gong, X. Fan, P. Wang, Q. Wang, and Y. Qiu, "Transglutaminase-modified wool keratin film and its potential application in tissue engineering," *Engineering in Life Sciences*, vol. 13, no. 2, pp. 149–155, 2013.

[21] L. Ajay Sharma, M. A. Ali, R. M. Love, M. J. Wilson, and G. J. Dias, "Novel keratin preparation supports growth and differentiation of odontoblast-like cells," *International Endodontic Journal*, vol. 49, no. 5, pp. 471–482, 2016.

[22] J. Choi, G. Panthi, Y. Liu et al., "Keratin/poly (vinyl alcohol) blended nanofibers with high optical transmittance," *Polymer*, vol. 58, pp. 146–152, 2015.

[23] P. Sierpinski, J. Garrett, J. Ma et al., "The use of keratin biomaterials derived from human hair for the promotion of rapid

regeneration of peripheral nerves," *Biomaterials*, vol. 29, no. 1, pp. 118–128, 2008.

[24] L. A. Pace, J. F. Plate, T. L. Smith, and M. E. Van Dyke, "The effect of human hair keratin hydrogel on early cellular response to sciatic nerve injury in a rat model," *Biomaterials*, vol. 34, no. 24, pp. 5907–5914, 2013.

[25] P. P. Salo-väänänen and P. E. Koivistoinen, "Determination of protein in foods: comparison of net protein and crude protein (N × 6.25) values," *Food Chemistry*, vol. 57, no. 1, pp. 27–31, 1996.

[26] P. Hill, H. Brantley, and M. Van Dyke, "Some properties of keratin biomaterials: kerateines," *Biomaterials*, vol. 31, no. 4, pp. 585–593, 2010.

[27] B. Ma, X. Qiao, X. Hou, and Y. Yang, "Pure keratin membrane and fibers from chicken feather," *International Journal of Biological Macromolecules*, vol. 89, pp. 614–621, 2016.

[28] V. Agarwal, A. G. Panicker, S. Indrakumar, and K. Chatterjee, "Comparative study of keratin extraction from human hair," *International Journal of Biological Macromolecules*, vol. 133, pp. 382–390, 2019.

[29] N. Ramakrishnan, S. Sharma, A. Gupta, and B. Y. Alashwal, "Keratin based bioplastic film from chicken feathers and its characterization," *International Journal of Biological Macromolecules*, vol. 111, pp. 352–358, 2018.

[30] I. Cruz-Maya, V. Guarino, A. Almaguer-Flores, M. A. Alvarez-Perez, A. Varesano, and C. Vineis, "Highly polydisperse keratin rich nanofibers: scaffold design and in vitro characterization," *Journal of Biomedical Materials Research Part A*, vol. 107, no. 8, pp. 1803–1813, 2019.

[31] M. He, M. Chen, Y. Dou et al., "Electrospun silver nanoparticles-embedded feather keratin/poly (vinyl alcohol)/poly(ethylene oxide) antibacterial composite nanofibers," *Polymers*, vol. 12, no. 2, p. 305, 2020.

Hindawi
Journal of Nanomaterials
Volume 2021, Article ID 4064983, 15 pages
https://doi.org/10.1155/2021/4064983

*Review Article*

# Nanoparticle-Based Drug Delivery System—A Target Strategy for Osteoarthritis Treatment

**Keda Liu, Dianjian Zhang, and Wei Wang**

*School and Hospital of Stomatology, China Medical University, Liaoning Provincial Key Laboratory of Oral Diseases, Shenyang 110001, China*

Correspondence should be addressed to Wei Wang; wwang75@cmu.edu.cn

Received 4 August 2021; Accepted 6 October 2021; Published 20 October 2021

Academic Editor: Hui Qi Xie



Osteoarthritis (OA) is a bone and joint disease with pathological characteristics such as articular cartilage degeneration injury and synovial and subchondral bone reactive hyperplasia. Once cartilage is damaged, it is difficult to repair it by itself. Current clinical practice is mainly limited to symptomatic treatment, not changing the degenerative process of osteoarthritis. The important goal of nanomedicine is targeted delivery. Nanoparticles (NPs) can provide many unique potential functions for the targeted treatment of arthritis. This review summarizes the research progress of nanomaterials as a drug delivery system in the treatment of osteoarthritis from three aspects: (1) the etiology of OA and the current research status of applying nanoparticles to treat OA, (2) the construction of osteoarthritis models, and (3) the classification of nanoparticle-based drug delivery systems.

## 1. Introduction

With the increase in life expectancy, obesity rates and sports injuries, the incidence of arthritis is rising steadily [1]. These reasons have promoted the research of tissue engineering materials in orthopedics or joint surgery. Osteoarthritis, also known as degenerative arthritis, senile arthritis, and hypertrophic arthritis, is a bone and joint disease with main pathological characteristics such as articular cartilage degeneration injury, joint edge and subchondral bone reactive hyperplasia, and synovial hyperplasia [2, 3]. Cartilage lacks nourishing pathways (such as blood vessels, nerves, and lymph), consisting of only a single type of cell with low proliferative activity (chondrocytes) [4]. Therefore, once damaged, it is extremely difficult to repair it by itself. The current traditional methods for the treatment of cartilage defects mainly include autologous cartilage transplantation, microfracture (bone marrow stimulation), and autologous chondrocyte transplantation [5]. Although these methods have certain curative effects, they have defects such as large damage to the donor site, inconsistent characteristics of the repaired area and surrounding cartilage, and poor interface healing. Current clinical practice is mainly limited to symptomatic treatment (pain relief and artificial joint replacement), not involving the underlying molecular cause of OA. This treatment does not change the degenerative process of osteoarthritis. Figure 1 shows the diagram of normal and cartilage osteoarthritis joints.

Nanomaterials refer to materials whose structure is at the nanometer scale in at least one dimension, or is composed of nanostructured units with special properties. It has been extensively studied in the field of tissue engineering, including as a cell growth scaffold to promote bone tissue regeneration and as a transplant material for repairing peripheral nerves [6, 7]. Nanomaterials can perform biological imaging through spectral and fluorescent signals to promote disease diagnosis [8]. At the same time, nanomaterials can also be used as biosensors to effectively monitor disease progression [9]. This review mainly focuses on the targeted delivery function of nanomaterials in the field of OA. Nanomaterials can provide many unique potential functions for the targeted treatment of arthritis, and they include the following: (1) maintaining the concentration of the drug in the target area to maximize the effect of the drug, (2) carrying more drug molecules and increasing the solubility of some hydrophobic drugs, and (3) loading target molecules

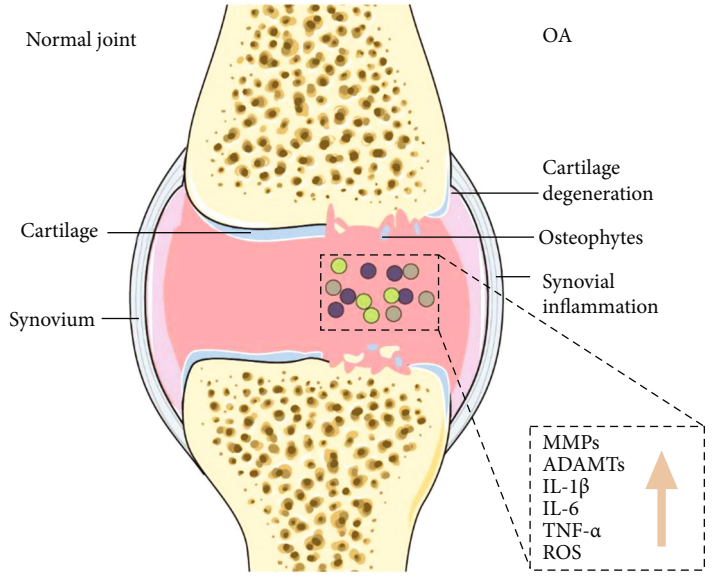


Figure 1: Diagram of normal and cartilage osteoarthritis joints.

to nanoparticles through surface modification for targeted delivery [10, 11].

This article summarizes the research progress of nanomaterials as a drug delivery system in the treatment of osteoarthritis from the following aspects: the etiology of OA, the current research status of applying nanoparticles to treat OA, the construction of OA models, and the classification of nanoparticle-based drug delivery systems. In Table 1, we summarize the latest research progress of applying nanoparticles to treat OA.

## 2. The Etiology of OA and the Current Research Status of Applying Nanoparticles to Treat OA

*2.1. Injury.* Osteoarthritis that develops after joint injury is considered as posttraumatic osteoarthritis (PTOA) [42]. Both anterior cruciate ligament injury (ACL) and meniscus injury can lead to a high risk of PTOA [43]. At the same time, the load change of the injured joint will promote the development of PTOA. ACL defect or joint reconstruction will change the biomechanical distribution of the tibiofemoral joint contact area, increasing the load on the cartilage area that was previously unloaded and reducing the load on the cartilage area that should have received a higher load during the weight-bearing process, eventually causing the articular cartilage to rupture [44–46]. Studies have shown that quadriceps weakness after knee injury is one of the causes of PTOA [47]. When the quadriceps muscles are weak, as in the case of anterior cruciate ligament injury and reconstruction, they cannot fully absorb the impact energy [48]. This will put more load on the articular cartilage, which will eventually lead to joint degeneration. Intra-articular fractures are also one of the causes of PTOA [49]. Acute mechanical damage and chronic abnormalities of joint load after intra-articular fractures may cause articular cartilage rupture.

Cartilage cells will enhance metabolism through mechanoreceptors on the surface of chondrocytes detecting mechanical load [50]. Through the process of mechanical transduction, mechanical signals are converted into chemical signals to regulate the biochemical activity of chondrocytes and induce molecular biosynthesis to maintain tissue integrity [51]. Mechanoreceptors of cell surface include integrins and mechanosensitive ion channels [52]. Integrin is a kind of transmembrane protein that activates intracellular signal transduction by attaching to downstream signal molecules. The activation of mechanoreceptors triggers a cascade of signals within the cell, causing the tissue remodeling process. Excessive mechanical load leads to the imbalance between synthesis and decomposition, causing the consumption of matrix components, and the lack of regeneration ability, resulting in irreversible damage, making it the most obvious trigger of OA [53, 54].

In past tissue engineering research, cartilage cells were loaded on the surface of biomaterials to promote cartilage repair. However, this method cannot solve the problem that resident chondrocytes secrete abnormal extracellular matrix, and it is difficult to maintain the survival rate of transplanted chondrocytes. To solve these problems, researchers invented a kind of cell-free HA nanoscaffold that provided two cytokines, namely, stromal cell-derived factor-1$\alpha$ (SDF) to increase MSC recruitment and infiltration, and transforming growth factor-$\beta$3 (TGF-$\beta$3; TGF) to promote the formation of cartilage tissue [31]. The ethylene glycol chitosan/fucoidan nanogels (GC/Fu @ KAFAK NGs) loaded with KAFAK (anti-inflammatory peptide) were prepared by electrostatic interaction and the natural compound genipin. Researchers found that intra-articular injection of this NP not only inhibited the expression of IL-6 and TNF-$\alpha$ but also increased the expression of the chondrogenesis markers type II collagen, proteoglycan, and Sox9 [30]. Based on the camouflage of the natural BMSC membrane, the researchers encapsulated kartogenin (KGN) as a cartilage regeneration

Table 1: Research summary of nanoparticle-based drug delivery systems.

| Type of NPs | Carrier | Cargo | Outcome | Ref |
|---|---|---|---|---|
| Liposomes | (HA)-liposomal | Diclofenac, dexamethasone | Effectively relieving the pain of OA and having good biocompatibility | [12] |
| | SLN system | Integrin $\beta$1 overexpression pDNA | Reducing chondrocyte apoptosis and enhancing tissue repair | [13] |
| Micelles | PNIPAM-PMPC | Diclofenac sodium | PNIPAM-PMPC nanospheres are biocompatible and upregulate anabolic genes, while downregulating articular cartilage catabolism genes | [14] |
| | Polyethylene oxide- (PEO-) and polypropylene oxide- (PPO-) based polymeric micelles | rAAV sox9 | Enhancing the deposition of ECM components and cell survival levels, inhibiting inflammation | [15] |
| | Acid-activatable polymer | Curcumin | Suppression of tumor necrosis factor-alpha (TNF-$\alpha$) and interleukin 1$\beta$ (IL-1$\beta$). Potent antioxidant and anti-inflammatory activities | [16] |
| Inorganic NPs | MSNs | $MnO_2$, gold-based nanoformulations, $CeO_2$ | COL2a1 and ACAN gene expression in chondrocytes was significantly decreased | [17–19] |
| | | pSBMA, colchicine | Due to the hydration lubrication mechanism, the wear resistance of the material is enhanced. Reducing nitric oxide, malondialdehyde, COX2, and TNF-$\alpha$ | [20, 21] |
| | Zeolitic imidazolate framework-8 | *S*-Methylisothiourea hemisulfate salt | Reducing the content of NO and $H_2O_2$, thereby inhibiting the production of HIF1$\alpha$ and M1 macrophages, alleviating mitochondrial function | [22] |
| | Membrane-disguised $Fe_3O_4$ | Kartogenin | Enabling rapid and high-quality cartilage regeneration | [23] |
| Polymer NPs | CD-PMPC | Silica | Enhancing penetration of dermal tissue and lubrication, inducing drug release | [24] |
| | PLGA-PEG | 4MAL, kartogenin (KGN) | Prolonging IA drug retention for the treatment of OA. Increasing sulfated glycosaminoglycans | [25–27] |
| | Electrostatic self-assembly heparin and $\varepsilon$-poly-l-lysine | Platelet lysate | Platelet lysate is evenly distributed | [28] |
| | Hollow dextran/PNIPAM | KAFAK | In cartilage explants to suppress inflammation | [29] |
| | Glycol chitosan/fucoidan nanogels | KAFAK | Inhibiting the expression of TNF-$\alpha$ and IL-6. Enhancing the expression of type II collagen, proteoglycan, and Sox9 | [30] |
| | Electro spun cell-free fibrous hyaluronic acid | SDF-1$\alpha$, TGF-$\beta$3 | Increasing recruitment and infiltration of MSCs to enhance cartilage tissue formation | [31] |
| | PLGA | Andrographolide, p66shc siRNA, diacerein | Inhibiting osteoclast function and inflammation | [32–34] |
| | Poly(D,L-lactic acid)-poly(ethylene glycol)-poly(D,L-lactic acid) | BMP2 | Inducing implant differentiation into cartilage and bone but also completely degraded without toxicity | [35] |
| | LbL polymer microcapsule | $MnO_2$ | Eliminating hydrogen peroxide $H_2O_2$ and protecting cells from oxidative stress | [36] |
| Exosomes | | miR-140, miR-9-5p, miR-100-5p, miR-135b, miR-1405p, and lncRNA KLF3-AS1 | Reducing inflammation and promoting cartilage marker production | [37–41] |

drug into $Fe_3O_4$ nanoparticles. As a result, a nanomaterial with excellent biocompatibility and good biosafety is obtained, achieving high-quality and fast cartilage regeneration [23]. Researchers synthesized cerium oxide nanoparticles ($CeO_2$) with a particle size of about 120 nm and combined them with hyaluronic acid (HA) to construct nanodelivery drugs. Through in vitro OA model studies, it was found that the delivery system can protect chondrocytes from oxidative stress, and the expression of COL2a1 and ACAN genes in chondrocytes was significantly increased [19]. Janus-based nanotubes (AAT) self-assemble from analogs of synthetic DNA bases (guanine-cytosine motif), which

can transport small RNA molecules to cells and tissues. Researchers encapsulated the nanotube AAT-packaged miR365 antagomir in the yeast cell wall to construct nanoadministrative particles. This nanodrug delivery system inhibited the content of miR365 by oral administration to treat PTOA (mice) [55].

*2.2. Inflammation.* OA is also a disease caused by underlying immune response leading to bone remodeling and cartilage degradation. Typical symptoms include swelling, pain, and stiffness [56]. By initiating the inflammatory process and inducing cartilage decomposition, the early changes in the cartilage surface are manifested as fibers extending distally, forming deep cracks, leading to cartilage delamination, forming calcified cartilage [57]. The thinning of articular cartilage is closely associated with dilation of basal calcified cartilage, which in turn leads to increased mechanical stress and further production of degrading factors [58]. Major signaling molecules involved in OA immune response are usually divided into the anti-inflammatory and inflammatory groups. The inflammatory cytokines include TNF-$\alpha$, IL-1$\beta$, IL-6, IL-8, and IL-17, and the anti-inflammatory cytokines include IL-13, IL-4, IL-10, and IL-1Ra [42, 49, 59]. Cytokines can participate in the pathological process of cartilage degeneration by mediating multiple signaling pathways, mainly including the mitogen-activated protein kinase (MAPK) signaling pathway [60], the AMPK signaling pathway [61], and the Wnt/$\beta$-catenin signaling pathways [62]. They can also promote the synthesis of $PGE_2$ and induce the production of chondrocytes to synthesize metalloproteinases (ADAMTS) [63], HIF2$\alpha$, NOS2, MMPs, and COX2, thereby promoting the inflammatory process and inhibiting the proliferation of chondrocytes [64, 65].

Therefore, implanting anti-inflammatory factors or enzymes into the joint cavity and maintaining the drug concentration is another research direction for OA treatment. Hollow dextran/PNIPAM nanoparticles loaded with KAFAK effectively deliver therapeutic peptides to inhibit inflammation. These heat-responsive nanoparticles may be an effective drug delivery system that can deliver anti-inflammatory therapeutic peptides in an OA environment [29]. The researchers encapsulated three hydrophobic anti-inflammatory drugs (tenoxicam, dexamethasone, and celecoxib) into core-shell terpolymer nanoparticles. Experiments have shown that these loaded nanoparticles have the activity of acting as inflammatory mediator production regulators in vitro [66]. $MnO_2$ nanoparticles, with excellent biocompatibility, can be used as artificial nanoenzymes to effectively eliminate reactive oxygen. Hollow $MnO_2$ (H-$MnO_2$) was synthesized by the Stober method and modified with $NH_2$-PEG-$NH_2$, reducing the inflammatory response of OA [17].

*2.3. Obesity.* Obesity is a state of excessive accumulation of fat in the body, which is believed to be directly related to some metabolic diseases such as high blood pressure, dyslipidemia, diabetes, and osteoarthritis [67–69]. Obesity plays an important role in the occurrence and development of weight-bearing and non-weight-bearing joint osteoarthritis. Increased joint load and systemic metabolic changes may be important factors in the occurrence of obesity-related osteoarthritis. Moderate mechanical load can maintain the dynamic balance and integrity of articular cartilage. Compared with normal BMI people, tibiofemoral cartilage of high BMI people withstand more compressive stress during short-term running tasks [70]. The proteoglycan content in obese subjects is reduced, indicating that the cartilage is in a "pre-osteoarthritis" state. Osteoarthritis caused by obesity is defined as a "metabolic osteoarthritis" phenotype [71]. Metabolic osteoarthritis is associated with increased fat deposits that release inflammatory cytokines/adipokines, leading to systemic inflammation, cartilage loss, and osteophyte formation [72].

In order to solve the abrasion caused by mechanical erosion, viscoelastic supplements based on hyaluronic acid (HA) have been widely used to treat knee joint injuries. However, current HA formulation cannot provide effective healing and recovery. Researchers have developed a nanofiber-HA membrane system to protect arthritic cartilage tissue from degeneration. The material has a unique scaffold structure that can provide a 3D microenvironment like natural ECM, and deliver biologically active signals that can activate chondrocyte proliferation and functional collagen I synthesis. Researchers injected the ankle joint to fill the joint cavity and found that this hybrid nanofiber membrane has a better therapeutic effect than the commercially available Hyalgan and Synvisc gels at a lower concentration, providing a simple and feasible alternative to OA treatment [73].

*2.4. Age.* Age is one of the main factors of osteoarthritis. There are literatures showing that the prevalence of knee arthritis increases almost linearly after the age of 40 [74]. The incidence of osteoarthritis increase with age, which may be due to the accumulation of various risk factors and the result of biological changes [75]. Osteoarthritis is characterized by the imbalance between catabolic and anabolic activities in the joints. Aging chondrocytes do not respond well to growth factor stimulation and cannot maintain the homeostasis of articular cartilage, leading to the occurrence of OA [76].

How to improve the response of aging chondrocytes to growth factors has received extensive attention. Platelet lysate (PL) is a cost-effective mixture of growth factors. Electrostatic self-assembly heparin (Hep) and $\varepsilon$-poly-l-lysine (EPL) nanoparticles (NPs) were engineered to enhance the sustained release ability of PL. This nanodrug delivery material retained the initial gelling ability and showed long-term PL release ability, ameliorating cartilage degeneration in the late stage of OA [28]. Researchers have prepared a cationic lipid nanoparticle (SLN) system that can efficiently deliver plasmid DNA (pDNA) into cells. This study reported that the overexpression of pDNA carrying integrin $\beta$1 was transported into rat chondrocytes via liposomes, reducing IL-1$\beta$-stimulated chondrocyte apoptosis and enhancing tissue repair [13]. Researchers developed a thermosensitive bifunctional nanosphere polymer (PNIPAM-PMPC) through emulsion polymerization. The nanospheres can enhance lubrication by forming a hydration layer around the base

of the zwitterion head, and deliver local drug by wrapping diclofenac sodium (an anti-inflammatory drug) [14, 77].

*2.5. Genetic Factors.* Epidemiological studies have confirmed that genetic factors play a major role in the pathogenesis of osteoarthritis. Studies based on the family history also confirmed that OA has hereditary susceptibility [78, 79]. The main mechanisms leading to OA were chemical modification of DNA, such as methylation, posttranslational modification of histones, and regulation of noncoding RNA.

(1) DNA methylation is a type of chemical modification of DNA that can alter the performance of genes without changing the DNA sequence. It refers to the covalent attachment of the methyl group to the 5th carbon position of cytosine in the genomic CpG dinucleotide under the action of DNA methyltransferase. Studies have shown that DNA methylation can cause changes in chromatin structure, DNA conformation, DNA stability, and the way DNA interacts with proteins, thereby controlling the gene expression. The analysis of the whole genome showed that the methylation of genes related to OA have changed, including genes encoding transcription factors, such as SOX9; genes encoding ECM protein and matrix degrading protease, including COL2a1, ACAN, and MMP13; and participating genes that signal growth factors and cytokines, such as GDF5 and BMP7 [80]. Some emerging trends indicate that methylation patterns may differ between different OA joints and stages of the disease [81]. For example, different methylation patterns may occur between knee cartilage and hip cartilage, and between mild and severe cartilage from the same joint [82, 83]

(2) Gene expression is a complex process regulated by multiple factors. Histones are an important part of the basic structure of chromosomes-nucleosomes, and their N-terminal amino acid residues can undergo acetylation, methylation, phosphorylation, and ubiquitination [84]

(3) Noncoding RNA (ncRNA) refers to RNA that does not encode protein. These include rRNA, tRNA, snRNA, snoRNA, microRNA, and other RNAs [85]. The common feature of these RNAs is that they can be transcribed from the genome, performing their biological functions at the RNA level without being translated into proteins [86]. For example, miR-140 can inhibit the expression of harmful genes ADAMTS5, MMP13, and IGFBP5 in OA [87]

Upregulating gene expression in target organs by delivering specific signaling molecules is a kind of method to treat OA caused by inheritance. Exosomes contain specific information about the source cell, with ability to deliver molecules targeting organs or tissues. The application of exosomes and their derivatives by intra-articular injection open up new possibilities for the treatment of OA. Studies have shown that exosomes derived from primary chondrocytes that overexpress miR-95-5p promoted cartilage development and cartilage matrix expression by directly targeting histone deacetylase [88]. Exosomal miR-8485 may regulate the expression of GSK-3 to suppress the production of glycogen synthase kinase, targeting the binding antagonist of DACT1 to activate the Wnt/$\beta$-catenin pathway and promote cartilage differentiation [89]. In Figure 2, we show the common predisposing factors of osteoarthritis.

## 3. Method of Constructing an OA Animal Model

Animal models are essential in studying the etiology of the disease and the effectiveness of various treatment tools. The ideal model should include the following features: (1) all joint tissues (as the human body) are affected; (2) early stages of the disease are included; (3) animal models can simulate human disease; (4) animal species are easy to handle and raise; (5) the results can be evaluated in different biochemical, genetic, and imaging biomarkers, and should be transferable to the specificity of human medical therapeutics and pathology. It is recommended to consider the following points when selecting the OA model: the stage of OA that needs to be studied, the expansion of the lesion (focal or systemic), the therapeutic effect, and the target tissue to be studied (cartilage, membrane, bones, or synovial fluid) [90].

OA models can be divided into induced models (surgery or injection) and spontaneous models (natural development and genetic models). Spontaneous models can be used to study the pathogenesis of OA, with high economic costs and long time to achieve goals [91, 92]. On the contrary, the induction model achieves a reproducible and early OA model, but it prevents researchers from studying the possible pathogenesis of diseases. Small mammals (mice, rats), rabbits, and guinea pigs are the most common models for studying the pathogenesis and pathophysiology of OA.

*3.1. Spontaneous Models (Age, Obesity, and Genetic Factor).* The main feature of spontaneous models is slow evolution, with a very long research cycle and high economic costs. However, they have an excellent correlation with natural processes from a pathophysiological point of view. Spontaneous models can be further subdivided into two subgroups: naturally occurring models or models produced by individual genetic manipulation.

*3.1.1. Age.* OA tends to occur in the elderly. The animal model of spontaneous osteoarthritis is close to the progression of human OA, as a valuable tool for studying the pathogenesis of osteoarthritis. When a Hartly guinea pig about 3 months old weighs 700 g, OA may appear on the medial tibial plateau of the knee joint. By the age of 18 months, the guinea pig's medial tibial plateau had severe OA pathological changes and there was no meniscus covering on the surface [93, 94]. OA is manifested by cartilage degradation, mainly histological changes in the cartilage in the weight-bearing area, which is similar to the occurrence and development of human osteoarthritis. The distribution

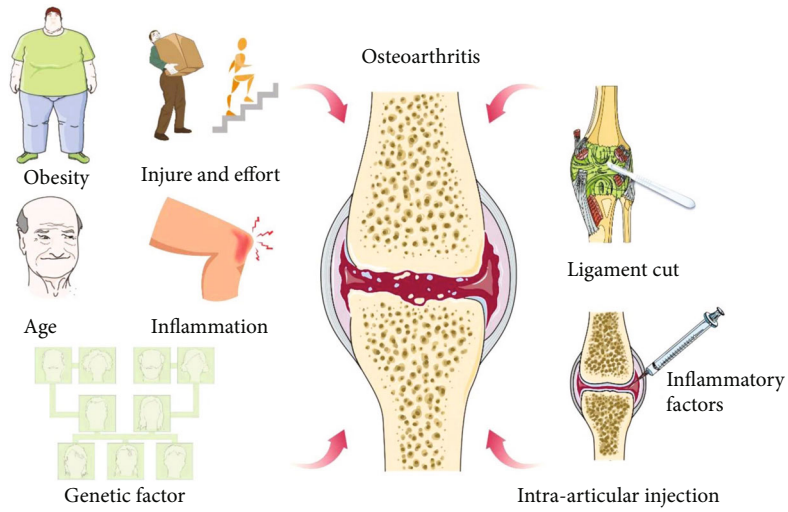


Figure 2: The etiology of osteoarthritis and the model construction method.

of glycosaminoglycans in cartilage is abnormal. Studies have found that the production of NO in guinea pig knee cartilage cells is positively correlated with age and the progression of OA, suggesting that it may be an important factor leading to mitochondrial dysfunction and calcification of OA chondrocytes [63, 95]. It can be observed that 12-20-week-old STR/ort mice have knee joint OA lesions [96]. The histological changes are mainly manifested as severe degeneration of the medial articular cartilage, similar to human OA, and calcification of the subchondral layer. This kind of mice also showed a marked increase in the release of local and systemic inflammatory factors, such as RAGE, AGE, IL-1, and IL-6 [97].

*3.1.2. Obesity.* Obesity can cause a variety of musculoskeletal system diseases, especially OA. The entire joint tissue, especially the synovial tissue, is affected by a high-fat diet. Obesity has been confirmed to be associated with the development of posttraumatic arthritis through a variety of mechanisms [98]. The mouse obesity model is usually induced by a high-fat diet. Louer et al. fed C57BL/6 mice with normal food (13% fat) and a high-fat diet (60% fat) from 4 weeks of age. After 16 weeks of age, the medial meniscus (destabilization of the medial meniscus (DMM)) was removed. The results showed that the serum levels of systemic inflammatory factors and proinflammatory factors increased in the high-fat group, including IL-12p70, IL-6, TNF-$\alpha$, and several other chemokines [99]. STR/ort mice are more prone to osteoarthritis and hyperlipidemia. Studies confirmed that STR/ort mice have same symptoms as human hyperlipidemia patients, such as high serum total cholesterol, high serum triglycerides, hyperinsulinemia, and insulin resistance. It is a good model for studying abnormal lipid metabolism and OA.

*3.1.3. Genetic Factor.* With the rapid development of transgenic technology, transgenic animal models provide new options for osteoarthritis research. Animal studies have found that in the process of OA, knockouting apoptosis-related genes will ultimately lead to the occurrence of OA. However, conventional gene knockout methods can easily cause embryonic death or severe bone deformation. In order to overcome this defect, conditionally inducible gene knockout technology is widely used, such as Bgn-Fbn double gene knockout mice [100, 101]. Biglycan and fibromodulin are two small molecular proteoglycans coexpressed in tissues such as tendon, cartilage, and bone. The double gene knockout mice can present heterotopic ossification and OA lesions similar to STR/ort mice. The genetically modified mice lack the expression of bone morphogenetic protein (BMP) receptor protein specifically in joints, resulting in the occurrence of multijoint OA lesions at an early stage. Genetically modified mouse OA models usually include mice lacking expression of type II collagen, mice lacking expression of type IX collagen, MMP13 transgenic mice, and aggrecan knockout mice [102–104].

Animal models of spontaneous OA formation have similar pathogenic characteristics to human OA: the initial stage and the progression of the disease are more moderate, which is better than operation animal models. It is worth noting that due to the slow development of the disease, the early diagnosis of OA is difficult, and researchers need to pay attention to the pathological changes.

### 3.2. Induced Models (Surgery or Injection)

*3.2.1. Surgical Induction Models.* The biomechanical changes of weight-bearing joints caused by instability are an important reason for OA, which can lead to the degeneration of articular cartilage cells, degrading the extracellular matrix. Surgery or man-made trauma causes the joints to lose stability and the stress changes on the joint contact surface, inducing the occurrence of OA. This modeling method usually shows the formation process of OA after trauma.

*(1) Anterior Cruciate Ligament Transection (ALCT).* This is the most commonly used method for establishing OA models in recent years. After the anterior cruciate ligament

is cut, the number of cartilage cells in the superficial zone decreases, swells, and becomes fibrotic [105, 106]. The degradation products of denatured type II collagen are significantly increased in the fibrotic area. It was reported that after cutting the anterior cruciate ligament of the canine knee joint, the synovial membrane of the canine joint was thickened, the cartilage surface was eroded and osteophytes formed [107]. This phenomenon is the same as the pathological changes of natural joint instability caused by the rupture of the anterior cruciate ligament. This kind of model is simple to operate with less traumatic. It can fully reflect the pathological process of cartilage degeneration. However, this method takes a long time to successfully model—at least 6 weeks. Some researchers fix the contralateral limb after the rabbit anterior cruciate ligament is removed, so that the surgical limb is overloaded, and the time to make the OA model is shorter [108].

*(2) Meniscal Destabilization*. The researchers removed part of the meniscus of the rabbit knee joint, causing the instability of the joint. The meniscus resection alone can reduce the damage caused by the operation, but the modeling time is correspondingly prolonged. 12 weeks after removal of the lateral meniscus of the miniature pig's knees, the number of chondrocytes and the proteoglycan content decreased, the number of cells arranged in clusters increased, the thickness of cartilage became thinner, the surface of cartilage became fibrotic, and the femoral intercondylar notch osteophytes formed [109, 110].

*(3) Hulth Model*. Under sterile conditions, a longitudinal cut is made on the inside of the knee joint, the cruciate ligament and medial collateral ligament are cut off, and the medial meniscus is completely resected without damaging the articular cartilage surface. After the operation, the injured limb was not fixed and moved freely. After experimental animals underwent the Hulth method surgery, due to joint instability, increased friction on the articular surface, and the lack of cushioning effect of the meniscus, osteoarthritis can easily occur [111].

*(4) Models for Generating Focal Defects*. In the OA model obtained through intra-articular surgery, joint instability is a factor that promotes the progress of OA. At the same time, in this type of OA model, the presence of synovial inflammation leads to joint degeneration, which will affect the therapeutic effect of treatment measures for cartilage protection and repair. An articular focal defect is a good model for observing the pathology development. Researchers used sharp tools to scratch the articular cartilage in the weight-bearing area of the joint, but they did not damage the subchondral bone. This method would lead to pathological changes in the bone and joint. The joint focal defect method is an ideal model for observing the early manifestations and treatment effects of OA. It is particularly sensitive in observing the therapeutic effects of cartilage protection and repair [112, 113].

*3.2.2. Intra-Articular Injection.* Toxic or inflammatory compounds were injected directly into the joint cavity of the knee joint to induce disease by destroying the extracellular matrix or articular cartilage cells. This method is simple to operate, reproducible, and has a short cycle. It is suitable for OA pathology and antiosteoarthritis drug research. Commonly used injections to induce osteoarthritis include papain, collagenase, and monosodium iodoacetate. Researchers have found that collagenase can cause cartilage destruction and joint tissue inflammation in rabbit knee joints in the early stage and articular cartilage degradation in the late stage [114]. The glycolysis inhibitor monosodium iodoacetate (MIA) was injected into the knee joints of Wistar rats. Within 1 week, chondrocytes became degenerated and necrotic, and full-thickness changes of cartilage could also appear in the tibia and femoral condyles. MIA injection-induced osteoarthritis is currently the most commonly used pharmaceutical preparation [115]. Vitamin A, hyaluronidase, cartilage fragments or foreign bodies, adrenal cortex hormones, etc. injected into the joint cavity of animals can also cause articular cartilage degeneration and form an OA model [116, 117].

*3.2.3. Joint Brake Modeling Method.* The composition, structure, and function of articular cartilage can be maintained only by ensuring the normal movement and function of the joints. Fixing limbs to break the joints can induce articular cartilage atrophy, resulting in cartilage thinning, edema, and decreased proteoglycan content [118]. Because these cartilage changes are similar to the pathological changes of human OA, this model is especially used for the study of cartilage degeneration. However, the use of this model has gradually decreased in the research on the differences in the basic morphology of cartilage. In the cartilage of OA, chondrocytes proliferate focally in cell clusters or cell nests, which are usually active at the later stage of OA. In the fixed-joint model, chondrocytes have no such changes. However, cell clusters often become necrotic, especially when the splint is firmly fixed without any movement. This change in cartilage may be caused by the lack of nutrients in cartilage cells. Moreover, if the immobilized limbs are allowed to move in a small range, the range of cartilage degeneration will be significantly reduced [119, 120]. In Table 2, we compare the characteristics of several osteoarthritis models.

## 4. Classification of Nanoparticle-Based Drug Delivery System

Nanomaterials have a close relationship with biological bodies in terms of size. For example, the ribonucleic acid protein complex, one of the elements of life, has a linearity between 15 and 20 nm. Nanobiomedical materials are the intersection of nanomaterials and biomedical materials. Nanoparticles and other materials are combined to make various composite materials. With the further deepening of research, nanomaterials have begun to penetrate into many disciplines, showing great potential application value. In recent years, the exuberant development of nanotechnology in drug delivery systems has spawned new methods for treating OA. This section describes the current development and new applications of NP-based drug delivery for the treatment of OA,

Table 2: Classification and characteristics of osteoarthritis animal models.

| | Spontaneous models | Surgical induction models | Intra-articular injection models |
|---|---|---|---|
| Principle of the experiment | The cause of OA is related to certain genetic mutations<br>OA spontaneously occurs with age<br>Genetically modified animals constructed using transgenic or gene knockout technologies can also spontaneously form OA | Using surgery to cause disease in the joint cavity to produce OA | Injecting toxic or inflammatory compounds directly into the joint cavity of the joint to induce disease by destroying extracellular matrix or articular cartilage cells |
| Types of commonly used models | Male Hartly guinea pig, STR/ort mice, Bgn-Fbn double gene knockout mice, Cre-Gdf5/Bmpr1a floxP mice | The Hulth method, anterior cruciate ligament transection (ACLT), partial or full meniscus resection, medial meniscus tear, joint mark method | Types of drugs: chemicals, enzymes, and hormones<br>Common injection drugs: MIA, collagenase, papain, etc. |
| Advantage | Animal models of spontaneous OA have similar pathogenic characteristics to humans | Using aseptic technique to induce, the results are highly reproducible and the modeling experiments are shorter | (1) The molding speed is fast<br>(2) The pathological changes of cartilage in the end-stage OA can be observed in a short time<br>(3) Less traumatic and easy to operate |
| Disadvantage | Early diagnosis of OA is difficult. The research time is long. The model may be restricted by environmental factors, ethical conditions, and high economic cost | (1) The trauma is large, and postoperative infection is prone to occur<br>(2) Traumatic arthritis and synovial inflammation may occur during the operation, which may affect the experimental results | It is difficult to have a certain standard for drug dosage. Different animals have different doses of drugs injected. Therefore, a poor grasp of the drug dosage will cause errors in experiments |

including liposomes, micelles, polymeric nanoparticles, exosomes, and inorganic nanoparticles [121].

*4.1. Exosome.* Exosomes are membrane vesicles with a diameter from 30 to 150 nm, reflecting complex molecular processes that occur in parent cells. Exosomes, as endogenous drugs, have diagnostic, drug delivery, and targeted therapy capabilities by transporting nucleic acids (DNA, mRNA, microRNA, and lncRNA), biologically active lipids, and proteins [122]. Exosomes do not require the same harsh storage conditions as seed cells, but can perform functions similar to seed cells. Therefore, it is more suitable for treatment and delivering active substances [123, 124].

Exosomes used to treat OA are principally derived from MSCs. Recent studies have shown that exosomal miRNA and lncRNA play a key role in anti-OA. It remains a major challenge to deliver a drug through the dense cartilage matrix. Liang et al. use lysosomal-membrane glycoprotein to fuse chondrocyte active peptide (CAP) on the surface of chondrocyte-derived exosomes. In vivo studies have shown that the delivery of miR-140 based on CAP exosomes significantly reduces the development of OA in a rat model by IA injection [37]. Several recent studies have shown that miRNA may participate in the regulation of several signals such as the SIRT1/p53 pathway, the Wnt/-catenin pathway, and the NF-$\kappa$B pathway, thereby regulating the expression of genes involved in the decomposition and anabolism of OA. By delivering miRNA, exosomes can inhibit the production of proteolytic enzymes and proinflammatory cytokines (e.g., IL-1, IL-6, and TNF-$\alpha$) to affect the treatment of OA [125, 126].

Natural exosomes have their own therapeutic agents and can be used for drug delivery. However, the number of exosomes released by cells is uncertain due to the lack of clinical research. Obtaining a sufficient number of exosomes for in vivo research is a technical challenge. In order to increase the production of exosomes, some studies are exploring the use of three-dimensional spheres or tetrahedrons to transport therapeutic substances. With the elucidation of exosomal mechanism and the maturity of exosomal manufacturing technology, it will create a new field of OA treatment [127].

*4.2. Liposome.* The liposome is an artificial membrane. When the hydrophilic head of the phospholipid molecule is inserted into the water, the hydrophobic tail of the liposome extends to the air. After agitation, a spherical liposome with a double layer of lipid molecules is formed, with a diameter ranging from 25 to 1000 nm [13]. Liposomes can be used for genetically modified or prepared medicines. The liposomes can fuse with the cell membrane to deliver the medicines into the cell. Liposomes are the first nanodrug carrier approved by the FDA, deemed to be the most ideal drug delivery vehicle. Liposome formulations have been extensively tested as drug delivery vehicles in OA, not only because of their ability to carry hydrophobic and hydrophilic drugs but also because of their excellent biocompatibility.

Adenosine is a key autocrine cytokine for maintaining cartilage homeostasis. The A2A receptor is a kind of receptor for adenosine. Researchers encapsulated adenosine and A2A receptor agonists in liposomes, and then they injected the liposomes to prevent the OA progression of obesity-

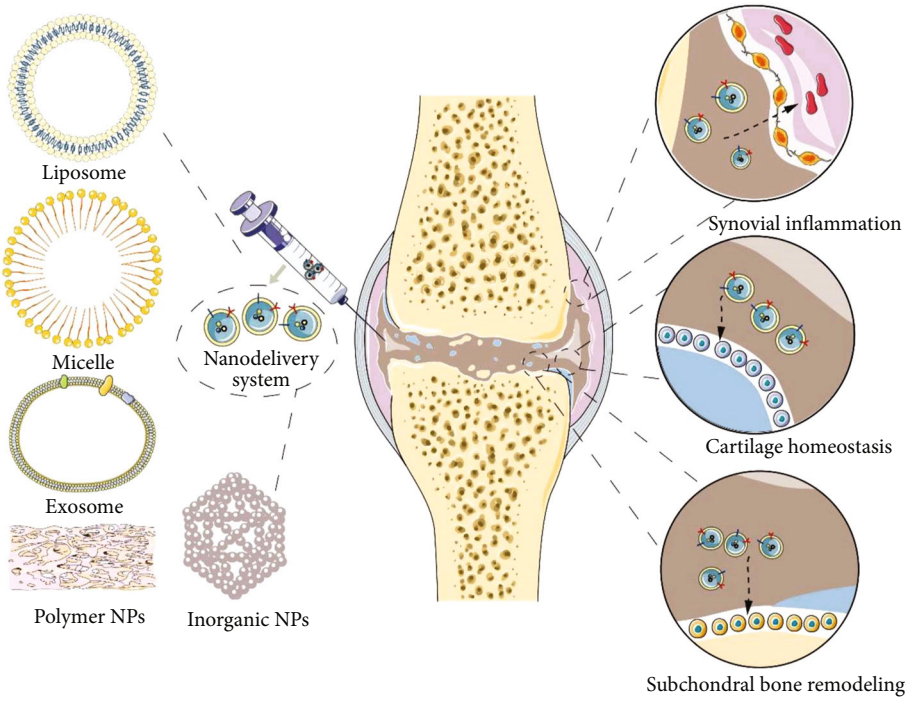


Figure 3: Classification and function of a nanoparticle-based drug delivery system.

induced mouse and rat posttraumatic OA [128]. Recent studies have shown that rapamycin encapsulated in liposomes has a notable anti-inflammatory effect in the spontaneous OA model [129].

*4.3. Micelle.* Micelle refers to the orderly aggregates of molecules that begin to form in large quantities after the surfactant concentration in an aqueous solution reaches the critical micelle concentration (CMC). In micelles, the hydrophobic groups of surfactant molecules aggregate to form the inner core of the micelle, and the hydrophilic polar groups form the outer layer of the micelle. Micelles can also be taken up by cells by binding to ligands, antibodies, or peptides. Because of its low CMC, polymer micelles have a longer cycle time and are more stable, so they are the most widely used in drug delivery systems [130, 131].

A study has reported that overexpression of the SOX9 transcription factor by using polymer micelles as a carrier can readjust the metabolic balance in OA. In the presence of inflammatory factors IL-1$\beta$ and TNF-$\alpha$, micellar-guided rAAV-sox9 increases the level of extracellular cartilage matrix (ECM) deposition and chondrocyte survival [15].

*4.4. Inorganic Nanoparticles.* Inorganic nanoparticles (INPs) are synthesized from inorganic particles and biodegradable polycations. Typical inorganic nanoparticles include metal, metal oxides, and carbon materials (such as fullerenes, nanotubes, and fibers) and magnetic nanoparticles composed of superparamagnetic iron oxide nanoparticles (SPION). The more commonly used is mesoporous silica nanoparticles (MSN), which have the characteristics of uniform pores, easy functionalization, biocompatibility, high specific surface area, large pore volume, and biodegradability. In order to improve the gene loading efficiency and cell absorption efficiency of MSN, its surface or inner pore will be coated with a cationic polymer [132, 133].

The researchers prepared mesoporous silica nanoparticles (MSN) and used them as an encapsulant for colchicine. The free colchicine or encapsulated drug is then embedded in the self-healing hydrogel. Treatment studies of this drug delivery in a rat osteoarthritis model induced by monoiodoacetic acid (MIA) have shown that nanoparticle/hydrogel patches have an effective and safe therapeutic potential for OA [21]. Oxidative stress is caused by the accumulation of reactive oxygen and nitrogen substances (ROS and RNS) in the cell microenvironment. These ROS and RNS can destroy the cell structure, leading to cell apoptosis and senescence. Researchers use the layer-by-layer (LbL) method to manufacture polymer microcapsules that encapsulate manganese dioxide nanoparticles to exert antioxidant effects [36].

*4.5. Polymer Nanoparticles.* Cationic polymers have become another major type of nonviral gene delivery vehicle due to their ease of synthesis and flexibility. For example, synthetic or natural siRNA nanopolymers are colloidal solid materials that are specifically designed to degrade in the body without producing toxic components. Polymers can be combined with nucleic acids to form multimeric complexes at physiological pH to facilitate gene delivery. Generally, polymer nanoparticles have positively charged units to promote electrostatic binding with nucleic acids [134]. However, by using a degradable linker (such as a disulfide bond or a sulfhydryl-maleimide bond), the covalent linkage of the nucleic acid and the polymer can also be achieved. Representatives in this category are synthetic polymers, such as poly-L-lysine, poly-L-ornithine, linear and branched polyethyleneimine (PEI),

Table 3: Classification and characteristics of nanoparticle-based drug delivery system.

| Nanocarriers | Classification | Advantage | Disadvantage |
|---|---|---|---|
| Lipid based | Liposome | Operability, stability, low toxicity. Embedding lipophilic and hydrophilic drug | Drug leakage, easily degraded |
| | Micelle | Improving the solubility of lipophilic drugs, operability, releasing the drug in a controlled manner | Nonencapsulated hydrophilic drugs, CMC dependency, toxicity |
| PNP | PLA, PLGA, PCL, chitosan, alginate, gelatin, albumin | Combining hydrophilic and hydrophobic drugs, stability, sustained release | Poor drug loading, toxicity |
| Exosome | | Natural source, biocompatibility, targeting | Low yield, uncertain dose |
| Inorganic NP | $CeO_2$, $MnO_2$, Pt | Simple to prepare | Toxicity, poor targeting ability |

diethylaminoethyl-dextran, polyamide-amine dendrimer (PAMAM), and polydimethylaminoethyl methacrylate (PDMAEMA). In addition, natural polymers, such as chitosan (CS), dextran and gelatin, and complex synthetic substances are currently under study [135, 136].

Studies have reported that polylactic-*co*-glycolic acid (PLGA), loaded with p66shc-siRNA, was injected into the knee joint of rats to inhibit the expression of p66shc and relief the pain, cartilage damage, and inflammatory cytokine production induced by sodium iodoacetate (MIA) [33]. Researchers designed the nanocomposite 4-arm-poly(ethylene glycol)-maleimide (PEG-4 MAL) microgels. This kind of gel presents the effect of joint tuberculosis peptide and overcomes the adverse effects caused by the gel after rapid clearance. The gel can stay in the joint space for at least 3 weeks without causing any joint-degenerative changes [26]. In Figure 3, we show the classification and functions of five NP-based drug delivery systems.

## 5. Conclusion and Prospects

Although the NP-based drug delivery system shows significant targeting ability in OA treatment, there are still some shortcomings in clinical application. We have listed the characteristics of different NP-based drug delivery systems in Table 3. PNP particles, such as PLGA, have been wildly used because of the diverse forms. However, due to immune rejection, it may cause a new inflammatory response in vivo. Polymer nanoparticles modified by HA, chitosan, or other materials are a new direction to improve the biocompatibility of nanomaterials [137]. On the contrary, as an endogenous substance, exosomes have good biocompatibility, but the purification methods and the extremely low yield hinder its further development. Significantly improving the yield of exosomes is an important direction for future exosome research [123]. Although liposome-based drug delivery systems have been extensively studied, they are not the best choice for hydrophilic drugs. For inorganic nanoparticles, the extremely low targeting and instability limit their further applications.

Current clinical treatments for OA are only to delay the symptom of the disease, relieve pain, and improve motor function [7]. There is still a major challenge in nanoparticle-based drug delivery systems for OA treatment. In addition to the common problems of treatment drugs in the body (immune response, ethical challenges, and biocompatibility issues), there is a fact that needs to be overcome: "resident chondrocytes cannot secrete matrix with the same characteristics as those formed during development [138]." The ultimate goal of NP-based drug delivery systems is the complete regeneration of the limbs, which requires "forming multiple types of tissues at the same time and assembling these into complex organ systems." As explained in this review, NP-based drug delivery systems are promising for the treatment of OA [139].

Although this article outlines the developments of NP-based drug delivery systems, there are still many challenges ahead: (1) Various nanomaterials need to be combined to produce an effective therapeutic delivery system. For example, the use of nanoscaffold materials loaded with cytokines can induce chondrocyte production while restoring cartilage defects. (2) Nanomaterials can be studied to deliver drugs to other joint tissues, including fat pads, ligaments, and meniscus, all of which contribute to the research of OA treatment. (3) NP-based drug delivery systems can be engineered by modifying liposome membranes to improve the targeting ability. NP-based drug delivery systems are one of the most promising methods in the field of tissue and organ repair. By improving new strategies and technologies, regenerative tissue engineering will eventually be able to deal with more complex tissue systems, organs, and limbs. The drug delivery system based on NPs may continue to push us to adopt a comprehensive treatment strategy and contribute to the treatment of OA.

## Conflicts of Interest

The authors declare that there are no conflicts of interest regarding the publication of this paper.

## Acknowledgments

This study was supported by the National Natural Science Foundation of China (No. 81970980), the Liaoning Provincial Key Research Plan Guidance Project (No. 2018225078), the Liaoning Provincial Natural Science Foundation Guidance Project (No. 2019-ZD-0749), the Shenyang Major Scientific and Technological Innovation Research and Development

Plan (No. 19-112-4-027), and the Shenyang Young and Middle-Aged Technological Innovation Talent Plan (No. RC200060).

## References


[1] T. Takeuchi, H. Yoshida, and S. Tanaka, "Role of interleukin-6 in bone destruction and bone repair in rheumatoid arthritis," *Autoimmunity Reviews*, vol. 20, no. 9, article 102884, 2021.

[2] A. Kiadaliri and M. Englund, "Variability in end-of-life healthcare use in patients with osteoarthritis: a population-based matched cohort study," *Osteoarthritis and Cartilage*, vol. 29, no. 10, pp. 1418–1425, 2021.

[3] B. Karaismailoglu, "High-intensity strength training, knee pain, and knee joint compressive forces in adults with knee osteoarthritis," *JAMA*, vol. 325, no. 22, pp. 2315-2316, 2021.

[4] W. Lin and J. Klein, "Recent progress in cartilage lubrication," *Advanced Materials*, vol. 33, no. 18, article 2005513, 2021.

[5] H. Binder, L. Hoffman, L. Zak, T. Tiefenboeck, S. Aldrian, and C. Albrecht, "Clinical evaluation after matrix-associated autologous chondrocyte transplantation: a comparison of four different graft types," *Bone & Joint Research*, vol. 10, no. 7, pp. 370–379, 2021.

[6] W. Wang, Z. Wang, Y. Fu et al., "Improved osteogenic differentiation of human amniotic mesenchymal stem cells on gradient nanostructured Ti surface," *Journal of Biomedical Materials Research Part A*, vol. 108, no. 9, pp. 1824–1833, 2020.

[7] Y. Qian, W. Yuan, Y. Cheng, Y. Yang, X. Qu, and C. Fan, "Concentrically integrative bioassembly of a three-dimensional black phosphorus nanoscaffold for restoring neurogenesis, angiogenesis, and immune homeostasis," *Nano Letters*, vol. 19, no. 12, pp. 8990–9001, 2019.

[8] C. D. Bocsa, V. Moisoiu, A. Stefancu, L. F. Leopold, N. Leopold, and D. Fodor, "Knee osteoarthritis grading by resonant Raman and surface-enhanced Raman scattering (SERS) analysis of synovial fluid," *Nanomedicine*, vol. 20, article 102012, 2019.

[9] S. Khan, A. Dunphy, M. Anike et al., "Recent advances in carbon nanodots: a promising nanomaterial for biomedical applications," *International Journal of Molecular Sciences*, vol. 22, no. 13, p. 6786, 2021.

[10] G.-Z. Jin, "Current nanoparticle-based technologies for osteoarthritis therapy," *Nanomaterials*, vol. 10, no. 12, p. 2368, 2020.

[11] S. Brown, S. Kumar, and B. Sharma, "Intra-articular targeting of nanomaterials for the treatment of osteoarthritis," *Acta Biomaterialia*, vol. 93, pp. 239–257, 2019.

[12] M. C. Chang, P. F. Chiang, Y. J. Kuo, C. L. Peng, K. Y. Chen, and Y. C. Chiang, "Hyaluronan-loaded liposomal dexamethasone-diclofenac nanoparticles for local osteoarthritis treatment," *International Journal of Molecular Sciences*, vol. 22, no. 2, p. 665, 2021.

[13] Y. Zhao, H. Chen, L. Wang, Z. Guo, S. Liu, and S. Luo, "Cationic solid lipid nanoparticles loaded by integrin $\beta$1 plasmid DNA attenuates IL-1$\beta$-induced apoptosis of chondrocyte," *Aging*, vol. 12, no. 22, pp. 22527–22537, 2020.

[14] K. Zhang, J. Yang, Y. Sun et al., "Thermo-sensitive dual-functional nanospheres with enhanced lubrication and drug delivery for the treatment of osteoarthritis," *Chemistry*, vol. 26, no. 46, pp. 10564–10574, 2020.

[15] J. Urich, M. Cucchiarini, and A. Rey-Rico, "Therapeutic delivery of rAAV sox9 via polymeric micelles counteracts the effects of osteoarthritis-associated inflammatory cytokines in human articular chondrocytes," *Nanomaterials*, vol. 10, no. 6, p. 1238, 2020.

[16] C. Kang, E. Jung, H. Hyeon, S. Seon, and D. Lee, "Acid-activatable polymeric curcumin nanoparticles as therapeutic agents for osteoarthritis," *Nanomedicine*, vol. 23, article 102104, 2020.

[17] L. Chen, S. R. Tiwari, Y. Zhang, J. Zhang, and Y. Sun, "Facile synthesis of hollow $MnO_2$ Nanoparticles for reactive oxygen species scavenging in osteoarthritis," *ACS Biomaterials Science & Engineering*, vol. 7, no. 4, pp. 1686–1692, 2021.

[18] P. Famta, M. Famta, J. Kaur et al., "Protecting the normal physiological functions of articular and periarticular structures by aurum nanoparticle-based formulations: an up-to-date insight," *AAPS PharmSciTech*, vol. 21, no. 3, 2020.

[19] Y. W. Lin, C. H. Fang, F. Q. Meng, C. J. Ke, and F. H. Lin, "Hyaluronic acid loaded with cerium oxide nanoparticles as antioxidant in hydrogen peroxide induced chondrocytes injury: an in vitro osteoarthritis model," *Molecules*, vol. 25, no. 19, article 4407, 2020.

[20] L. Wan, X. Tan, T. Sun, Y. Sun, J. Luo, and H. Zhang, "Lubrication and drug release behaviors of mesoporous silica nanoparticles grafted with sulfobetaine-based zwitterionic polymer," *Materials Science & Engineering C, Materials for Biological Applications*, vol. 112, article 110886, 2020.

[21] A. L. Mohamed, H. Elmotasem, and A. A. A. Salama, "Colchicine mesoporous silica nanoparticles/hydrogel composite loaded cotton patches as a new encapsulator system for transdermal osteoarthritis management," *International Journal of Biological Macromolecules*, vol. 164, pp. 1149–1163, 2020.

[22] F. Zhou, J. Mei, S. Yang et al., "Modified ZIF-8 nanoparticles attenuate osteoarthritis by reprogramming the metabolic pathway of synovial macrophages," *ACS Applied Materials & Interfaces*, vol. 12, no. 2, pp. 2009–2022, 2020.

[23] X. Zhang, J. Chen, Q. Jiang et al., "Highly biosafe biomimetic stem cell membrane-disguised nanovehicles for cartilage regeneration," *Journal of Materials Chemistry B*, vol. 8, no. 38, pp. 8884–8893, 2020.

[24] W. Zhao, H. Wang, H. Wang et al., "Light-responsive dual-functional biodegradable mesoporous silica nanoparticles with drug delivery and lubrication enhancement for the treatment of osteoarthritis," *Nanoscale*, vol. 13, no. 13, pp. 6394–6399, 2021.

[25] L. Zerrillo, K. Gupta, F. Lefeber et al., "Novel fluorinated poly(lactic-*co*-glycolic acid) (PLGA) and polyethylene glycol (PEG) nanoparticles for monitoring and imaging in osteoarthritis," *Pharmaceutics*, vol. 13, no. 2, p. 235, 2021.

[26] L. M. Mancipe Castro, A. Sequeira, A. J. García, and R. E. Guldberg, "Articular cartilage- and synoviocyte-binding poly(ethylene glycol) nanocomposite microgels as intra-articular drug delivery vehicles for the treatment of osteoarthritis," *ACS Biomaterials Science & Engineering*, vol. 6, no. 9, pp. 5084–5095, 2020.

[27] B. Almeida, Y. Wang, and A. Shukla, "Effects of nanoparticle properties on kartogenin delivery and interactions with mesenchymal stem cells," *Annals of Biomedical Engineering*, vol. 48, no. 7, pp. 2090–2102, 2020.

[28] Q. Tang, T. Lim, L. Y. Shen et al., "Well-dispersed platelet lysate entrapped nanoparticles incorporate with injectable PDLLA-PEG-PDLLA triblock for preferable cartilage engineering application," *Biomaterials*, vol. 268, article 120605, 2021.

[29] Y. Song, T. Zhang, H. Cheng et al., "Imidazolium-based ionic liquid-assisted preparation of nano-spheres loaded with bioactive peptides to decrease inflammation in an osteoarthritis Model:Ex VivoEvaluations," *Journal of Biomedical Nanotechnology*, vol. 17, no. 5, pp. 859–872, 2021.

[30] T. Li, J. Yang, C. Weng et al., "Intra-articular injection of anti-inflammatory peptide-loaded glycol chitosan/fucoidan nanogels to inhibit inflammation and attenuate osteoarthritis progression," *International Journal of Biological Macromolecules*, vol. 170, pp. 469–478, 2021.

[31] A. R. Martin, J. M. Patel, R. C. Locke et al., "Nanofibrous hyaluronic acid scaffolds delivering TGF-$\beta$3 and SDF-1$\alpha$ for articular cartilage repair in a large animal model," *Acta Biomaterialia*, vol. 126, pp. 170–182, 2021.

[32] T. Kulsirirat, K. Sathirakul, N. Kamei, and M. Takeda-Morishita, "The *in vitro* and *in vivo* study of novel formulation of andrographolide PLGA nanoparticle embedded into gelatin-based hydrogel to prolong delivery and extend residence time in joint," *International Journal of Pharmaceutics*, vol. 602, article 120618, 2021.

[33] H. J. Shin, H. Park, N. Shin et al., "p66shc siRNA nanoparticles ameliorate chondrocytic mitochondrial dysfunction in osteoarthritis," *International Journal of Nanomedicine*, vol. 15, pp. 2379–2390, 2020.

[34] J. H. Jung, S. E. Kim, H. J. Kim, K. Park, G. G. Song, and S. J. Choi, "A comparative pilot study of oral diacerein and locally treated diacerein- loaded nanoparticles in a model of osteoarthritis," *International Journal of Pharmaceutics*, vol. 581, article 119249, 2020.

[35] R. Wu, G. Gao, and Y. Xu, "Electrospun fibers immobilized with BMP-2 mediated by polydopamine combined with autogenous tendon to repair developmental dysplasia of the hip in a porcine model," *International Journal of Nanomedicine*, vol. 15, pp. 6563–6577, 2020.

[36] E. Marin, C. Tapeinos, S. Lauciello, G. Ciofani, J. R. Sarasua, and A. Larrañaga, "Encapsulation of manganese dioxide nanoparticles into layer-by-layer polymer capsules for the fabrication of antioxidant microreactors," *Materials Science & Engineering C, Materials for Biological Applications*, vol. 117, article 111349, 2020.

[37] Y. Liang, X. Xu, X. Li et al., "Chondrocyte-targeted microRNA delivery by engineered exosomes toward a cell-free osteoarthritis therapy," *ACS Applied Materials & Interfaces*, vol. 12, no. 33, pp. 36938–36947, 2020.

[38] Z. Jin, J. Ren, and S. Qi, "Exosomal miR-9-5p secreted by bone marrow-derived mesenchymal stem cells alleviates osteoarthritis by inhibiting syndecan-1," *Cell and Tissue Research*, vol. 381, no. 1, pp. 99–114, 2020.

[39] J. Wu, L. Kuang, C. Chen et al., "miR-100-5p-abundant exosomes derived from infrapatellar fat pad MSCs protect articular cartilage and ameliorate gait abnormalities via inhibition of mTOR in osteoarthritis," *Biomaterials*, vol. 206, pp. 87–100, 2019.

[40] S. Tao, T. Yuan, Y. Zhang, W. Yin, S. Guo, and C. Zhang, "Exosomes derived from miR-140-5p-overexpressing human synovial mesenchymal stem cells enhance cartilage tissue regeneration and prevent osteoarthritis of the knee in a rat model," *Theranostics*, vol. 7, no. 1, pp. 180–195, 2017.

[41] Y. Liu, R. Zou, Z. Wang, C. Wen, F. Zhang, and F. Lin, "Exosomal KLF3-AS1 from hMSCs promoted cartilage repair and chondrocyte proliferation in osteoarthritis," *The Biochemical Journal*, vol. 475, no. 22, pp. 3629–3638, 2018.

[42] R. Zhao, Z. Dong, X. Wei et al., "Inflammatory factors are crucial for the pathogenesis of post-traumatic osteoarthritis confirmed by a novel porcine model: "Idealized" anterior cruciate ligament reconstruction and gait analysis," *International Immunopharmacology*, vol. 99, article 107905, 2021.

[43] Y. Kharaz, H. Birch, A. Chester et al., "The effect of exercise on the protein profile of rat knee joint intra- and extra-articular ligaments," *Scandinavian Journal of Medicine & Science in Sports*, 2021.

[44] J. Soul, M. Barter, C. Little, and D. Young, "OATargets: a knowledge base of genes associated with osteoarthritis joint damage in animals," *Annals of the Rheumatic Diseases*, vol. 80, no. 3, pp. 376–383, 2021.

[45] R. Tang, N. Harasymowicz, C. Wu et al., "Gene therapy for follistatin mitigates systemic metabolic inflammation and post-traumatic arthritis in high-fat diet-induced obesity," *Science Advances*, vol. 6, no. 19, p. eaaz7492, 2020.

[46] J. Whittaker and E. Roos, "Infographic. Risk profile for sport-related post-traumatic knee osteoarthritis," *British Journal of Sports Medicine*, vol. 54, no. 6, pp. 362-363, 2020.

[47] B. Tayfur, C. Charuphongsa, D. Morrissey, and S. Miller, "Neuromuscular function of the knee joint following knee injuries: does it ever get back to normal? A systematic review with meta-analyses," *Sports Medicine*, vol. 51, no. 2, pp. 321–338, 2021.

[48] T. Blackburn, D. Padua, B. Pietrosimone et al., "Vibration improves gait biomechanics linked to posttraumatic knee osteoarthritis following anterior cruciate ligament injury," *Journal of Orthopaedic Research*, vol. 39, no. 5, pp. 1113–1122, 2021.

[49] T. Pham, J. Erichsen, J. Kowal, S. Overgaard, and H. Schmal, "Elevation of pro-inflammatory cytokine levels following intra-articular fractures—a systematic review," *Cells*, vol. 10, no. 4, p. 902, 2021.

[50] N. Hirose, Y. Okamoto, M. Yanoshita et al., "Protective effects of cilengitide on inflammation in chondrocytes under excessive mechanical stress," *Cell Biology International*, vol. 44, no. 4, pp. 966–974, 2020.

[51] Z. du, X. Feng, G. Cao et al., "The effect of carbon nanotubes on osteogenic functions of adipose-derived mesenchymal stem cells *in vitro* and bone formation *in vivo* compared with that of nano-hydroxyapatite and the possible mechanism," *Bioactive Materials*, vol. 6, no. 2, pp. 333–345, 2021.

[52] H. Jin, S. Jiang, R. Wang, Y. Zhang, J. Dong, and Y. Li, "Mechanistic insight into the roles of integrins in osteoarthritis," *Frontiers in Cell and Developmental Biology*, vol. 9, article 693484, 2021.

[53] H. Wang, M. Zhang, Y. Zhang et al., "The decreased expression of integrin $\alpha$v is involved in T-2 toxin-induced extracellular matrix degradation in chondrocytes," *Toxicon*, vol. 199, pp. 109–116, 2021.

[54] G. Zhen, Q. Guo, Y. Li et al., "Mechanical stress determines the configuration of TGF$\beta$ activation in articular cartilage," *Nature communications*, vol. 12, no. 1, p. 1706, 2021.

[55] L. Zhang, H. Peng, W. Zhang, Y. Li, L. Liu, and T. Leng, "Yeast cell wall particle mediated nanotube-RNA delivery system loaded with miR365 antagomir for post-traumatic osteoarthritis therapy via oral route," *Theranostics*, vol. 10, no. 19, pp. 8479–8493, 2020.

[56] J. von Heideken, S. Chowdhry, J. Borg, K. James, and M. Iversen, "Reporting of harm in randomized controlled trials of therapeutic exercise for knee osteoarthritis: a systematic review," *Physical Therapy*, 2021.

[57] D. Reece, T. Thote, A. Lin, N. Willett, and R. Guldberg, "Contrast enhanced $\mu$CT imaging of early articular changes in a pre-clinical model of osteoarthritis," *Osteoarthritis and Cartilage*, vol. 26, no. 1, pp. 118–127, 2018.

[58] S. Haysom, M. Vickers, L. Yu, C. Reynolds, E. Firth, and S. McGlashan, "Post-weaning high-fat diet results in growth cartilage lesions in young male rats," *PLoS One*, vol. 12, no. 11, article e0188411, 2017.

[59] Z. Tian, F. Zeng, C. Zhao, and S. Dong, "Angelicin alleviates post-trauma osteoarthritis progression by regulating macrophage polarization via STAT3 signaling pathway," *Frontiers in Pharmacology*, vol. 12, article 669213, 2021.

[60] C. Yu, H. Zang, C. Yang et al., "Study of chondroitin sulfate E oligosaccharide as a promising complement C5 inhibitor for osteoarthritis alleviation," *Materials Science & Engineering C, Materials for Biological Applications*, vol. 127, article 112234, 2021.

[61] D. Yi, H. Yu, K. Lu et al., "AMPK signaling in energy control, cartilage biology, and osteoarthritis," *Frontiers in Cell and Developmental Biology*, vol. 9, article 696602, 2021.

[62] H. Yu, Y. Liu, X. Yang et al., "Strontium ranelate promotes chondrogenesis through inhibition of the Wnt/$\beta$-catenin pathway," *Stem Cell Research & Therapy*, vol. 12, no. 1, p. 296, 2021.

[63] M. Abshirini, B. Ilesanmi-Oyelere, and M. Kruger, "Potential modulatory mechanisms of action by long-chain polyunsaturated fatty acids on bone cell and chondrocyte metabolism," *Progress in Lipid Research*, vol. 83, article 101113, 2021.

[64] Z. Yang, L. Feng, J. Huang et al., "Asiatic acid protects articular cartilage through promoting chondrogenesis and inhibiting inflammation and hypertrophy in osteoarthritis," *European Journal of Pharmacology*, vol. 907, article 174265, 2021.

[65] D. Wilkinson, A. Falconer, H. Wright et al., "Matrix metalloproteinase-13 is fully activated by neutrophil elastase and inactivates its serpin inhibitor, alpha-1 antitrypsin: implications for osteoarthritis," *The FEBS Journal*, 2021.

[66] G. M. Pontes-Quero, L. Benito-Garzón, J. Pérez Cano, M. R. Aguilar, and B. Vázquez-Lasa, "Modulation of inflammatory mediators by polymeric nanoparticles loaded with anti-inflammatory drugs," *Pharmaceutics*, vol. 13, no. 2, p. 290, 2021.

[67] M. Seward, L. Briggs, P. Bain, and A. Chen, "Preoperative nonsurgical weight loss interventions before total hip and knee arthroplasty: a systematic review," *The Journal of Arthroplasty*, 2021.

[68] H. Yarizadeh, L. Setayesh, N. Majidi et al., "Nutrient patterns and their relation to obesity and metabolic syndrome in Iranian overweight and obese adult women," *Eating and Weight Disorders*, 2021.

[69] J. Evans, S. Mouchti, A. Blom et al., "Obesity and revision surgery, mortality, and patient-reported outcomes after primary knee replacement surgery in the National Joint Registry: a UK cohort study," *PLoS Medicine*, vol. 18, no. 7, article e1003704, 2021.

[70] I. Szilagyi, J. Waarsing, D. Schiphof, J. van Meurs, and S. Bierma-Zeinstra, "Towards sex-specific osteoarthritis risk models: evaluation of risk factors for knee osteoarthritis in males and females," *Rheumatology*, 2021.

[71] L. Kuusalo, D. Felson, N. Wang et al., "Metabolic osteoarthritis - relation of diabetes and cardiovascular disease with knee osteoarthritis," *Osteoarthritis and Cartilage*, vol. 29, no. 2, pp. 230–234, 2021.

[72] K. Collins, D. Hart, R. Reimer, R. Seerattan, and W. Herzog, "Response to diet-induced obesity produces time-dependent induction and progression of metabolic osteoarthritis in rat knees," *Journal of Orthopaedic Research*, vol. 34, no. 6, pp. 1010–1018, 2016.

[73] E. Arslan, M. Sardan Ekiz, C. Eren Cimenci et al., "Protective therapeutic effects of peptide nanofiber and hyaluronic acid hybrid membrane in *in vivo* osteoarthritis model," *Acta Biomaterialia*, vol. 73, pp. 263–274, 2018.

[74] M. Thomas, T. Rathod-Mistry, E. Parry, C. Pope, T. Neogi, and G. Peat, "Triggers for acute flare in adults with, or at risk of, knee osteoarthritis: a web-based case-crossover study in community-dwelling adults," *Osteoarthritis and Cartilage*, vol. 29, no. 7, pp. 956–964, 2021.

[75] A. Mohamadi, K. Momenzadeh, A. Masoudi et al., "Evolution of knowledge on meniscal biomechanics: a 40 year perspective," *BMC Musculoskeletal Disorders*, vol. 22, no. 1, p. 625, 2021.

[76] S. Poudel, M. Dixit, G. Yildirim et al., "Sexual dimorphic impact of adult-onset somatopause on life span and age-induced osteoarthritis," *Aging Cell*, no. article e13427, 2021.

[77] C. Wang, B. Yu, Y. Fan et al., "Incorporation of multi-walled carbon nanotubes to PMMA bone cement improves cytocompatibility and osseointegration," *Materials Science & Engineering C, Materials for Biological Applications*, vol. 103, article 109823, 2019.

[78] B. Plotz, F. Bomfim, M. Sohail, and J. Samuels, "Current epidemiology and risk factors for the development of hand osteoarthritis," *Current Rheumatology Reports*, vol. 23, no. 8, p. 61, 2021.

[79] Y. Badshah, M. Shabbir, H. Hayat et al., "Genetic markers of osteoarthritis: early diagnosis in susceptible Pakistani population," *Journal of Orthopaedic surgery and Research*, vol. 16, no. 1, p. 124, 2021.

[80] A. Miranda-Duarte, "DNA methylation in osteoarthritis: current status and therapeutic implications," *The Open Rheumatology Journal*, vol. 12, no. 1, pp. 37–49, 2018.

[81] M. Rushton, L. Reynard, M. Barter et al., "Characterization of the cartilage DNA methylome in knee and hip osteoarthritis," *Arthritis & Rheumatology*, vol. 66, no. 9, pp. 2450–2460, 2014.

[82] F. Moazedi-Fuerst, M. Hofner, G. Gruber et al., "Epigenetic differences in human cartilage between mild and severe OA," *Journal of Orthopaedic Research*, vol. 32, no. 12, pp. 1636–1645, 2014.

[83] W. den Hollander, Y. Ramos, S. Bos et al., "Knee and hip articular cartilage have distinct epigenomic landscapes: implications for future cartilage regeneration approaches," *Annals of the Rheumatic Diseases*, vol. 73, no. 12, pp. 2208–2212, 2014.

[84] A. Michael and N. Thomä, "Reading the chromatinized genome," *Cell*, vol. 184, no. 14, pp. 3599–3611, 2021.

[85] Y. Ramos and I. Meulenbelt, "The role of epigenetics in osteoarthritis: current perspective," *Current Opinion in Rheumatology*, vol. 29, no. 1, pp. 119–129, 2017.

[86] R. Vicente, D. Noël, Y. Pers, F. Apparailly, and C. Jorgensen, "Deregulation and therapeutic potential of microRNAs in arthritic diseases," *Nature Reviews Rheumatology*, vol. 12, no. 4, pp. 211–220, 2016.

[87] G. Tardif, J. Pelletier, H. Fahmi et al., "NFAT3 and TGF-$\beta$/SMAD3 regulate the expression of miR-140 in osteoarthritis," *Arthritis Research & Therapy*, vol. 15, no. 6, p. R197, 2013.

[88] G. Mao, S. Hu, Z. Zhang et al., "Exosomal miR-95-5p regulates chondrogenesis and cartilage degradation via histone deacetylase 2/8," *Journal of Cellular and Molecular Medicine*, vol. 22, no. 11, pp. 5354–5366, 2018.

[89] Z. Li, Y. Wang, S. Xiang et al., "Chondrocytes-derived exosomal miR-8485 regulated the Wnt/$\beta$-catenin pathways to promote chondrogenic differentiation of BMSCs," *Biochemical and Biophysical Research Communications*, vol. 523, no. 2, pp. 506–513, 2020.

[90] M. Choi, J. Jo, M. Lee, J. Park, and Y. Park, "Intra-articular administration of cramp into mouse knee joint exacerbates experimental osteoarthritis progression," *International Journal of Molecular Sciences*, vol. 22, no. 7, p. 3429, 2021.

[91] W. Zeng, Y. Zhang, D. Wang et al., "Intra-articular injection of kartogenin-enhanced bone marrow-derived mesenchymal stem cells in the treatment of knee osteoarthritis in a rat model," *The American Journal of Sports Medicine*, vol. 49, no. 10, pp. 2795–2809, 2021.

[92] Y. Henrotin, S. Patrier, A. Pralus, M. Roche, and A. Nivoliez, "Protective actions of oral administration ofBifidobacterium longumCBi0703 in spontaneous osteoarthritis in dunkin hartley guinea pig model," *Cartilage*, 2019.

[93] A. Spittler, M. Afzali, S. Bork et al., "Age- and sex-associated differences in hematology and biochemistry parameters of Dunkin Hartley guinea pigs (*Cavia porcellus*)," *PLoS One*, vol. 16, no. 7, article e0253794, 2021.

[94] A. Spittler, M. Afzali, R. Martinez et al., "Evaluation of electroacupuncture for symptom modification in a rodent model of spontaneous osteoarthritis," *Acupuncture in Medicine*, 2021.

[95] C. Bartholdy, S. Nielsen, S. Warming, D. Hunter, R. Christensen, and M. Henriksen, "Poor replicability of recommended exercise interventions for knee osteoarthritis: a descriptive analysis of evidence informing current guidelines and recommendations," *Osteoarthritis and Cartilage*, vol. 27, no. 1, pp. 3–22, 2019.

[96] L. Ramos-Mucci, B. Javaheri, R. van 't Hof et al., "Meniscal and ligament modifications in spontaneous and post-traumatic mouse models of osteoarthritis," *Arthritis Research & Therapy*, vol. 22, no. 1, p. 171, 2020.

[97] S. Kyostio-Moore, B. Nambiar, E. Hutto et al., "STR/ort mice, a model for spontaneous osteoarthritis, exhibit elevated levels of both local and systemic inflammatory markers," *Comparative Medicine*, vol. 61, no. 4, pp. 346–355, 2011.

[98] D. Bradley, "The intriguing intersection of type 2 diabetes, obesity-related insulin resistance, and osteoarthritis," *The Journal of Clinical Endocrinology and Metabolism*, vol. 106, no. 5, pp. e2370–e2372, 2021.

[99] C. Louer, B. Furman, J. Huebner, V. Kraus, S. Olson, and F. Guilak, "Diet-induced obesity significantly increases the severity of posttraumatic arthritis in mice," *Arthritis and Rheumatism*, vol. 64, no. 10, pp. 3220–3230, 2012.

[100] L. van de Stadt, F. Kroon, F. Rosendaal et al., "Real-time-vsstatic scoring in musculoskeletal ultrasonography in patients with inflammatory hand osteoarthritis," *Rheumatology*, 2021.

[101] M. Kim, I. Koh, Y. Sung, D. Park, S. Yang, and Y. in, "Efficacy and safety of celecoxib combined with JOINS in the treatment of degenerative knee osteoarthritis: study protocol of a randomized controlled trial," *Therapeutic Advances in Musculoskeletal Disease*, vol. 13, 2021.

[102] C. Woo, H. Kim, G. Jung et al., "Small extracellular vesicles from human adipose-derived stem cells attenuate cartilage degeneration," *Journal of Extracellular Vesicles*, vol. 9, no. 1, article 1735249, 2020.

[103] Y. Ito, T. Matsuzaki, F. Ayabe et al., "Both microRNA-455-5p and -3p repress hypoxia-inducible factor-2$\alpha$ expression and coordinately regulate cartilage homeostasis," *Nature communications*, vol. 12, no. 1, article 4148, 2021.

[104] H. Ling, Q. Zeng, Q. Ge et al., "Osteoking decelerates cartilage degeneration in DMM-induced osteoarthritic mice model through TGF-$\beta$/smad-dependent manner," *Frontiers in Pharmacology*, vol. 12, article 678810, 2021.

[105] Z. Liu, H. Wang, S. Wang, J. Gao, and L. Niu, "PARP-1 inhibition attenuates the inflammatory response in the cartilage of a rat model of osteoarthritis," *Bone & Joint Research*, vol. 10, no. 7, pp. 401–410, 2021.

[106] J. Qian, Q. Xu, W. Xu, R. Cai, and G. Huang, "Expression of VEGF-A signaling pathway in cartilage of ACLT-induced osteoarthritis mouse model," *Journal of Orthopaedic Surgery and Research*, vol. 16, no. 1, p. 379, 2021.

[107] M. Teunissen, A. Miranda Bedate, K. Coeleveld et al., "Enhanced extracellular matrix breakdown characterizes the early distraction phase of canine knee joint distraction," *Cartilage*, 2021.

[108] S. Kamekura, K. Hoshi, T. Shimoaka et al., "Osteoarthritis development in novel experimental mouse models induced by knee joint instability," *Osteoarthritis and Cartilage*, vol. 13, no. 7, pp. 632–641, 2005.

[109] T. Ernest and P. Kondrashov, "The role of excessive body weight and meniscal instability in the progression of osteoarthritis in a rat model," *The Knee*, vol. 25, no. 6, pp. 1151–1156, 2018.

[110] K. Waller, K. Chin, G. Jay et al., "Intra-articular recombinant human proteoglycan 4 mitigates cartilage damage after destabilization of the medial meniscus in the Yucatan minipig," *The American Journal of Sports Medicine*, vol. 45, no. 7, pp. 1512–1521, 2017.

[111] F. Liu, H. Yang, D. Li, X. Wu, and Q. Han, "Punicalagin attenuates osteoarthritis progression via regulating Foxo1/Prg4/HIF3$\alpha$ axis," *Bone*, vol. 152, article 116070, 2021.

[112] G. Pattappa, J. Krueckel, R. Schewior et al., "Physioxia expanded bone marrow derived mesenchymal stem cells have improved cartilage repair in an early osteoarthritic focal defect model," *Biology*, vol. 9, no. 8, p. 230, 2020.

[113] R. Stefani, A. Lee, A. Tan et al., "Sustained low-dose dexamethasone delivery via a PLGA microsphere-embedded agarose implant for enhanced osteochondral repair," *Acta Biomaterialia*, vol. 102, pp. 326–340, 2020.

[114] J. Xu, L. Yan, B. Yan, L. Zhou, P. Tong, and L. Shan, "Osteoarthritis pain model induced by intra-articular injection of mono-iodoacetate in rats," *Journal of Visualized Experiments*, no. 159, 2020.

[115] T. Pitcher, J. Sousa-Valente, and M. Malcangio, "The monoiodoacetate model of osteoarthritis pain in the mouse," *Journal of Visualized Experiments*, no. 111, 2016.

[116] D. Apostu, O. Lucaciu, A. Mester et al., "Systemic drugs with impact on osteoarthritis," *Drug Metabolism Reviews*, vol. 51, no. 4, pp. 498–523, 2019.

[117] M. F. Hsueh, P. Önnerfjord, and V. B. Kraus, "Biomarkers and proteomic analysis of osteoarthritis," *Matrix Biology*, vol. 39, pp. 56–66, 2014.

[118] X. Ouyang, J. Wang, S. D. Hong et al., "Establishment of a rat model for osteoarthritis resulting from anterior cruciate ligament rupture and its significance," *Experimental and Therapeutic Medicine*, vol. 10, no. 6, pp. 2035–2038, 2015.

[119] R. Beraud, M. Moreau, and B. Lussier, "Effect of exercise on kinetic gait analysis of dogs afflicted by osteoarthritis," *Veterinary and Comparative Orthopaedics and Traumatology*, vol. 23, no. 2, pp. 87–92, 2010.

[120] N. P. Fey, G. K. Klute, and R. R. Neptune, "Optimization of prosthetic foot stiffness to reduce metabolic cost and intact knee loading during below-knee amputee walking: a theoretical study," *Journal of Biomechanical Engineering*, vol. 134, no. 11, article 111005, 2012.

[121] L. Wang, C. Wang, S. Wu, Y. Fan, and X. Li, "Influence of the mechanical properties of biomaterials on degradability, cell behaviors and signaling pathways: current progress and challenges," *Biomaterials Science*, vol. 8, no. 10, pp. 2714–2733, 2020.

[122] P. H. L. Tran, D. Xiang, T. T. D. Tran et al., "Exosomes and nanoengineering: a match made for precision therapeutics," *Advanced Materials*, 2020.

[123] K. Liu, N. Cao, Y. Zhu, and W. Wang, "Exosome: a novel nanocarrier delivering noncoding RNA for bone tissue engineering," *Journal of Nanomaterials*, vol. 2020, Article ID 2187169, 14 pages, 2020.

[124] S. Zhu, Y. Zhu, Z. Wang et al., "Bioinformatics analysis and identification of circular RNAs promoting the osteogenic differentiation of human bone marrow mesenchymal stem cells on titanium treated by surface mechanical attrition," *PeerJ*, vol. 8, article e9292, 2020.

[125] J. Lamas, L. Rodriguez-Rodriguez, A. Vigo et al., "Large-scale gene expression in bone marrow mesenchymal stem cells: a putative role for COL10A1 in osteoarthritis," *Annals of the Rheumatic Diseases*, vol. 69, no. 10, pp. 1880–1885, 2010.

[126] M. Xu, M. Feng, H. Peng, Z. Qian, L. Zhao, and S. Wu, "Epigenetic regulation of chondrocyte hypertrophy and apoptosis through Sirt1/P53/P21 pathway in surgery-induced osteoarthritis," *Biochemical and Biophysical Research Communications*, vol. 528, no. 1, pp. 179–185, 2020.

[127] Z. Ni, S. Zhou, S. Li et al., "Exosomes: roles and therapeutic potential in osteoarthritis," *Bone Research*, vol. 8, no. 1, p. 25, 2020.

[128] C. Corciulo, C. Castro, T. Coughlin et al., "Intraarticular injection of liposomal adenosine reduces cartilage damage in established murine and rat models of osteoarthritis," *Scientific Reports*, vol. 10, no. 1, article 13477, 2020.

[129] C. Chen, S. Kuo, Y. Tien, P. Shen, Y. Kuo, and H. Huang, "Steady augmentation of anti-osteoarthritic actions of rapamycin by liposome-encapsulation in collaboration with low-intensity pulsed ultrasound," *International Journal of Nanomedicine*, vol. 15, pp. 3771–3790, 2020.

[130] V. Grippo, M. Mojovic, A. Pavicevic et al., "Electrophilic characteristics and aqueous behavior of fatty acid nitroalkenes," *Redox Biology*, vol. 38, article 101756, 2021.

[131] D. Miele, L. Catenacci, M. Sorrenti et al., "Chitosan oleate coated poly lactic-glycolic acid (PLGA) nanoparticles versus chitosan oleate self-assembled polymeric micelles, loaded with resveratrol," *Marine Drugs*, vol. 17, no. 9, p. 515, 2019.

[132] L. Valot, M. Maumus, L. Brunel et al., "A collagen-mimetic organic-inorganic hydrogel for cartilage engineering," *Gels*, vol. 7, no. 2, p. 73, 2021.

[133] M. Velásquez-Hernández, E. Astria, S. Winkler et al., "Modulation of metal-azolate frameworks for the tunable release of encapsulated glycosaminoglycans," *Chemical Science*, vol. 11, no. 39, pp. 10835–10843, 2020.

[134] X. Bi, L. Li, Z. Mao et al., "The effects of silk layer-by-layer surface modification on the mechanical and structural retention of extracellular matrix scaffolds," *Biomaterials Science*, vol. 8, no. 14, pp. 4026–4038, 2020.

[135] B. Geiger, S. Wang, R. Padera, A. Grodzinsky, and P. Hammond, "Cartilage-penetrating nanocarriers improve delivery and efficacy of growth factor treatment of osteoarthritis," *Science Translational Medicine*, vol. 10, no. 469, article eaat8800, 2018.

[136] N. Truong, W. Gu, I. Prasadam et al., "An influenza virus-inspired polymer system for the timed release of siRNA," *Nature Communications*, vol. 4, no. 1, p. 1902, 2013.

[137] S. Lo and M. B. Fauzi, "Current Update of collagen nanomaterials-fabrication, characterisation and its applications: a review," *Pharmaceutics*, vol. 13, no. 3, p. 316, 2021.

[138] J. Lam, S. Lu, F. Kasper, and A. Mikos, "Strategies for controlled delivery of biologics for cartilage repair," *Advanced Drug Delivery Reviews*, vol. 84, pp. 123–134, 2015.

[139] O. S. Manoukian, C. Dieck, T. Milne, C. N. Dealy, S. Rudraiah, and S. G. Kumbar, "Nanomaterials/nanocomposites for osteochondral tissue," *Advances in Experimental Medicine and Biology*, vol. 1058, pp. 79–95, 2018.

Hindawi
Journal of Nanomaterials
Volume 2021, Article ID 3762490, 14 pages
https://doi.org/10.1155/2021/3762490

*Review Article*

# Synthesis and Application of Iron Oxide Nanoparticles in Bone Tissue Repair

**Da Lu**,[1,2,3] **Xueqing Wu**,[1,2,3] **Wei Wang**,[1,2,3] **Chenghao Ma**,[1,2,3] **Baoqing Pei**,[1,2,3] **and Shuqin Wu**[4]

[1]*School of Biological Science and Medical Engineering, Beihang University, Beijing /100191, China*
[2]*Beijing Key Laboratory for Design and Evaluation Technology of Advanced Implantable & Interventional Medical Devices, Beihang University, Beijing /100191, China*
[3]*Beijing Advanced Innovation Center for Biomedical Engineering, Beihang University, Beijing /100191, China*
[4]*School of Big Data and Information, Shanxi Polytechnic Institute, Shanxi 036000, China*

Correspondence should be addressed to Baoqing Pei; pbq@buaa.edu.cn and Shuqin Wu; wushuqin@nuc.edu.cn

Received 6 May 2021; Accepted 14 August 2021; Published 16 September 2021

Academic Editor: Domenico Acierno



Nanoparticles play a vital role in bone tissue repair engineering, especially iron oxide nanoparticles (IONPs), which have magnetic properties, semiconductor properties, and nontoxicity at the same time, and their applications in biomedicine have received widespread attention. This review summarizes the excellent performance of IONPs in enhancing scaffold functions, promoting stem cell differentiation, and labeling positioning, in order to understand the research progress and future development trends of IONPs in bone tissue repair engineering, as well as the security issues. Firstly, IONPs can affect the expression of genes and proteins to accelerate the process of biomineralization under a magnetic field. Then, the composite of IONPs and polymers can synthesize a scaffold which can promote the attachment, proliferation, and bone differentiation of stem cells. Furthermore, IONPs can also mark the location of drugs in the body to follow up the process of bone repair. Therefore, extensive research on the manufacturing and application range of IONPs is of great significance to bone tissue repair engineering.

## 1. Introduction

As we all know, physical stimulation enhances the bone rebuilding capacity significantly, including stretching, compression, fluid shear stress, and heat [1, 2]. Additionally, the magnetic stimulation of static magnetic fields (SMFs) and electromagnetic fields (EMFs) also improve the bone rebuilding capacity greatly [3, 4]. So, the application of MNPs as an intermediate medium has received extensive attention in medical research, such as targeted drug delivery, magnetic resonance imaging (MRI), local tissue hyperthermia, tumor treatment, bioseparation, and biosensing [5], and compared to other materials, MNPs have lower production cost, more stable physical and chemical properties, and better biocompatibility [6].

Magnetic particles are slowly deposited on the surface of the cell membrane under the action of a magnetic field and are endocytosed by the cell. After the magnetic particles enter the cell, it is easier to affect the physiological function of the cell [7, 8]. If a magnetic field is applied, each magnetic particle will become a magnetic source, so that the magnetic scaffold material can play the role of bone tissue repair treatment. Once magnetic particles are exposed to an external magnetic field, they will be rapidly magnetized. Magnetic particles and magnetic fields work together to improve the effectiveness of bone tissue repair [9, 10]. MNPs can be synthesized through different techniques including coprecipitation [11], microemulsion [12], hydrothermal synthesis [13], sol-gel process [14], polyol synthesis [15], flow injection [16], sonolysis/sonochemical method [17], microwave

irradiation [18], electrochemical synthesis [19], solvothermal method [20], chemical vapor deposition [21], laser pyrolysis [22], green synthesis [23], and using biomass or biological templates.

Scaffolds used to reconstruct an injured bone must have sufficient mechanical strength to carry the load. Therefore, other types of scaffold materials, such as ceramics and biodegradable polymers, are usually not suitable for bone tissue engineering. Porous metals and alloy materials may be used as alternative scaffolds to promote new bone formation. However, other metal particles may release toxic substances and cause tissue pollution [24], and the issues can be overcome by using biodegradable metal materials such as irons and their alloys. In view of the advantages of IONPs, some researchers have incorporated $Fe_3O_4$ nanoparticles into tissue engineering biomaterials [25–27]. For example, Pan et al. [28] prepared $Fe_3O_4$/polylactide composites with extrusion process, and they found that the composites containing IONPs had no cytotoxic effect on fibroblasts and enhanced osteogenesis in vitro experiments. Ge et al. [29] prepared a magnetic scaffold containing $Fe_3O_4$/chitosan, which has high biocompatibility to $C_2C_{12}$ cells. Similarly, De Santis et al. designed a magnetic scaffold for bone tissue combining PCL and $Fe_3O_4$ with different ratios. The results showed that the nanoparticles mechanically enhanced the PCL matrix; the elastic modulus and maximum stress increased by about 10% and 30%, respectively [30]. Thus, IONPs are expected to provide a strategy for bone repair. IONPs improve the three key factors of bone regeneration including stem cells, scaffolds, and growth factors via magnetic fields. Among the factors, magnetic cells' strategies contain cell labeling, targeting, and genetic modification. Magnetic scaffolds can enhance cell differentiation through magnetic-mechanical simulation [31]. And IONPs can also be used as delivery media for growth factors, drugs, and gene [32, 33].

## 2. Synthesis and Application of IONPs in Bone Tissue Engineering

*2.1. Synthesis Method of IONPs.* The preparation method has developed well due to its application value, and various element compositions have been used in magnetic nanomaterials, including $Fe_3O_4$, Fe, Co, Ni, $MgFe_2O_4$, and $CoFe_2O_4$ [34–37]. The most common component of magnetic nanomaterials is $Fe_3O_4$, and the preparation methods of magnetic $Fe_3O_4$ mainly include dry and wet methods [38, 39]. Among them, the wet method is more commonly used and mainly includes the following technologies: hydrothermal method, solution thermal method, chemical coprecipitation method, ball milling method, sol-gel method, and atomic layer deposition method. The advantages and disadvantages of each preparation method are summarized (see Table 1).

*2.2. Application of IONPs in the Function of Scaffold*

*2.2.1. Scaffold Material Type.* Guiding and controlling the delivery of bioactive drugs to bone injuries has always been a hot research area. The design of the delivery platform plays a vital role in the treatment of bone diseases and the activation of bone regeneration, because they can provide a suitable environment for the cell adhesion and growth and, at the same time, provide a valuable platform for delivery strategies [64]. The nanostructured materials used in the platform have the characteristics of biocompatibility, nontoxicity, and noncarcinogenicity. Several common nanomaterials for the attachment platform of IONPs are exhibited (see Table 2). Nanomaterials can be divided into organic materials and inorganic materials. Organic materials are a combination of the few lightest elements, especially hydrogen, nitrogen, and oxygen, as well as carbon-containing compounds located in organisms. Organic materials include lipids, liposomes, dendrimers, and polymers, including chitosan, gelatin, and collagen [65]. And inorganic materials refer to materials lacking carbon, which are widely used in in vivo and in vitro biomedical research [66].

IONPs with superparamagnetic properties have a high specific surface energy and are prone to agglomeration. Polymers, which can improve the stability of nanoparticle dispersion in water, are often used as wrapping materials on the surface of particles formatting shell-core structure. In addition, polymer-encapsulated magnetic nanoparticles have the characteristics of strong surface modification and easy modification or functionalization, which greatly broaden the application fields of magnetic materials. Polymers frequently used to encapsulate magnetic nanoparticles including proteins, dendrimers, liposomes, chitosan, glucose, starch, polyethylene glycol (PEG), polyvinyl alcohol (PVA), polyvinylpyrrolidone, and polyglyceryl acrylate (PGA). Among them, PEG is used for drug slow-release system because of its electrical neutrality, water solubility, low toxicity, and nonimmunogenic properties. Glycopolymers are often used in medical imaging studies to improve the diagnosis of diseased tissues such as tumors. PGA/PGMA is also a good class of polymers that has a stronger ability to bind to IONPs, greatly improving the stability of the particles. In addition, human-made biodegradable polymers are widely used as tissue engineering scaffold materials because they can be degraded to small molecules in vivo and excreted through the body metabolism. And they have good histocompatibility, mechanical properties, and controllable degradation rate.

There are many ways to synthesize IONP composite scaffolds, and the manufacturing process and the shortcomings shown are also different (see Table 3).

Among these methods, electrostatic spinning technology has become an important process for producing scaffolds due to its modulable properties and simplicity. The basic method of high-voltage electrostatic spinning technology is to apply a voltage of tens of thousands of volts between the jetting device and the receiving device, forming an electrostatic field. As the spinning fluid drips out of the jet, a jet is formed at the cone end of the droplet and is stretched in the electric field. The final result is the formation of long, irregular fibers on the receiving device, with fiber diameters typically in the tens to hundreds of the nanometer range. From the above description of the electrospinning principle, we find that the shape of the electrospun filament can be regulated by several parameters. These parameters include the viscosity and concentration of the spinning solution, the

Table 1: Synthesis method of IONPs.

| Method | Advantage | Disadvantage | Reference |
|---|---|---|---|
| Organic based | High particle dispersion | Unruly IONPs' appearance | [40–42] |
| Hydrothermal/solvothermal | Simple operation<br>High reaction efficiency<br>Suitable for wider temperature range | Hard to replicate metastable phase and nanomorphology in other ways | [43–47] |
| Coprecipitation | Simple operation<br>High-yield | Poor controllability of its particle size and distribution | [48–51] |
| Ball milling | Granularity reproducibility | IONP aggregation<br>Expensive<br>Long cycle<br>Hard to realize industrial production | [52–55] |
| Sol-gel | Small particle size<br>Good dispersion | Expensive<br>Long duration<br>Easy to shrink during drying | [56–60] |
| Atomic layer deposition | Accurate thickness control<br>Good uniformity | Slow deposition rate | [61–63] |

conductivity, the charge concentration of the solution, the electric field strength/voltage surface tension, the distance between the needle and the collecting screen, the design and placement of the needle tip, and the composition and geometry of the collecting screen. Of course, there are other factors like ambient constant, dipole moment, dielectric constant, and surface tension that also affect high-voltage electrostatic spinning.

*2.2.2. IONPs Enhance Scaffold Function.* Artificial bone transplantation has been extensively studied for bone repair due to less immune rejection and low disease transmission ability [102, 103]. Bone morphogenetic proteins and transformation factors are usually incorporated into artificial scaffolds to improve cell viability. However, there is still a phenomenon of slow cell binding. If magnetic field stimulation activates more receptors on the cell surface and further activates related signal pathway, the cell activity will be enhanced [104, 105]. Magnetic scaffolds can attract growth factors and stem cells to migrate in the body through magnetic drive and promote bone repair and regeneration [106]. In addition, magnetic field stimulation can promote the integration of the scaffold with the host bone and increase calcium content and new bone density, thereby accelerating bone healing [107–109]. At present, the role of magnetic scaffold in promoting cell proliferation and new bone tissue growth has been confirmed [110]. The magnetic scaffold has a wide range of components including biological macromolecules, synthetic polymers, polyethylene glycol, and inorganic materials [111–115].

Liu et al. [116] fabricated a magnetic coating composed of $Fe_3O_4$ nanoparticles and polyamine on the surface of the scaffold, thereby enhancing the cell attachment, proliferation, and bone differentiation of mesenchymal stem cell (MSC) in vitro, and forming new bones at the defect of the rabbit femur. It is found that the magnetic $Fe_3O_4$/PDA coating is related to strengthening the regulation signal pathway by protein analysis. Shuai et al. [117] constructed a magnetic microenvironment by selectively sintering $Fe_3O_4$ magnetic nanoparticles on the PLLA/PGA scaffold. Each nanoparticle in the environment provides a nanometer-scale magnetic field to activate the cell response. The in vitro results show that the magnetic scaffold not only stimulates cell adhesion and activity but also improves the rate of growth and alkaline phosphatase activity (see Figure 1). Yang et al. [118] used calcium phosphate cement (CPC) and IONPs to prepare a new type of scaffold and explored the effect of the new composite material on the formation and bone formation of human dental pulp stem cells (hDPSC). They found that the addition of IONPs greatly promote the bone formation of hDPSC, enhanced mechanical strength and cell activity, and increased the expression of bone marker genes by 1.5-2 times.

Quite a few studies have shown that IONPs have a significant effect on the function of the scaffold. In fact, the 3D platform with IONPs shows tighter cell-to-cell connections, and highly developed filamentous protrusions (increased number and extension length) enhance the interaction between cells and the platform. The distribution of nanoparticles on the surface of the 3D scaffold increased the surface area of the scaffold, enhanced the mechanical signal transduction of cells, and stabilized the cell's anchoring to the matrix, thus promoting the cell adhesion process. Adding IONPs to the 3D scaffold significantly increases the expression of the osteogenic transcription factor RUNX2 and its two downstream factors. IONPs may promote bone formation through different mechanisms, but they rely more on magnetic genetic responses that activate intracellular magnetic receptors and generate endogenous magnetic fields to promote bone formation even in the absence of external magnetic fields [119].

When nanoparticles are absorbed on the surface of the tissue scaffold, they are in direct contact with the cells and may have unknown effects on the cells through ingestion. Hsin-Yi Lin et al. discussed how to use a three-dimensional printing device to make a chitosan hydrogel scaffold and embed nanoparticles in the hydrogel, so that the surrounding cells do not directly contact the nanoparticles. Some studies have shown that the coupling force induced by the magnetic chitosan scaffold promotes the growth and mineralization of bone cells.

Table 2: Types of materials for the attachment platform of IONPs.

| Types of nanomaterials | Description | Size (nm) | Applications | Reference |
|---|---|---|---|---|
| Lipid | Small hydrophobic or amphiphilic molecules | <100 | Nanocarriers for anticancer Drug doxorubicin Osteoblastic bone formation Osteoporosis treatment | [67–70] |
| Liposome | Same bilayer structure as the skin cell membrane structure and excellent moisturizing effect on the skin | >25 | High encapsulation of hydrophilic Drug delivery Growth factor delivery Therapeutic gene delivery Used as a template | [71–73] |
| Dendrimers | Organic molecules with dendritic structure | <10 | Multidrug delivery system | [71, 74, 75] |
| Chitosan | A natural nontoxic linear biopolymer | 20-200 | Scaffolds Drug delivery Support chondrocyte adhesion Implant coating Osteogenic differentiation | [76–80] |
| Collagen | The main structural protein of soft and hard tissues in living organisms | — | Drug delivery Scaffolds | [81] |
| Gelatin | Derivatives of collagen | <200 | Scaffolds Drug-loaded gelatin nanoparticles Promote cell growth | [82, 83] |
| PLGA | A degradable functional polymer organic compound | 100-250 | Drug delivery Scaffolds Nanostructured film Enhanced cell attachment and growth Promote gene expression | [84–87] |
| Carbon nanotubes | With cylindrical or tapered structure of different diameters and lengths | 20-100 | Drug delivery Biosensing Scaffolds | [88–91] |

Table 3: Synthesis method of IONP composite scaffolds.

| Synthesis method | Advantages | Disadvantages | Reference |
|---|---|---|---|
| Traditional method (physical adsorption) | Simple, cheap, stable performance | Lack of control measures for magnetic field gradients | [92, 93] |
| IONPs mixed with other ingredients | Stable performance, excellent mechanical properties | Difficult to control the surface characteristics of the bracket | [94–97] |
| Electrospinning | Easy to operate, easy to control the surface characteristics of the bracket | Low output and low strength | [98–100] |
| 3D printing | Good stability, good three-dimensional structure, high efficiency | Expensive, material limitations | [101] |

Under the action of inductively coupled magnetic force, the signal transduction in bone cells is achieved through the release of intracellular Ca+. This leads to an increase in cytoplasmic Ca ions and an increase in cytoskeletal calmodulin. The increase in cytoplasmic calcium in bone cells will cause cellular bones to shrink. Calcium-dependent contraction promotes the release of extracellular vesicles. These extracellular vesicles contain key bone regulatory proteins, including cellular skeletal calmodulin. Calmodulin is a calcium-sensing protein that is involved in signal pathways that regulate many key processes in bone cells, such as growth, cell division, and movement (see Figure 2).

In addition to its outstanding performance in promoting cell proliferation and osteogenic differentiation, the excellent mechanical strength of the magnetic scaffold also deserves our attention. For example, Ghorbani et al. investigated the

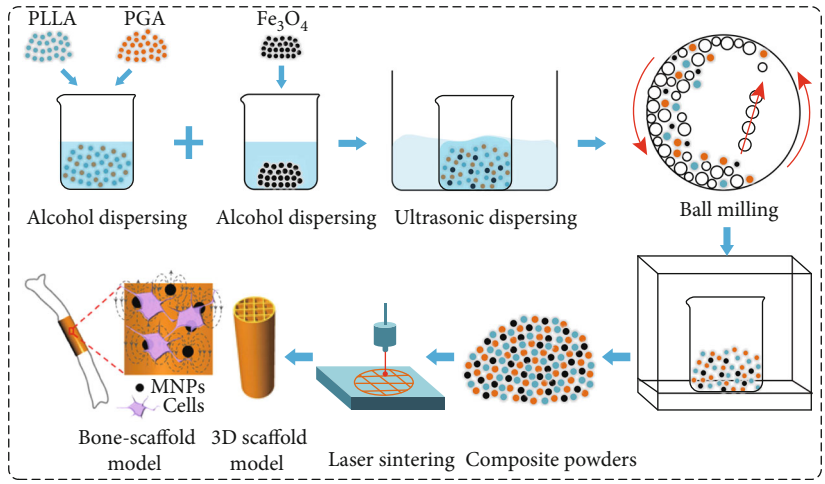


FIGURE 1: Schematic of the magnetic scaffold preparation process. Reproduced with permission from [117].

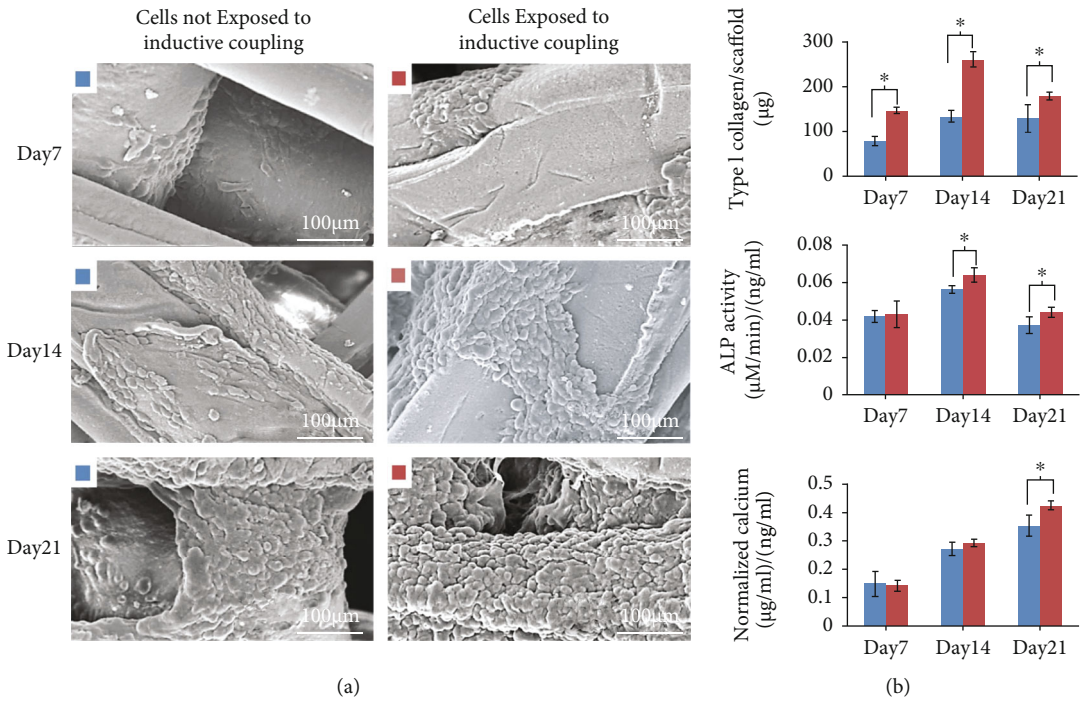


FIGURE 2: (a, b) Cell surface morphology and osteogenic differentiation with and without the inductive coupling magnetic force for 7, 14, and 21 days. (a) The morphology of osteoblast cells on the chitosan hydrogel scaffolds. (b) Osteoblast cell proliferation and differentiation. Reproduced with permission from [120].

effect of IONPs on the scaffold structure. Compared with scaffolds without IONPs, scaffolds with IONPs reduced the pore size, thus improving the mechanical strength of the scaffold, but the absorption capacity and biodegradation ratio were reduced [121]. Similar to Ghorbani et al.'s study, Kim et al. also found that the mechanical stiffness of the PCL scaffold increased significantly with the addition of IONPs. The initial adhesion of cells to the magnetic scaffold was substantially increased by 1.4-fold compared to the pure PCL scaffold [122]. Wang et al. fabricated borosilicate bioactive glass scaffolds loaded with different amounts (5-15 wt%) of $Fe_3O_4$ nanoparticles and evaluated their performance in vitro and in vivo. They found that the $Fe_3O_4$ content was proportional to the compressive strength of the scaffold, and the compressive strength of the scaffolds increased with increasing content of IONPs, from $2.6 \pm 0.6$ MPa for the BG scaffolds to $3.6 \pm 0.6$ MPa for the scaffolds loaded with 15 wt% $Fe_3O_4$ [123]. In the meantime, that scaffold has the largest magnetic saturation and highest temperature of aqueous suspension.

These findings suggest that the scaffold with IONPs has excellent physicochemical, magnetic, mechanical, and biological

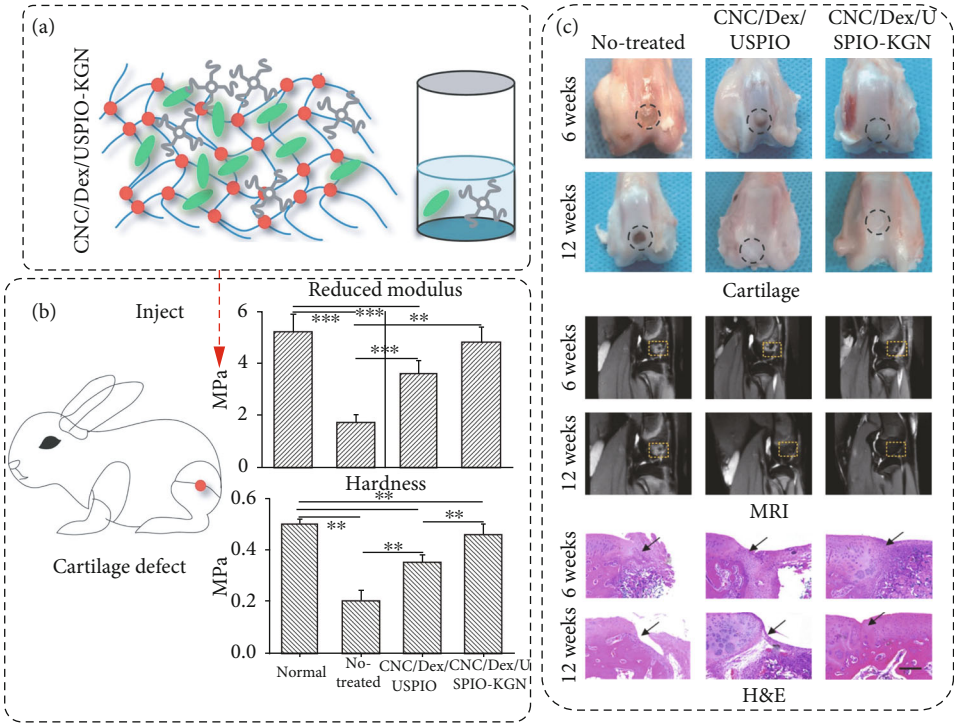


FIGURE 3: Synthesis in vitro and physicochemical properties in rabbit cartilage of CNC/Dex/USPIO-KGN. (a) Schematic illustration of preparation and utilization of USPIO-labeled Dex/CNC/USPIO-KGN hydrogels for engineering artificial cartilage repair. (b) Reduced modulus and hardness (reduced modulo is a "combined" modulus of the tip and the sample and can be directly evaluated from analysis of stress-strain data according to specific equations). (c) Observations of cartilage harvested; MRI and H&E during 6 weeks and 12 weeks. H&E staining shows that the neocartilage integrated with the adjacent normal cartilage. Reproduced with permission from [127].

properties, supporting the potential application of magnetic scaffolds for bone repair and regeneration.

*2.2.3. IONPs Promote Stem Cell Differentiation.* In addition to scaffolds, stem cells are another vital factor in tissue regeneration. In recent years, although stem cell therapy has provided a strategy for large-scale bone repair and has been successful in the treatment of animal bone defect models, these traditional stem cell transplants have not achieved the desired effect [124]. With the development of materials science and chemical biology, people have been trying to use IONPs as a tool for research and control of stem cells for many years [125]. By combining IONPs with an external magnetic field, it will affect the cell adhesion, proliferation, movement and distribution, and osteogenic differentiation of stem cells. In addition, IONPs can be used to label cells for in vivo tracking and monitoring.

MSCs are a key participant in bone regeneration, and promoting the differentiation of MSCs is an important basis for evaluating the performance of nanoparticles. The combination of different polymers and IONPs greatly promote the differentiation of MSCs. Jia et al. [126] synthesized medium-porous silicon-coated magnetic $Fe_3O_4$ nanoparticles and evaluated their potential to accelerate bone regeneration in a rat osteoporosis model. After X-ray imaging, micro-CT, mechanical testing, histological examination, and immunochemical analysis, local injection of MNPs significantly accelerated bone regeneration. Yang et al. [127] transplanted kartogenin (KGN), which can promote the differentiation of bone marrow-derived mesenchymal stem cells into chondrocytes, onto a modified magnetic oxide surface, and then integrated into the cellulose nanocrystalline hydrogel. Release and recruit endogenous host cells and differentiate BMSCs into chondrocytes, thereby achieving original cartilage regeneration. The regenerated cartilage tissue is very similar to a natural cartilage. This innovative diagnosis and treatment system improve the convenience and effectiveness of cartilage regeneration (see Figure 3).

Xu et al. [128] prepared hollow IONPs, HMFN, which is of spherical shape with a diameter of about 320 nanometers. It has a negative charge on the surface and has huge supernegative magnetic properties. The -OH bond in it improves the affinity of nanoparticles. For water and biocompatibility, as a result, it was found that electromagnetic fields can use intracellular supersuspended magnetic nanoparticles to manipulate the bone differentiation of BMSCs.

In addition, human dental pulp stem cells (hDPSCs) also provide great potential for research of bone tissue engineering. Their advantages include easy isolation, nonimmunogenicity, strong proliferation, and differentiation ability, similar to bone marrow stem cells (BMSCs) [129]. The osteogenic differentiation ability of hDPSCs has been fully confirmed by previous studies, which is manifested by increased ALP activity [130] and increased expression of bone-specific markers [131, 132]. The WNT/$\beta$-catenin signaling pathway plays an important role in osteogenesis. Previous studies have shown that by activating the SMAD pathway or interacting with the WNT pathway to upregulate

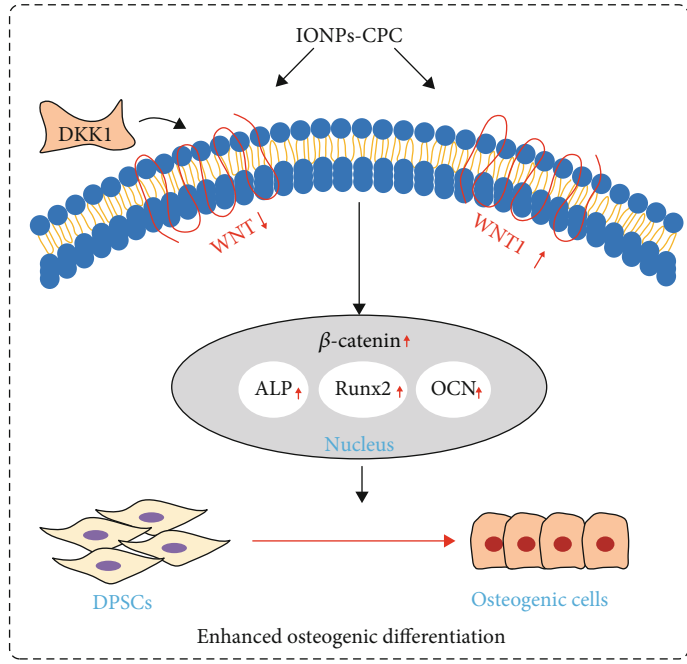


Figure 4: WNT signaling pathway promotes osteoblast differentiation.

osteogenic genes, IONPs can promote stem cells by upregulating BMP2, which plays a key role in bone morphogenesis. They added hydrophilic IONP solution to CPC powder to prepare IONP-CPC scaffolds and explored the effect of new composite materials on the formation of bone matrix and osteogenic differentiation of hDPSCs. As the ionosphere content increases, the color of the scaffold turns darker, and the surface of the scaffold forms agglomerates, which significantly enhances the adsorption of proteins. Through the analysis of the WNT pathway, it was found that CPC+IONPs can significantly enhance the expression of $\beta$-catenin protein, proving its important role in the osteogenic differentiation of stem cells (see Figure 4) [118]. In fact, another study also confirmed that IONPs can activate the BMP/SMAD pathway [133].

*2.2.4. Marking and Positioning of IONPs.* Cell migration, distribution, survival, and differentiation play a crucial role in therapeutic efficacy [134]. We understand that these parameters can optimize cell selection, administration route, and therapeutic dose and provide cell-based therapy for specific clinical applications. To solve this problem, researchers have been looking for tools that allow real-time, quantitative, and long-term monitoring of cell behavior in the body. This phenomenon is called cell tracking. IONPs are used as an NMR contrast agent for cell tracking [135].

Because the healing potential of the articular cartilage is limited, the treatment of osteoporotic defects continues to pose a major challenge to patients and orthopedic surgeons. MSCs have a therapeutic potential for the treatment of osteoporotic pain and pathology. However, it is necessary to use appropriate stem cell labels and imaging agents to decipher its role after transplantation. Silva et al. [136] incubated MSCs with magnetic nanoparticles and used external magnetic fields to guide magnetized MSCs in vitro and enhanced their retention in the lungs in vivo. The results showed that MT improved MSC translocation and expression of chemical hormone receptor. Shelat et al. [137] evaluated the efficacy of bone marrow-derived mesenchymal stem cells (BMSCs) for the treatment of osteoporosis defects in rats and used L-lysine functionalized IONPs (lys-IONPs) to treat stem cells. In vivo monitoring showed that the particles can be used as long-term stem cell markers and imaging agents. Yao et al. [138] used amine-modified silicon-coated nanoparticles to label bone marrow-derived mesenchymal stem cells and then evaluated the stem cell potential. The study found that after labeling, the viability of BM-MSC remained good and the migration ability was enhanced and had no effect on bone production and adipogenesis, which means that this kind of nanoparticles can not only serve as an ideal tracking marker but also become an accelerator for stem cell positioning during tissue repair (see Figure 5). In addition, scholars have also discovered the advantages of magnetic IONPs as markers in the treatment of diseases such as ischemic heart disease and pulmonary fibrosis [139, 140].

*2.2.5. Security Issues of IONPs.* IONPs are among the most versatile and safe nanoparticles for a variety of biomedical applications. The dramatic increase in the use of nanoparticles in research, industry, and medicine raises many questions about potential toxicity [141], since the nanoscale properties can potentially induce cytotoxicity by impairing the functions of mitochondria, nucleus, and DNA [141–143]. It is well known that excess reactive oxygen species (ROS), including superoxide anions, hydroxyl radicals, and nonradical hydrogen peroxide, can be toxic intracellularly and in vivo [141, 144, 145]. The ROS can be generated from the leaching of iron ions from the surface degradation by enzymatic degradation. Furthermore, ROS can react with macromolecules and damage cells by peroxidizing lipids,

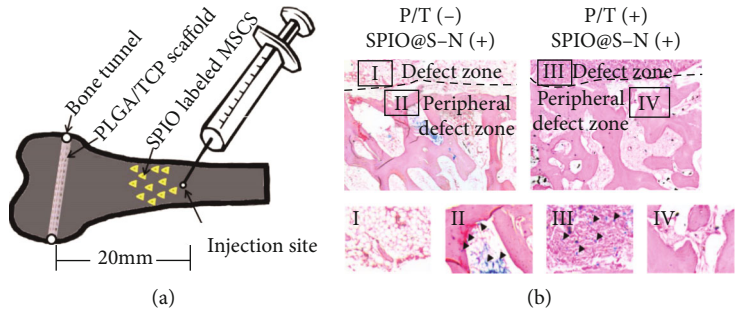


Figure 5: (a, b) Marking and positioning of IONPs. (a) Rabbit SAON bone defect model was established, and PLGA/TCP was implanted into the rabbit at the distal femur to track BM-MSC migration in vivo. (b) Dynamic MRI was performed at day 0 and day 7, respectively, after implantation. Reproduced with permission from [140].

changing proteins, disrupting DNA, interfering with signaling functions, modulating gene transcription, and finally causing cell death either by apoptosis or necrosis. Another mechanism by which IONPs can induce toxicity is via iron overload. Since IONPs require magnetic targeting to specific tissues [146], high concentrations of free iron ions may lead to abnormal cellular responses including cytotoxicity, oxidative stress, epigenetic events, inflammation, and DNA damage that may trigger carcinogenesis or have significant effects on offspring [142, 147–150].

The cytotoxicity of IONPs is highly dependent on a number of factors related to their physical properties, such as size, shape, and surface coating. The type of surface coating materials of IONPs and their decomposition products are important in determining their toxicity [151]. As mentioned previously, there are many polymers that can be used to coat IONPs; however, some studies have shown that PEG-coated IONPs produce negligible aggregation in cell culture media and reduce nonspecific uptake by macrophages [152], while dextran-coated IONPs can lead to cell death and reduced proliferation with observable visible membrane disruption [153, 154]. The oxidation state of iron ($Fe^{2+}$ or $Fe^{3+}$) in IONPs is an additional key factor that determines the cytotoxicity of IONPs [150]. It has been demonstrated that maghemite ($Fe_2O_3$) with an $Fe^{2+}/Fe^{3+}$ ratio of 0.118 has a more significant genotoxicity than magnetite ($Fe_3O_4$) with an $Fe^{2+}/Fe^{3+}$ ratio of 0.435. More efforts are needed to design and prepare IONPs with good chemical stability.

In vivo, the toxicity of IONPs is dose dependent and is also related to the type of tissue cells on which they act. For example, Hanini et al. [155] reported that IONPs in vivo can induce toxicity in the liver, kidneys, and lungs while the brain and heart organs remained unaffected. Additionally, hemocompatibility is also an aspect that should be taken into account for the in vivo application of IONPs. If IONPs are incompatible with biological fluids such as blood, this can trigger coagulation and clot formation through adsorption of plasma proteins, platelet adhesion, and activation of the complement cascade. IONPs will exist in different proportions in different organs of the body; how to remove the excess particles is also related to the toxic side effects. Generally, clearance and opsonization of IONPs depend on their sizes and surface characteristics [156, 157]. For example, 55% oleic acid/pluronic-coated IONPs of injected dosage were accumulated in the liver of a rat. However, in the same animal model, 25% of injected dextran-coated IONPs was eliminated via urine and feces [158]. Therefore, the toxic effects of IONPs on humans can be effectively reduced by controlling the physical properties of IONPs and selecting the appropriate type of surface coating material and the dose of IONPs. Also, more attention should be paid to the kinetic and metabolic mechanisms of IONPs with different surface coatings, which would allow the development of predictive models of nanotoxicity.

## 3. Summary and Prospect

We briefly describe the synthesis method of IONPs and the merit and demerit of each method. And the applications of the IONPs in the function of scaffold are also elaborated. Among them, we firstly mentioned the material used to make the scaffold and statistics on their size. Each material has unique properties including nanocarriers for anticancer, drug doxorubicin, osteoblastic bone formation, and osteoporosis treatment. And then, we have mentioned the merit and demerit of several scaffold synthesis methods. Furthermore, the mechanism by which IONPs enhance the function of the scaffold is described. IONPs can impart a magnetic effect to the scaffold, which can attract growth factors and stem cells to migrate in the body, and promote bone repair and regeneration. IONPs can also be used as accelerators to accelerate the binding of the scaffold to the host bone and enhance related signal pathways to promote the attachment, proliferation, and bone differentiation of mesenchymal stem cells. At the same time, as a marker and imaging agent, it is an important tool for drug delivery and stem cell localization.

Through the above literature research, we have summarized the development status and development direction of IONPs. (a) How to precisely control the arrangement of the IONPs to obtain a better magnetocaloric effect has broad prospects. (b) There are many ways to prepare composite scaffolds of iron oxide particles, all of which have excellent performance and significant shortcomings in specific scenarios. How to obtain a scaffold that can control the surface characteristics of the scaffold and has high yield and low cost will become the focus of research. (c) How to maintain long-lasting and effective stem cell characteristics is the key to successful treatment. Therefore, for cells expanded in vitro,

maintaining a stable cell phenotype and reducing the necrosis and loss of the cells at the defect site after transplantation in vitro are necessary for bone defect repair. (d) At present, most researches on IONPs focus on labeling methodologies and monitoring curative effects, but there are not many studies on their effects on labeled cells. IONPs have different effects on different types of cells, even the same type of cell, in different aspects. Functional activities also react differently to IONPs. Therefore, it is necessary to extensively study the short-term and long-term potential cytotoxicities of IONPs to different labeled cells, which is an important reference for avoiding the adverse reactions of IONPs when cell magnetic labeling really enters the clinical trial stage in the future.

With the in-depth research of human cells and virus particles, the continuous improvement of the feasibility and practicability of nanoparticles as drug carriers will inevitably provide a breakthrough in the research of drug carrier systems. It is reasonable to believe that the multifunctional magnetic nanodrug carrier with fluorescence detection, multiple targeting, efficient drug loading, quantitative time-released drug, and nontoxic side effects is of great significance for the diagnosis and treatment of major diseases such as cancer.

## Data Availability

The data used to support the findings of this study are included within the article.

## Conflicts of Interest

There are no conflicts of interest in this study.

## Authors' Contributions

All authors have read and approved this version of the article, and due care has been taken to ensure the integrity of the work.

## Acknowledgments

This research was supported by National Natural Science Foundation of China (No. 11972065) and Beijing Natural Science Foundation (L202006).

## References

[1] H. Y. Xu and N. Gu, "Magnetic responsive scaffolds and magnetic fields in bone repair and regeneration," *Frontiers of Materials Science*, vol. 8, no. 1, pp. 20–31, 2014.

[2] E. Chung, A. C. Sampson, and M. N. Rylander, "Influence of heating and cyclic tension on the induction of heat shock proteins and bone-related proteins by MC3T3-E1 cells," *BioMed Research International*, vol. 2014, Article ID 354260, 16 pages, 2014.

[3] M. Quittan, O. Schuhfried, G. F. Wiesinger, and V. Fialka-Moser, "Clinical effectiveness of magnetic field therapy–a review of the literature," *Acta Medica Austriaca*, vol. 27, no. 3, pp. 61–68, 2000.

[4] M. Gujjalapudi, C. Anam, P. Mamidi, R. Chiluka, A. G. Kumar, and R. Bibinagar, "Effect of magnetic field on bone healing around endosseous implants - an in-vivo study," *Journal of Clinical and Diagnostic Research*, vol. 10, no. 10, pp. ZF01–ZF04, 2016.

[5] R. V. Ferreira, P. P. Silva-Caldeira, E. C. Pereira-Maia et al., "Bio-inactivation of human malignant cells through highly responsive diluted colloidal suspension of functionalized magnetic iron oxide nanoparticles," *Journal of Nanoparticle Research*, vol. 18, no. 4, p. 92, 2016.

[6] A. Özbey, M. Karimzadehkhouei, S. E. Yalçın, D. Gozuacik, and A. Koşar, "Modeling of ferrofluid magnetic actuation with dynamic magnetic elds in small channels," *Microfluidics and Nanofluidics*, vol. 18, no. 3, pp. 447–460, 2015.

[7] A. J. Theruvath, H. Nejadnik, A. M. Muehe et al., "Tracking cell transplants in femoral osteonecrosis with magnetic resonance imaging: a proof-of-concept study in patients," *Clinical Cancer Research*, vol. 24, no. 24, pp. 6223–6229, 2018.

[8] Y. Xia, J. Sun, L. Zhao et al., "Magnetic field and nanoscaffolds with stem cells to enhance bone regeneration," *Biomaterials*, vol. 183, pp. 151–170, 2018.

[9] D. Fan, Q. Wang, T. Zhu et al., "Recent advances of magnetic nanomaterials in bone tissue repair," *Frontiers in Chemistry*, vol. 8, 2020.

[10] Y. Zhao, T. Fan, J. Chen et al., "Magnetic bioinspired micro/-nanostructured composite scaffold for bone regeneration," *Colloids and Surfaces. B, Biointerfaces*, vol. 174, pp. 70–79, 2019.

[11] M. I. Khalil, "Co-precipitation in aqueous solution synthesis of magnetite nanoparticles using iron(III) salts as precursors," *Arabian Journal of Chemistry*, vol. 8, no. 2, pp. 279–284, 2015.

[12] M. A. Malik, M. Y. Wani, and M. A. Hashim, "Microemulsion method: A novel route to synthesize organic and inorganic nanomaterials: 1st Nano Update," *Arabian Journal of Chemistry*, vol. 5, no. 4, pp. 397–417, 2012.

[13] T. J. Daou, G. Pourroy, S. Bégin-Colin et al., "Hydrothermal synthesis of monodisperse magnetite nanoparticles," *Chemistry of Materials*, vol. 18, no. 18, pp. 4399–4404, 2006.

[14] Z. I. Takai, M. K. Mustafa, S. Asman, and K. A. Sekak, "Preparation and characterization of magnetite ($Fe_3O_4$) nanoparticles by sol-gel method," *International Journal of Nanoelectronics and Materials*, vol. 12, pp. 37–46, 2019.

[15] R. Hachani, M. Lowdell, M. Birchall et al., "Polyol synthesis, functionalisation, and biocompatibility studies of superparamagnetic iron oxide nanoparticles as potential MRI contrast agents," *Nanoscale*, vol. 8, no. 6, pp. 3278–3287, 2016.

[16] G. Salazar-Alvarez, M. Muhammed, and A. Zagorodni, "Novel flow injection synthesis of iron oxide nanoparticles with narrow size distribution," *Chemical Engineering Science*, vol. 61, no. 14, pp. 4625–4633, 2006.

[17] A. Hassanjani-Roshan, M. R. Vaezi, A. Shokuhfar, and Z. Rajabali, "Synthesis of iron oxide nanoparticles via sonochemical method and their characterization," *Particuology*, vol. 9, no. 1, pp. 95–99, 2011.

[18] E. Aivazoglou, E. Metaxa, and E. Hristoforou, "Microwave-assisted synthesis of iron oxide nanoparticles in biocompatible organic environment," *AIP Advances*, vol. 8, article 48201, 2017.

[19] M. Starowicz, P. Starowicz, J. Żukrowski et al., "Electrochemical synthesis of magnetic iron oxide nanoparticles with

controlled size," *Journal of Nanoparticle Research*, vol. 13, no. 12, pp. 7167–7176, 2011.

[20] Y. Huang, L. Zhang, W. Huan, X. Liang, X. Liu, and Y. Yang, "A study on synthesis and properties of $Fe_3O_4$ nanoparticles by solvothermal method," *Glass Physics and Chemistry*, vol. 36, no. 3, pp. 325–331, 2010.

[21] D. Wei, Y. Liu, L. Cao et al., "A magnetism-assisted chemical vapor deposition method to produce branched or iron-encapsulated carbon nanotubes," *Journal of the American Chemical Society*, vol. 129, no. 23, pp. 7364–7368, 2007.

[22] O. Bomati-Miguel, L. Mazeina, A. Navrotsky, and S. Veintemillas-Verdaguer, "Calorimetric study of maghemite nanoparticles synthesized by laser-induced pyrolysis," *Chemistry of Materials*, vol. 20, no. 2, pp. 591–598, 2008.

[23] V. C. Karade, P. P. Waifalkar, T. D. Dongle et al., "Greener synthesis of magnetite nanoparticles using green tea extract and their magnetic properties," *Materials Research Express*, vol. 4, no. 9, p. 96102, 2017.

[24] V. S. A. Challa, S. Mali, and R. D. K. Misra, "Reduced toxicity and superior cellular response of preosteoblasts to Ti-6Al-7Nb alloy and comparison with Ti-6Al-4V," *Journal of Biomedical Materials Research Part A*, vol. 101, no. 7, pp. 2083–2089, 2013.

[25] T. Long, Y. P. Guo, S. Tang, Y. J. Guo, and Z. A. Zhu, "Emulsion fabrication of magnetic mesoporous carbonated hydroxyapatite microspheres for treatment of bone infection," *RSC Advances*, vol. 4, no. 23, pp. 11816–11825, 2014.

[26] J. Li, Y. Hu, J. Yang et al., "Hyaluronic acid-modified $Fe_3O_4$@Au core/shell nanostars for multimodal imaging and photothermal therapy of tumors," *Biomaterials*, vol. 38, pp. 10–21, 2015.

[27] W. Chen, T. Long, Y. J. Guo, Z. A. Zhu, and Y. P. Guo, "Magnetic hydroxyapatite coatings with oriented nanorod arrays: hydrothermal synthesis, structure and biocompatibility," *Journal of Materials Chemistry B*, vol. 2, no. 12, pp. 1653–1660, 2014.

[28] Y. H. Pan, H. T. Wang, T. L. Wu, K. H. Fan, H. M. Huang, and W. J. Chang, "Fabrication of $Fe_3O_4$/PLLA composites for use in bone tissue engineering," *Polymer Composites*, vol. 38, 2016.

[29] J. H. Ge, M. Z. Zhai, Y. Zhang, J. Bian, and J. Wu, "Biocompatible $Fe_3O_4$/chitosan scaffolds with high magnetism," *International Journal of Biological Macromolecules*, vol. 128, pp. 406–413, 2019.

[30] R. de Santis, A. Gloria, T. Russo et al., "A basic approach toward the development of nanocomposite magnetic scaffolds for advanced bone tissue engineering," *Journal of Applied Polymer Science*, vol. 122, no. 6, pp. 3599–3605, 2011.

[31] X. Zhao, J. Kim, C. A. Cezar et al., "Active scaffolds for on-demand drug and cell delivery," *Proceedings of the National Academy of Sciences of the United States of America*, vol. 108, no. 1, pp. 67–72, 2011.

[32] D. Singh, J. M. McMillan, A. V. Kabanov, M. Sokolsky-Papkov, and H. E. Gendelman, "Bench-to-bedside translation of magnetic nanoparticles," *Nanomedicine (Lond)*, vol. 9, no. 4, pp. 501–516, 2014.

[33] E. Delyagina, W. Li, N. Ma, and G. Steinhoff, "Magnetic targeting strategies in gene delivery," *Nanomedicine (Lond)*, vol. 6, no. 9, pp. 1593–1604, 2011.

[34] H. Hamidian and T. Tavakoli, "Preparation of a new $Fe_3O_4$/starch- *g* -polyester nanocomposite hydrogel and a study on swelling and drug delivery properties," *Carbohydrate Polymers*, vol. 144, pp. 140–148, 2016.

[35] Q. Chen, D. Liu, C. Wu et al., "Co-immobilization of cellulase and lysozyme on amino-functionalized magnetic nanoparticles: an activity-tunable biocatalyst for extraction of lipids from microalgae," *Bioresource Technology*, vol. 263, pp. 317–324, 2018.

[36] J. Wu, X. Cheng, and G. Yang, "Preparation of nanochitin-contained magnetic chitosan microfibers via continuous injection gelation method for removal of Ni(II) ion from aqueous solution," *International Journal of Biological Macromolecules*, vol. 125, pp. 404–413, 2019.

[37] X. Xue, R. Lu, M. Liu, Y. Li, J. Li, and L. Wang, "A facile and general approach for the preparation of boronic acid-functionalized magnetic nanoparticles for the selective enrichment of glycoproteins," *Analyst*, vol. 144, no. 2, pp. 641–648, 2019.

[38] C. Yu, J. Geng, Y. Zhuang et al., "Preparation of the chitosan grafted poly (quaternary ammonium)/$Fe_3O_4$ nanoparticles and its adsorption performance for food yellow 3," *Carbohydrate Polymers*, vol. 152, pp. 327–336, 2016.

[39] J. Huang, W. Liu, Y. Liang et al., "Preparation and biocompatibility of diphasic magnetic nanocomposite scaffold," *Materials Science & Engineering. C, Materials for Biological Applications*, vol. 87, pp. 70–77, 2018.

[40] A. Maleki, "One-pot multicomponent synthesis of diazepine derivatives using terminal alkynes in the presence of silica-supported superparamagnetic iron oxide nanoparticles," *Tetrahedron Letters*, vol. 54, no. 16, pp. 2055–2059, 2013.

[41] A. Maleki, "One-pot three-component synthesis of pyrido[2′,1′:2,3]imidazo[4,5-c]isoquinolines using $Fe_3O_4$@$SiO_2$-$OSO_3H$ as an efficient heterogeneous nanocatalyst," *RSC Advances*, vol. 4, no. 109, pp. 64169–64173, 2014.

[42] A. Maleki, "Green oxidation protocol: selective conversions of alcohols and alkenes to aldehydes, ketones and epoxides by using a new multiwall carbon nanotube-based hybrid nanocatalyst via ultrasound irradiation," *Ultrasonics Sonochemistry*, vol. 40, Part A, pp. 460–464, 2018.

[43] H. Gan and H. Xu, "A novel aptamer-based online magnetic solid phase extraction method for simultaneous determination of urinary 8-hydroxy-2′-deoxyguanosine and monohydroxylated polycyclic aromatic hydrocarbons," *Talanta*, vol. 201, pp. 271–279, 2019.

[44] K. Pandi, N. Viswanathan, and S. Meenakshi, "Hydrothermal synthesis of magnetic iron oxide encrusted hydrocalumite-chitosan composite for defluoridation studies," *International Journal of Biological Macromolecules*, vol. 132, pp. 600–605, 2019.

[45] H. Saygili, "Hydrothermal synthesis of magnetic nanocomposite from biowaste matrix by a green and one-step route: Characterization and pollutant removal ability," *Bioresource Technology*, vol. 278, pp. 242–247, 2019.

[46] Y. Liu, T. Cui, T. Wu, Y. Li, and G. Tong, "Excellent microwave-absorbing properties of elliptical $Fe_2O_2$ nanorings made by a rapid microwave-assisted hydrothermal approach," *Nanotechnology*, vol. 27, no. 16, p. 165707, 2016.

[47] X. Wang, P. Y. Gao, Y. Y. Yang, H. Guo, and D. Wu, "Dynamic and programmable morphology and size evolution via a living hierarchical self-assembly strategy," *Nature Communications*, vol. 9, no. 1, p. 2772, 2018.

[48] C. Wan and J. Li, "Synthesis of well-dispersed magnetic $CoFe_2O_4$ nanoparticles in cellulose aerogels via a facile

oxidative co-precipitation method," *Carbohydrate Polymers*, vol. 134, pp. 144–150, 2015.

[49] H. Nosrati, M. Salehiabar, H. K. Manjili, H. Danafar, and S. Davaran, "Preparation of magnetic albumin nanoparticles via a simple and one-pot desolvation and co-precipitation method for medical and pharmaceutical applications," *International Journal of Biological Macromolecules*, vol. 108, pp. 909–915, 2018.

[50] M. S. A. Darwish, H. Kim, H. Lee, C. Ryu, J. Y. Lee, and J. Yoon, "Synthesis of magnetic ferrite nanoparticles with high hyperthermia performance via a controlled co-precipitation method," *Nanomaterials*, vol. 9, no. 8, p. 1176, 2019.

[51] S. Majidi, F. Zeinali Sehrig, S. M. Farkhani, M. Soleymani Goloujeh, and A. Akbarzadeh, "Current methods for synthesis of magnetic nanoparticles," *Artificial Cells, Nanomedicine, and Biotechnology*, vol. 44, no. 2, pp. 722–734, 2016.

[52] W. Zhang, X. Li, R. Zou et al., "Multifunctional glucose biosensors from $Fe_3O_4$ nanoparticles modified chitosan/graphene nanocomposites," *Scientific Reports*, vol. 5, no. 1, p. 11129, 2015.

[53] Q. Yang, M. Zhou, M. Yang et al., "Highyield production of few-layer graphene via new-fashioned strategy combining resonance ball milling and hydrothermal exfoliation," *Nanomaterials*, vol. 10, no. 4, p. 667, 2020.

[54] V. Narayanaswamy, I. M. Obaidat, A. S. Kamzin et al., "Synthesis of graphene oxide-$Fe_3O_4$ based nanocomposites using the mechanochemical method and in vitro magnetic hyperthermia," *International Journal of Molecular Sciences*, vol. 20, no. 13, p. 3368, 2019.

[55] M. Amiri, K. Eskandari, and M. Salavati-Niasari, "Magnetically retrievable ferrite nanoparticles in the catalysis application," *Advances in Colloid and Interface Science*, vol. 271, p. 101982, 2019.

[56] H. M. Kayili and B. Salih, "Fast and efficient proteolysis by reusable pepsin-encapsulated magnetic sol- gel material for mass spectrometry-based proteomics applications," *Talanta*, vol. 155, pp. 78–86, 2016.

[57] J. Lin, J. Zhang, H. Sun et al., "Structural and magnetic property of Cr3+ substituted cobalt ferrite nanomaterials prepared by the sol-gel method," *Materials*, vol. 11, no. 11, p. 2095, 2018.

[58] J. Wang, Q. Zhang, X. Shao, J. Ma, and G. Tian, "Properties of magnetic carbon nanomaterials and application in removal organic dyes," *Chemosphere*, vol. 207, pp. 377–384, 2018.

[59] W. R. Bao, M. L. Li, Y. Y. Yang et al., "Advancements and frontiers in the high performance of natural hydrogels for cartilage tissue engineering," *Frontiers in Chemistry*, vol. 8, p. 53, 2020.

[60] L. Gao, Y. Tang, C. Wang et al., "Highly-efficient amphiphilic magnetic nanocomposites based on a simple sol-gel modification for adsorption of phthalate esters," *Journal of Colloid and Interface Science*, vol. 552, pp. 142–152, 2019.

[61] U. T. Sanli, C. Jiao, M. Baluktsian et al., "3D nanofabrication of high-resolution multilayer fresnel zone plates," *Advanced Science*, vol. 5, no. 9, article 1800346, 2018.

[62] Y. Li, T. Liang, R. Wang, B. He, Y. Gong, and H. Wang, "Encapsulation of $Fe_3O_4$ between copper nanorod and thin TiO2 film by ALD for lithium-ion capacitors," *ACS Applied Materials & Interfaces*, vol. 11, no. 21, pp. 19115–19122, 2019.

[63] A. Ponti, M. H. Raza, F. Pantò et al., "Structure, defects, and magnetism of electrospun hematite nanofibers silica-coated by atomic layer deposition," *Langmuir*, vol. 36, no. 5, pp. 1305–1319, 2020.

[64] X. W. Bi, L. H. Li, Z. N. Mao et al., "The effects of silk layer-by-layer surface modification on the mechanical and structural retention of extracellular matrix scaffolds," *Biomaterials Science*, vol. 8, no. 14, pp. 4026–4038, 2020.

[65] C. Y. Wang, B. Yu, Y. B. Fan et al., "Incorporation of multi-walled carbon nanotubes to PMMA bone cement improves cytocompatibility and osseointegration," *Materials Science and Engineering: C*, vol. 103, p. 109823, 2019.

[66] Q. Chen, C. Zhu, and G. A. Thouas, "Progress and challenges in biomaterials used for bone tissue engineering: bioactive glasses and elastomeric composites," *Progress in Biomaterials*, vol. 1, no. 1, p. 2, 2012.

[67] G. Wang, N. Z. Mostafa, V. Incani, C. Kucharski, and H. Uludağ, "Bisphosphonate-decorated lipid nanoparticles designed as drug carriers for bone diseases," *Journal of Biomedial Materials Research Part A*, vol. 100, pp. 684–693, 2012.

[68] G. Zhang, B. Guo, H. Wu et al., "A delivery system targeting bone formation surfaces to facilitate RNAi-based anabolic therapy," *Nature Medicine*, vol. 18, no. 2, pp. 307–314, 2012.

[69] J. Liu, H. Zhang, Y. Dong et al., "Bi-directionally selective bone targeting delivery for anabolic and antiresorptive drugs: a novel combined therapy for osteoporosis?," *Medical Hypotheses*, vol. 83, no. 6, pp. 694–696, 2014.

[70] S. Hirsjärvi, L. Sancey, S. Dufort et al., "Effect of particle size on the biodistribution of lipid nanocapsules: comparison between nuclear and fluorescence imaging and counting," *International Journal of Pharmaceutics*, vol. 453, no. 2, pp. 594–600, 2013.

[71] M. Nahar, T. Dutta, S. Murugesan et al., "Functional polymeric nanoparticles: an efficient and promising tool for active delivery of bioactives," *Critical Reviews in Therapeutic Drug Carrier Systems*, vol. 23, no. 4, pp. 259–318, 2006.

[72] S. Y. An, M.-P. N. Bui, Y. J. Nam et al., "Preparation of monodisperse and size-controlled poly(ethylene glycol) hydrogel nanoparticles using liposome templates," *Journal of Colloid and Interface Science*, vol. 331, no. 1, pp. 98–103, 2009.

[73] N. Monteiro, A. Martins, R. L. Reis, and N. M. Neves, "Liposomes in tissue engineering and regenerative medicine," *Journal of the Royal Society Interface*, vol. 11, pp. 281–297, 2014.

[74] R. Qi, I. Majoros, A. C. Misra et al., "Folate receptor-targeted dendrimer-methotrexate conjugate for inflammatory arthritis," *Journal of Biomedical Nanotechnology*, vol. 11, pp. 1370–1384, 2014.

[75] R. Duncan and L. Izzo, "Dendrimer biocompatibility and toxicity," *Advanced Drug Delivery Reviews*, vol. 57, no. 15, pp. 2215–2237, 2005.

[76] B. De la Riva, E. Sánchez, A. Hernández et al., "Local controlled release of VEGF and PDGF from a combined brushite-chitosan system enhances bone regeneration," *Journal of Controlled Release*, vol. 143, no. 1, pp. 45–52, 2010.

[77] A. Rampino, M. Borgogna, P. Blasi, B. Bellich, and A. Cesàro, "Chitosan nanoparticles: preparation, size evolution and stability," *International Journal of Pharmaceutics*, vol. 455, no. 1-2, pp. 219–228, 2013.

[78] W. S. Vedakumari, P. Prabu, and T. P. Sastry, "Chitosan-fibrin nanocomposites as drug delivering and wound healing

materials," *Journal of Biomedical Nanotechnology*, vol. 11, no. 4, pp. 657–667, 2015.

[79] I. K. Shim, W. H. Suh, S. Y. Lee et al., "Chitosan nano-/microfibrous double-layered membrane with rolled-up three-dimensional structures for chondrocyte cultivation," *Journal of Biomedial Materials Research Part A*, vol. 90, pp. 595–602, 2009.

[80] N. Poth, V. Seiffart, G. Gross, H. Menzel, and W. Dempwolf, "Biodegradable chitosan nanoparticle coatings on titanium for the delivery of BMP-2," *Biomolecules*, vol. 5, no. 1, pp. 3–19, 2015.

[81] U. Nagarajan, K. Kawakami, and S. Zhang, "Fabrication of solid collagen nanoparticles using electrospray deposition," *Pharmaceutical Bulletin*, vol. 62, no. 5, pp. 422–428, 2014.

[82] Y. Liu, Y. Lu, X. Tian et al., "Segmental bone regeneration using an rhBMP-2-loaded gelatin/nanohydroxyapatite/fibrin scaffold in a rabbit model," *Biomaterials*, vol. 30, no. 31, pp. 6276–6285, 2009.

[83] M. Jahanshahi, M. H. Sanati, S. Hajizadeh, and Z. Babaei, "Gelatin nanoparticle fabrication and optimization of the particle size," *Physica Status Solidi (a)*, vol. 205, no. 12, pp. 2898–2902, 2008.

[84] D. C. Miller, A. Thapa, K. M. Haberstroh, and T. J. Webster, "Endothelial and vascular smooth muscle cell function on poly(lactic-co- glycolic acid) with nano-structured surface features," *Biomaterials*, vol. 25, no. 1, pp. 53–61, 2004.

[85] F. Danhier, E. Ansorena, J. M. Silva, R. Coco, A. le Breton, and V. Préat, "PLGA-based nanoparticles: an overview of biomedical applications," *Journal of Controlled Release*, vol. 161, no. 2, pp. 505–522, 2012.

[86] M. A. Pattison, S. Wurster, T. J. Webster, and K. M. Haberstroh, "Three-dimensional, nano-structured PLGA scaffolds for bladder tissue replacement applications," *Biomaterials*, vol. 26, no. 15, pp. 2491–2500, 2005.

[87] C. Soundrapandian, A. Mahato, B. Kundu, S. Datta, B. Sa, and D. Basu, "Development and effect of different bioactive silicate glass scaffolds: in vitro evaluation for use as a bone drug delivery system," *Journal of the Mechanical Behavior of Biomedical Materials*, vol. 40, pp. 1–12, 2014.

[88] M. Baldrighi, M. Trusel, and R. Tonini, "Carbon nanomaterials interfacing with neurons: an in vivo perspective," *Frontiers in Neuroscience*, vol. 10, p. 250, 2016.

[89] B. Gorain, H. Choudhury, M. Pandey et al., "Carbon nanotube scaffolds as emerging nanoplatform for myocardial tissue regeneration: a review of recent developments and therapeutic implications," *Biomedicine & Pharmacotherapy*, vol. 104, pp. 496–508, 2018.

[90] Z. Zhu, "An overview of carbon nanotubes and graphene for biosensing applications," *Nano-Micro Letters*, vol. 9, no. 3, p. 25, 2017.

[91] L. Wang, C. Y. Wang, S. Wu, Y. Fan, and X. Li, "Influence of the mechanical properties of biomaterials on degradability, cell behaviors and signaling pathways: current progress and challenges," *Biomaterials Science*, vol. 8, no. 10, pp. 2714–2733, 2020.

[92] N. Bock, A. Riminucci, C. Dionigi et al., "A novel route in bone tissue engineering: magnetic biomimetic scaffolds," *Acta Biomaterialia*, vol. 6, no. 3, pp. 786–796, 2010.

[93] N. A. Usov, S. A. Gudoshnikov, N. Serebryakova, M. L. Fdez-Gubieda, A. Muela, and J. M. Barandiarán, "Properties of dense assemblies of magnetic nanoparticles promising for application in biomedicine," *Journal of Superconductivity and Novel Magnetism*, vol. 26, no. 4, pp. 1079–1083, 2013.

[94] E. Akaraonye, J. Filip, M. Safarikova et al., "Composite scaffolds for cartilage tissue engineering based on natural polymers of bacterial origin, thermoplastic poly(3-hydroxybutyrate) and micro-fibrillated bacterial cellulose," *Polymer International*, vol. 65, no. 7, pp. 780–791, 2016.

[95] A. Bhowmick, P. Jana, N. Pramanik et al., "Multifunctional zirconium oxide doped chitosan based hybrid nanocomposites as bone tissue engineering materials," *Carbohydrate Polymers*, vol. 151, pp. 879–888, 2016.

[96] S. Aliramaji, A. Zamanian, and M. Mozafari, "Super-paramagnetic responsive silk fibroin/chitosan/magnetite scaffolds with tunable pore structures for bone tissue engineering applications," *Materials Science and Engineering: C*, vol. 70, Part 1, pp. 736–744, 2017.

[97] J. H. Huang, J. Y. Xiong, D. P. Wang et al., "Performance of magnetic nanocomposite artificial bone scaffolds prepared by low-temperature rapid prototyping 3D printing," *Hainan Medical Journal (Hai Nan Yi Xue)*, vol. 6, no. 7, pp. 678–687, 2017.

[98] J. Meng, B. Xiao, Y. Zhang et al., "Super-paramagnetic responsive nanofibrous scaffolds under static magnetic field enhance osteogenesis for bone repair *in vivo*," *Scientific Reports*, vol. 3, no. 1, article 2655, 2013.

[99] R. K. Singh, K. D. Patel, J. H. Lee et al., "Potential of magnetic nanofiber scaffolds with mechanical and biological properties applicable for bone regeneration," *PloS One*, vol. 9, no. 4, article e91584, 2014.

[100] Y. J. Li, H. Chen, J. Wu et al., "Preparation and characterization of APTES modified magnetic MMT capable of using as anisotropic nanoparticles," *Applied Surface Science*, vol. 447, pp. 393–400, 2018.

[101] S. C. Zhao, M. Zhu, J. H. Zhang et al., "Three dimensionally printed mesoporous bioactive glass and poly(3-hydroxybutyrate-co-3-hydroxyhexanoate) composite scaffolds for bone regeneration," *Journal of Materials Chemistry, B*, vol. 2, no. 36, pp. 6106–6118, 2014.

[102] Z. du, X. X. Feng, G. X. Cao et al., "The effect of carbon nanotubes on osteogenic functions of adipose-derived mesenchymal stem cells _in vitro_ and bone formation _in vivo_ compared with that of nano-hydroxyapatite and the possible mechanism," *Bioactive Materials*, vol. 6, no. 2, pp. 333–345, 2021.

[103] C. Shuai, P. Feng, P. Wu et al., "A combined nanostructure constructed by graphene and boron nitride nanotubes reinforces ceramic scaffolds," *Chemical Engineering Journal*, vol. 313, pp. 487–497, 2017.

[104] K. Wójcik-Piotrowicz, J. Kaszuba-Zwoińska, E. Rokita, and P. Thor, "Cell viability modulation through changes of $Ca^{2+}$-dependent signalling pathways," *Progress in Biophysics and Molecular Biology*, vol. 121, no. 1, pp. 45–53, 2016.

[105] Y. Zhu, Q. Yang, M. Yang et al., "Protein corona of magnetic hydroxyapatite scaffold improves cell proliferation via activation of mitogen-activated protein kinase signaling pathway," *ACS Nano*, vol. 11, no. 4, pp. 3690–3704, 2017.

[106] E. Díaz, M. B. Valle, S. Ribeiro, S. Lanceros-Mendez, and J. Barandiarán, "Development of magnetically active scaffolds for bone regeneration," *Nanomaterials*, vol. 8, no. 9, p. 678, 2018.

[107] J. Wang, Y. An, F. Li et al., "The effects of pulsed electromagnetic field on the functions of osteoblasts on implant surfaces

with different topographies," *Acta Biomaterialia*, vol. 10, no. 2, pp. 975–985, 2014.

[108] A. Tampieri, S. Sprio, M. Sandri, and F. Valentini, "Mimicking natural bio-mineralization processes: a new tool for osteochondral scaffold development," *Trends in Biotechnology*, vol. 29, no. 10, pp. 526–535, 2011.

[109] M. Arjmand, A. Ardeshirylajimi, H. Maghsoudi, and E. Azadian, "Osteogenic differentiation potential of mesenchymal stem cells cultured on nanofibrous scaffold improved in the presence of pulsed electromagnetic field," *Journal of Cellular Physiology*, vol. 233, 2017.

[110] J. W. Lu, F. Yang, Q. Ke, X. T. Xie, and Y. P. Guo, "Magnetic nanoparticles modified-porous scaffolds for bone regeneration and photothermal therapy against tumors," *Nanomedicine*, vol. 14, no. 3, pp. 811–822, 2018.

[111] M. Cruz-Acuña, J. R. Halman, K. A. Afonin, J. Dobson, and C. Rinaldi, "Magnetic nanoparticles loaded with functional RNA nanoparticles," *Nanoscale*, vol. 10, no. 37, pp. 17761–17770, 2018.

[112] J. H. Kuai, Q. Wang, A. J. Zhang et al., "Epidermal growth factor receptor-targeted immune magnetic liposomes capture circulating colorectal tumor cells efficiently," *World Journal of Gastroenterology*, vol. 24, no. 3, pp. 351–359, 2018.

[113] C. Luo, X. Yang, M. Li et al., "A novel strategy forin vivoangiogenesis and osteogenesis: magnetic micromovement in a bone scaffold," *Artificial Cells, Nanomedicine, and Biotechnology*, vol. 46, Supplement 2, pp. 636–645, 2018.

[114] F. D. Cojocaru, V. Balan, M. I. Popa et al., "Biopolymers - calcium phosphates composites with inclusions of magnetic nanoparticles for bone tissue engineering," *International Journal of Biological Macromolecules*, vol. 125, pp. 612–620, 2019.

[115] Z. Y. Liu, J. H. Liu, X. Cui, X. Wang, L. Zhang, and P. Tang, "Recent advances on magnetic sensitive hydrogels in tissue engineering," *Frontiers in Chemistry*, vol. 8, p. 124, 2020.

[116] Z. F. Huang, Y. He, X. Chang et al., "A magnetic iron oxide/-polydopamine coating can improve osteogenesis of 3D-Printed porous titanium scaffolds with a static magnetic field by upregulating the TGF$\beta$-Smads pathway," *Advanced Healthcare Materials*, vol. 9, no. 14, p. 2000318, 2020.

[117] C. Shuai, W. Yang, C. He et al., "A magnetic microenvironment in scaffolds for stimulating bone regeneration," *Materials & Design*, vol. 185, article 108275, 2019.

[118] Y. Xia, Y. Guo, Z. Yang et al., "Iron oxide nanoparticle-calcium phosphate cement enhanced the osteogenic activities of stem cells through WNT/$\beta$-catenin signalling - ScienceDirect," *Materials Science and Engineering: C*, vol. 104, 2019.

[119] A. S. Saraiva, I. A. C. Ribeiro, M. H. Fernandes et al., "3D-printed platform multi-loaded with bioactive, magnetic nanoparticles and an antibiotic for re-growing bone tissue," *International Journal of Pharmaceutics X*, vol. 593, pp. 120097–120097, 2020.

[120] H.-Y. Lin, H.-Y. Huang, S.-J. Shiue, and J.-K. Cheng, "Osteogenic effects of inductive coupling magnetism from magnetic 3D printed hydrogel scaffold," *Journal of Magnetism and Magnetic Materials*, vol. 504, 2020.

[121] F. Ghorbani, A. Zamanian, A. Shams, A. Shamoosi, and A. Aidun, "Fabrication and characterisation of super-paramagnetic responsive PLGA–gelatine–magnetite scaffolds with the unidirectional porous structure: a physicochemical, mechanical, andin vitroevaluation," *IET Nanobiotechnology*, vol. 13, no. 8, pp. 860–867, 2019.

[122] J. J. Kim, R. K. Singh, S. J. Seo et al., "Magnetic scaffolds of polycaprolactone with functionalized magnetite nanoparticles: physicochemical, mechanical, and biological properties effective for bone regeneration," *RSC Advances*, vol. 4, no. 33, pp. 17325–17336, 2014.

[123] H. Wang, S. Zhao, J. Zhou et al., "Biocompatibility and osteogenic capacity of borosilicate bioactive glass scaffolds loaded with Fe3O4magnetic nanoparticles," *Journal of Materials Chemistry B*, vol. 3, no. 21, article 4377, 4387 pages, 2015.

[124] Y. Watanabe, N. Harada, K. Sato, S. Abe, K. Yamanaka, and T. Matushita, "Stem cell therapy: is there a future for reconstruction of large bone defect?," *Injury*, vol. 47, pp. S47–S51, 2016.

[125] M. Barrow, A. Taylor, P. Murray, M. J. Rosseinsky, and D. J. Adams, "Design considerations for the synthesis of polymer at iron oxide nanoparticles for stem labelling and tracking using MRI," *Chemical Society Reviews*, vol. 44, no. 19, pp. 6733–6748, 2015.

[126] Y. Jia, P. Zhang, Y. Sun et al., "Regeneration of large bone defects using mesoporous silica coated magnetic nanoparticles during distraction osteogenesis," *Nanomedicine: Nanotechnology, Biology and Medicine*, vol. 21, article 102040, 2019.

[127] W. Yang, P. Zhu, H. Huang et al., "Functionalization of novel theranostic hydrogels with kartogenin-grafted USPIO nanoparticles to enhance cartilage regeneration," *ACS Applied Materials & Interfaces*, vol. 11, no. 38, pp. 34744–34754, 2019.

[128] C. Xu, S. Wang, L. Liu, S. Yu, X. Wu, and H. Dai, "Manipulating mesenchymal stem cells differentiation under sinusoidal electromagnetic fields using intracellular superparamagnetic nanoparticles," *Journal of Biomedical Nanotechnology*, vol. 15, no. 2, pp. 301–310, 2019.

[129] M. Tatullo, M. Marrelli, K. M. Shakesheff, and L. J. White, "Dental pulp stem cells: function, isolation and applications in regenerative medicine," *Journal of Tissue Engineering and Regenerative Medicine*, vol. 9, no. 11, pp. 1205–1216, 2015.

[130] B. Lindroos, K. Mäenpää, T. Ylikomi, H. Oja, R. Suuronen, and S. Miettinen, "Characterisation of human dental stem cells and buccal mucosa fibroblasts," *Biochemical and Biophysical Research Communications*, vol. 368, no. 2, pp. 329–335, 2008.

[131] R. d'Aquino, A. Graziano, M. Sampaolesi et al., "Human postnatal dental pulp cells co-differentiate into osteoblasts and endotheliocytes: a pivotal synergy leading to adult bone tissue formation," *Cell Death and Differentiation*, vol. 14, no. 6, pp. 1162–1171, 2007.

[132] R. d'Aquino, G. Papaccio, G. Laino, and A. Graziano, "Dental pulp stem cells: a promising tool for bone regeneration," *Stem Cell Reviews*, vol. 4, no. 1, pp. 21–26, 2008.

[133] Q. Wang, B. Chen, F. Ma et al., "Magnetic iron oxide nanoparticles accelerate osteogenic differentiation of mesenchymal stem cells via modulation of long noncoding RNA INZEB2," *Nano Research*, vol. 10, no. 2, pp. 626–642, 2017.

[134] A. H. Silva, E. Lima, M. V. Mansilla et al., "Superparamagnetic iron-oxide nanoparticles mPEG350- and mPEG2000-coated: cell uptake and biocompatibility evaluation," *Nanomedicine*, vol. 12, no. 4, pp. 909–919, 2016.

[135] P. Hua, Y. Y. Wang, L. B. Liu et al., "In vivo magnetic resonance imaging tracking of transplanted superparamagnetic iron oxide-labeled bone marrow mesenchymal stem cells in

rats with myocardial infarction," *Molecular Medicine Reports*, vol. 11, no. 1, pp. 113–120, 2015.

[136] L. H. A. Silva, M. C. Silva, J. B. Vieira et al., "Magnetic targeting increases mesenchymal stromal cell retention in lungs and enhances beneficial effects on pulmonary damage in experimental silicosis," *Stem Cells Translational Medicine*, vol. 9, no. 10, pp. 1244–1256, 2020.

[137] R. Shelat, L. K. Bhatt, B. Paunipagar, T. Kurian, A. Khanna, and S. Chandra, "Regeneration of hyaline cartilage in osteochondral lesion model using L-lysine magnetic nanoparticles labeled mesenchymal stem cells and their In Vivo imaging," *Journal of Tissue Engineering and Regenerative Medicine*, vol. 14, no. 11, pp. 1604–1617, 2020.

[138] D. Yao, N. N. Liu, and B. W. Mo, "Assessment of proliferation, migration and differentiation potentials of bone marrow mesenchymal stem cells labeling with silica-coated and amine-modified superparamagnetic iron oxide nanoparticles," *Cytotechnology*, vol. 72, no. 4, pp. 513–525, 2020.

[139] A. B. Mathiasen, A. A. Qayyum, E. Jørgensen et al., "In vivo MRI tracking of mesenchymal stromal cells labeled with ultrasmall paramagnetic iron oxide particles after intramyocardial transplantation in patients with chronic ischemic heart disease," *Stem Cells International*, vol. 2019, Article ID 2754927, 10 pages, 2019.

[140] R. Jiang, Y. Liao, F. Yang, Y. Cheng, X. Dai, and J. Chao, "SPIO nanoparticle-labeled bone marrow mesenchymal stem cells inhibit pulmonary EndoMT induced by $SiO_2$," *Experimental Cell Research*, vol. 383, no. 1, p. 111492, 2019.

[141] A. Nel, T. Xia, L. Mädler, and N. Li, "Toxic potential of materials at the nanolevel," *Science*, vol. 311, no. 5761, pp. 622–627, 2006.

[142] U. O. Häfeli, J. S. Riffle, L. Harris-Shekhawat et al., "Cell uptake and in vitro toxicity of magnetic nanoparticles suitable for drug delivery," *Molecular Pharmaceutics*, vol. 6, no. 5, pp. 1417–1428, 2009.

[143] G. Oberdorster, V. Stone, and K. Donaldson, "Toxicology of nanoparticles: a historical perspective," *Nanotoxicology*, vol. 1, no. 1, pp. 2–25, 2007.

[144] P. Møller, N. R. Jacobsen, J. K. Folkmann et al., "Role of oxidative damage in toxicity of particulates," *Free Radical Research Communications*, vol. 44, no. 1, pp. 1–46, 2010.

[145] K. Unfried, C. Albrecht, L.-O. Klotz, A. Von Mikecz, S. Grether-Beck, and R. P. F. Schins, "Cellular responses to nanoparticles: target structures and mechanisms," *Nanotoxicology*, vol. 10, no. 6, pp. 52–71, 2007.

[146] A. Elias, "Imaging circulating cells and lymphoid tissues with iron oxide nanoparticles," *Hematology*, vol. 2009, no. 1, pp. 720–726, 2009.

[147] B. Ankamwar, T. C. Lai, J. H. Huang et al., "Biocompatibility of Fe3O4nanoparticles evaluated byin vitrocytotoxicity assays using normal, glia and breast cancer cells," *Nanotechnology*, vol. 21, no. 7, p. 075102, 2010.

[148] J. Bulte, T. Douglas, B. Witwer et al., "Magnetodendrimers allow endosomal magnetic labeling and _in vivo_ tracking of stem cells," *Nature Biotechnology*, vol. 19, no. 12, pp. 1141–1147, 2001.

[149] J. M. Veranth, E. G. Kaser, M. M. Veranth, M. Koch, and G. S. Yost, "Cytokine responses of human lung cells (BEAS-2B) treated with micron-sized and nanoparticles of metal oxides compared to soil dusts," *Particle and Fibre Toxicology*, vol. 4, no. 1, pp. 1–18, 2007.

[150] N. Singh, "Conference scene - nanotoxicology: health and environmental impacts," *Nanomedicine*, vol. 4, no. 4, pp. 385–390, 2009.

[151] Z. G. M. Lacava, R. B. Azevedo, L. M. Lacava et al., "Toxic effects of ionic magnetic fluids in mice," *Journal of Magnetism and Magnetic Materials*, vol. 194, no. 1-3, pp. 90–95, 1999.

[152] J. Xie, G. Liu, H. S. Eden, H. Ai, and X. Chen, "Surface-engineered magnetic nanoparticle platforms for cancer imaging and therapy," *Accounts of Chemical Research*, vol. 44, no. 10, pp. 883–892, 2011.

[153] C. C. Berry, S. Wells, S. Charles, and A. S. G. Curtis, "Dextran and albumin derivatised iron oxide nanoparticles: influence on fibroblasts in vitro," *Biomaterials*, vol. 24, no. 25, pp. 4551–4557, 2003.

[154] C. C. Berry, S. Wells, S. Charles, G. Aitchison, and A. S. G. Curtis, "Cell response to dextran-derivatised iron oxide nanoparticles post internalisation," *Biomaterials*, vol. 25, no. 23, pp. 5405–5413, 2004.

[155] A. Hanini, A. Schmitt, K. Kacem, F. Chau, S. Ammar, and J. Gavard, "Evaluation of iron oxide nanoparticle biocompatibility," *International Journal of Nanomedicine*, vol. 6, pp. 787–794, 2011.

[156] J. Curtis, M. Greenberg, J. Kester, S. Phillips, and G. Krieger, "Nanotechnology and nanotoxicology," *Toxicological Reviews*, vol. 25, no. 4, pp. 245–260, 2006.

[157] S. M. Moghimi, A. C. Hunter, and J. C. Murray, "Nanomedicine: current status and future prospects," *Faseb Journal*, vol. 19, no. 3, pp. 311–330, 2005.

[158] R. Weissleder, D. D. Stark, B. L. Engelstad et al., "Superparamagnetic iron oxide: pharmacokinetics and toxicity," *American Journal of Roentgenology*, vol. 152, no. 1, pp. 167–173, 1989.

Hindawi
Journal of Nanomaterials
Volume 2021, Article ID 6237130, 11 pages
https://doi.org/10.1155/2021/6237130

*Research Article*

# Repair of Osteoporotic Bone Defects Using Adipose-Derived Stromal Cells and Umbilical Vein Endothelial Cells Seeded in Chitosan/Nanohydroxyapatite-P24 Nanocomposite Scaffolds

**Yifei Fang**,[1] **Yong Gong**,[2] **Zhijian Yang**,[1] **and Yan Chen**[3]

[1]*Department of Orthopedics, Zhujiang Hospital, Southern Medical University, Guangzhou 510282, China*
[2]*Department of Orthopedics, The Sixth Affiliated Hospital, Sun Yat-sen University, Guangzhou 510655, China*
[3]*Department of Ultrasonic Diagnosis, Zhujiang Hospital, Southern Medical University, Guangzhou 510282, China*

Correspondence should be addressed to Yan Chen; smu_chen@163.com

Received 27 May 2021; Accepted 29 July 2021; Published 21 August 2021

Academic Editor: Hui Qi Xie



*Background*. The cell regeneration and blood supply of bone defect lesions are restricted under osteoporotic pathological conditions, which make the healing of bone defect of osteoporosis still a great challenge. The current therapeutic strategies that mainly inhibit bone resorption are not always satisfactory for osteoporotic bone defects, which make the development of new therapies an urgent need. *Methods*. Previously, we prepared chitosan/nanohydroxyapatite (CS/nHA) biomimetic nanocomposite scaffolds for controlled delivery of bone morphogenetic protein 2-derived peptide (P24). In this study, we determined the effect of coculturing adipose-derived stromal cells (ADSCs) and human umbilical vein endothelial cells (HUVECs) with the CS-P24/nHA nanocomposite scaffolds on osteoporotic bone defect healing. In vitro mixed coculture models were employed to assess the direct effects of coculture. *Results*. ADSCs cocultured with HUVECs showed significantly greater osteogenic differentiation and mineralization compared with ADSCs or HUVECs alone. The CS-P24/nHA scaffold cocultured with ADSCs and HUVECs was more effective in inducing osteoporotic bone repair, as demonstrated by micro-computed tomography and histology of critical-sized calvariae defects in ovariectomized rats. Calvariae defects treated with the CS-P24/nHA nanocomposite scaffold plus ADSC/HUVEC coculture had a greater area of repair and better reconstitution of osseous structures compared with defects treated with the scaffold plus ADSCs or the scaffold plus HUVECs after 4 and 8 weeks. *Conclusion*. Taken together, coculture of ADSCs and HUVECs with the CS-P24/nHA nanocomposite scaffold is an effective combination to repair osteoporotic bone defects.

## 1. Introduction

Osteoporosis is a metabolic systemic bone disease characterized by decreased bone mass, increased bone fragility, and weakened bone strength [1]. More than 8 million fractures are caused by osteoporosis every year worldwide, and osteoporosis is the leading cause of fracture in older women [2]. More than one-third of older women experience osteoporosis-induced fracture [2]. Antibone resorption drugs are the most widely used in the clinic, including parathyroid hormone, bisphosphonate, raloxifene, and dinozumab [3, 4]. These drugs exert therapeutic effects by inhibiting osteoclast activity and bone resorption; however, they do not influence bone regeneration, so it is difficult to reconstruct bone using these approaches [5, 6]. For patients with osteoporotic bone defects, due to the significantly weakened ability of mesenchymal stem cell (MSC) regeneration and osteogenic differentiation, antibone resorption therapy alone is insufficient; thus, bone regeneration therapy is required [7, 8]. Existing bone defect implants, such as autogenous bone and artificial bone, are considered to lack sufficient biological activity to induce differentiation of endogenous MSCs into osteoblasts in patients with osteoporosis. They also have an insufficient effect on osteoporotic bone regeneration [9]. Therefore, there is an urgent need to improve bone defect implants to achieve osteoporotic bone regeneration.

Although biological implants have more advantages compared with autogenous bone, they do have shortcomings such as ischemic necrosis and apoptosis of implanted cells in the early stage of transplantation, which are caused by an insufficient blood supply [10]. In bone tissue engineering, neovascularization can facilitate oxygen and nutrient exchange between implants and cells, which is important for the survival and differentiation of stem cells in scaffolds [11, 12]. Studies have shown that microvessel formation is a prerequisite for bone formation in implants [11]. Whether it is the exchange of oxygen and nutrients or the calcium and phosphorus needed for mineralization, a complete vascular network is essential [13].

Methods to promote microvessel growth include the use of cytokines, such as vascular endothelial growth factor (VEGF) and basic fibroblast growth factor (bFGF), as well as endothelial cell transplantation [11]. Cytokines are expensive, and their release and onset of effects in the body are difficult to control, so endothelial cells are preferred [14]. Endothelial cells are the cellular source of microangiogenesis and play an important role in vasculogenesis and angiogenesis [15]. Moreover, endothelial cells can be simply extracted from peripheral blood, which not only causes little damage to the donor but also reduces the likelihood of rejection after autologous cell transplantation [15]. Implantation of endothelial cells into the scaffold can provide nutritional support to the vasculature for osteogenic differentiation of stem cells. Previous studies have shown that coculturing endothelial cells and stem cells in the scaffold can induce graft blood vessel formation and achieve vascularization and osteogenesis simultaneously [12, 13, 15, 16]. Therefore, efforts to establish a system to coculture endothelial cells and stem cells in bone tissue engineering have been made. To apply the concept of endothelial cell and stem cell coculture in the clinic, it is important to determine whether endothelial cells and stem cells are beneficial or harmful in osteogenic differentiation and angiogenesis when used to treat bone defects.

Sulfhydrylated chitosan (CS) is obtained by amino modification of CS [17]. Compared with ordinary CS, sulfhydrylated CS has better adhesion, stability, and protein release properties [18]. The CS/nanohydroxyapatite (HA) nanocomposite scaffold prepared using sulfhydrylated CS and nanohydroxyapatite has widespread application potential in cell colonization and factor release because of its porous structure, excellent biocompatibility, and moderate degradation rate [19]. P24 is a peptide derived from bone morphogenetic protein (BMP-2). It has a low molecular weight and a stable structure, as well as similar biological effects to BMP-2 [19]. P24 can regulate the adhesion and osteogenic differentiation of MSCs, promote deposition of calcium and phosphate ions, and accelerate nucleation and mineralization [20]. Due to the high therapeutic dose of BMP-2 in clinical application, it is easy to lead to complications such as excessive bone resorption, heterotopic ossification, and tumor angiogenesis [21]. P24, which has similar biological effects and is more absorbable, is an excellent alternative to BMP-2. In a previous study, CS/nHA nanocomposite scaffold was prepared using chemical grafting modification technology, and this scaffold was used to control P24 delivery [19]. The results show that the scaffold has a good effect on repairing bone defects in rats. To further expand the application of this CS/nHA nanocomposite scaffold in the treatment of osteoporotic bone defects, we intend to use cell coculture to further enhance the ability of this scaffold to repair bone defects.

The purpose of this study was to investigate the effect of adipose-derived stromal cell (ADSC) and human umbilical endothelial cell (HUVEC) coculture with the CS-P24/nHA nanocomposite scaffold in repairing osteoporotic bone defects. We also aimed to explore the application prospects of this coculture system.

## 2. Methods

*2.1. Materials.* Chitosan (CS, viscosity: 50–800 mPa·s, degree of deacetylation: 80%–95%) was purchased from Macklin, China. Peptide 24 (P24) derived from BMP-2 (N → C: KIPKA SSVPT ELSAI STLYL SGGC) was synthesized by Shanghai ZiYu Biotech Co., China. 2-Iminothiolane hydrochloride, 2-iminothiolane hydrochloride, and dimethyl sulfoxide (DMSO) were purchased from Sigma-Aldrich, USA. nHA powder was obtained from Institute of Nuclear and New Energy Technology, Tsinghua University, China.

*2.2. Culture of ADSCs and HUVECs.* Human ADSCs were isolated following established methods. The procedure was approved by the Research Committee of South Medical University. Briefly, adipose tissue samples were collected from patients undergoing reconstructive surgery. Adipose tissue was digested in 50-200 U/ml collagenase type I (Sigma-Aldrich, USA) for 2 h. The suspension was oscillated at a constant temperature of 37°C for 2 hours and then centrifuged at 5000$g$ for 10 minutes. The cells obtained after centrifugation were cultured in expansion medium consisting of Dulbecco's modified Eagle's medium/F-12, 10% fetal bovine serum (FBS; Gibco BRL), and 1% penicillin/streptomycin. HUVECs were obtained from the American Type Culture Collection (Rockville, MD, USA) and cultured in RPMI 1640 medium (Gibco, USA) containing 10% FBS and 1% penicillin/streptomycin [1]. Cells at passages 3–4 were used in this study. Cells were cultured under standard conditions (5% $CO_2$, 37°C).

*2.3. Scaffold Synthesis and ADSC/HUVEC Coculture.* Scaffolds containing CS with 0% P24 and nHA (CS-0%P24/nHA) and scaffolds containing CS with 10% P24 and nHA (CS-10%P24/nHA) were prepared as outlined previously [19]. Briefly, 40 mg of 2-iminothiolane hydrochloride was added to 200 ml of 0.2% ($w/v$) chitosan solution (in 1% acetic acid). P24 (0% or 10% of the weight of chitosan in 15 ml DMSO) was then added into the chitosan solution. After continuous stirring at room temperature for 4 h, the mixture was dialyzed against deionized water for 5 days and lyophilized at −50°C and 20 Pa in order to immobilize the peptide within the chitosan (chitosan-peptide 24, CS-0%P24, and CS-10%P24).

200 mg of CS-0%P24 and CS-10%P24 were hydrated in 10 ml 0.1 M HCl, respectively. nHA powder (200 mg) was added with continuous stirring until uniformly distributed.

Thereafter, the hybrid of CS-P24 and HA was lyophilized at −50°C and 20 Pa using a 96-well plate (Corning, USA) as a mold to obtain the CS-0%P24/HA and CS-10%P24/HA scaffold.

With the CS-10%P24/nHA scaffold cultured with ADSCs and HUVECs, these two cell types were trypsinized separately and subcultured in 24-well plates at ratios of 1 : 1, 1 : 3, and 3 : 1 during the same seeding phase. The CS-10%P24/nHA scaffold cultured with ADSCs or HUVECs served as a control.

*2.4. Cell Proliferation Assay.* Cell proliferation was measured using the Cell Counting Kit-8 (CCK-8; Dojindo). With the CS-10%P24/nHA scaffold cultured with ADSCs and HUVECs, cells were trypsinized separately and subcultured in 96-well plates at ratios of 1 : 1, 1 : 3, and 3 : 1. Each group has 6 experimental samples. After 1, 3, and 7 days, cells in each group were incubated in 10% CCK-8 solution in a 5% $CO_2$ incubator at 37°C for 4 h. The absorbance of the culture medium was measured at 450 nm.

*2.5. Alizarin Red S Staining.* Alizarin Red S staining and quantification were performed as described previously [22]. Cells in different groups were stained 21 days after culture, and each group has 6 experimental samples. Cells were fixed in 4% paraformaldehyde (Leagene, China) for 15 min. After being fixed, cells were stained with 1% Alizarin Red S for 30 min. Stained samples were air dried, and images were taken using an optical microscope (Leica, DM2500 LED).

*2.6. Real-Time Quantitative PCR.* After 10 days of coculture, total RNA was isolated by lysis in TRIzol (Invitrogen Inc., Carlsbad, CA, USA). PCR was performed using the Transcriptor cDNA Synthesis Kit and FastStart Universal SYBR Green Master (Roche Diagnostics, Indianapolis, IN, USA). The mRNA expressions of osteogenic-specific genes (OCN, ALP, and RUNX2) were assessed by real-time quantitative PCR using SYBR Green Master (Roche Diagnostics). The sequences of all primers (Invitrogen Inc.) were designed using Primer 5.0 software (Table 1). $\beta$-Actin was amplified as an internal control. Each real-time quantitative PCR run was performed using three experimental samples. Error bars reflect one standard deviation from the mean of technical replicates.

*2.7. In Vivo Calvaria Defect Repair*

*2.7.1. Osteoporotic Rat Model and Transplantation Procedure.* To generate osteoporotic rat models, 36 female Sprague-Dawley rats (200-220 g) at 7 weeks of age ($n = 6$) were purchased from the Center of Experimental Animals of Guangdong Province. Rats were ovariectomized bilaterally with a dorsal approach. After 4 weeks, under general anesthesia, the cranium was exposed through a medial incision. Bilateral full-thickness circular defects of 5 × 5 mm were generated using a dental bur. The defects were implanted with CS-0%P24/nHA, CS-10%P24/nHA, CS-10%P24/nHA with ADSCs, CS-10%P24/nHA with HUVECs, or CS-10%P24/nHA with ADSC/HUVEC coculture. The coculture ration of ADSCs and HUVECs was 3 : 1. The control groups were left untreated. In all animals, the wound was irrigated, and the fascia and skin were closed. Postoperatively, animals were allowed free cage activity. To establish an osteoporosis model, the rats were injected with cyclosporine A (5 mg/kg of body weight) and methylprednisolone hemisuccinate (1 mg/kg body weight) daily after surgery. Whole calvariae were harvested for evaluation 4 and 8 weeks of postimplantation.

Table 1: Forward and reverse primer sequences used in real-time PCR analysis.

| Gene | | Primer (5′–3′) |
|---|---|---|
| OCN | Forward primer | GCTCTGTGCTCCTGCATCTG |
| | Reverse primer | GCTCTGTGCTCCTGCATCTG |
| ALP | Forward primer | ACCATTCCCACGTCTTCACATTT |
| | Reverse primer | AGACATTCTCTCGTTCACCGCC |
| RUNX2 | Forward primer | GCCTTCAAGGTGGTAGCCC |
| | Reverse primer | CGTTACCCGCCATGACAGTA |

*2.7.2. Micro-Computed Tomography (CT) Analysis of Calvaria Defect Repair.* After harvesting calvariae at 4 and 8 weeks postoperatively, specimens were immediately fixed in 10% (*v*/*v*) neutral-buffered formalin for 24 h. Specimens were scanned at a resolution of 9 $\mu$m for undecalcified samples using an advanced micro-CT instrument (ZKKS-MC-Sharp-IV; Zhongke Kaisheng Bio, Inc.). Three-dimensional reconstruction of images was performed, and histomorphometric parameters, including bone mineral density (BMD), trabecular number (Tb.N), and bone volume/total tissue volume (BV/TV), were evaluated.

*2.7.3. Immunofluorescence, Immunohistochemistry, and Histomorphometry.* Specimens were decalcified in neutral 10% EDTA solution for 2 weeks at room temperature. Slices were then cut into 6 $\mu$m sections and further stained with anti-OCN (1 : 500 dilution; Abcam) and anti-CD31 (1 : 600 dilution; Abcam), respectively, at 4°C overnight, followed by horseradish peroxidase-conjugated goat anti-rabbit secondary antibodies (Boster Company of Biotechnology, China). Images of stained specimens were obtained using a microscope (BX51; Olympus, Tokyo, Japan). The expression intensity of each molecule was quantified using ImageJ analysis software (1.8.0 64-bit, US National Institutes of Health).

For immunofluorescence analysis, slides or chondrocytes were fixed in 4% buffered formalin and incubated with fluorescence-conjugated secondary antibody for 90 min at room temperature. Sections were also stained with hematoxylin and eosin, Masson's trichrome, or tartrate-resistant acid phosphatase (TRAP).

*2.7.4. Cell Tracking Using Anti-Human Nuclear Antibody.* Sections from each group at 4 and 8 weeks were used postoperatively for cell tracking analysis. Sections were stained with mouse anti-human nuclei monoclonal antibody (MAB1281; 1 : 500 dilution; Merck Millipore, Germany) for immunofluorescence and immunohistochemistry. MAB1281-labeled cells were marked.

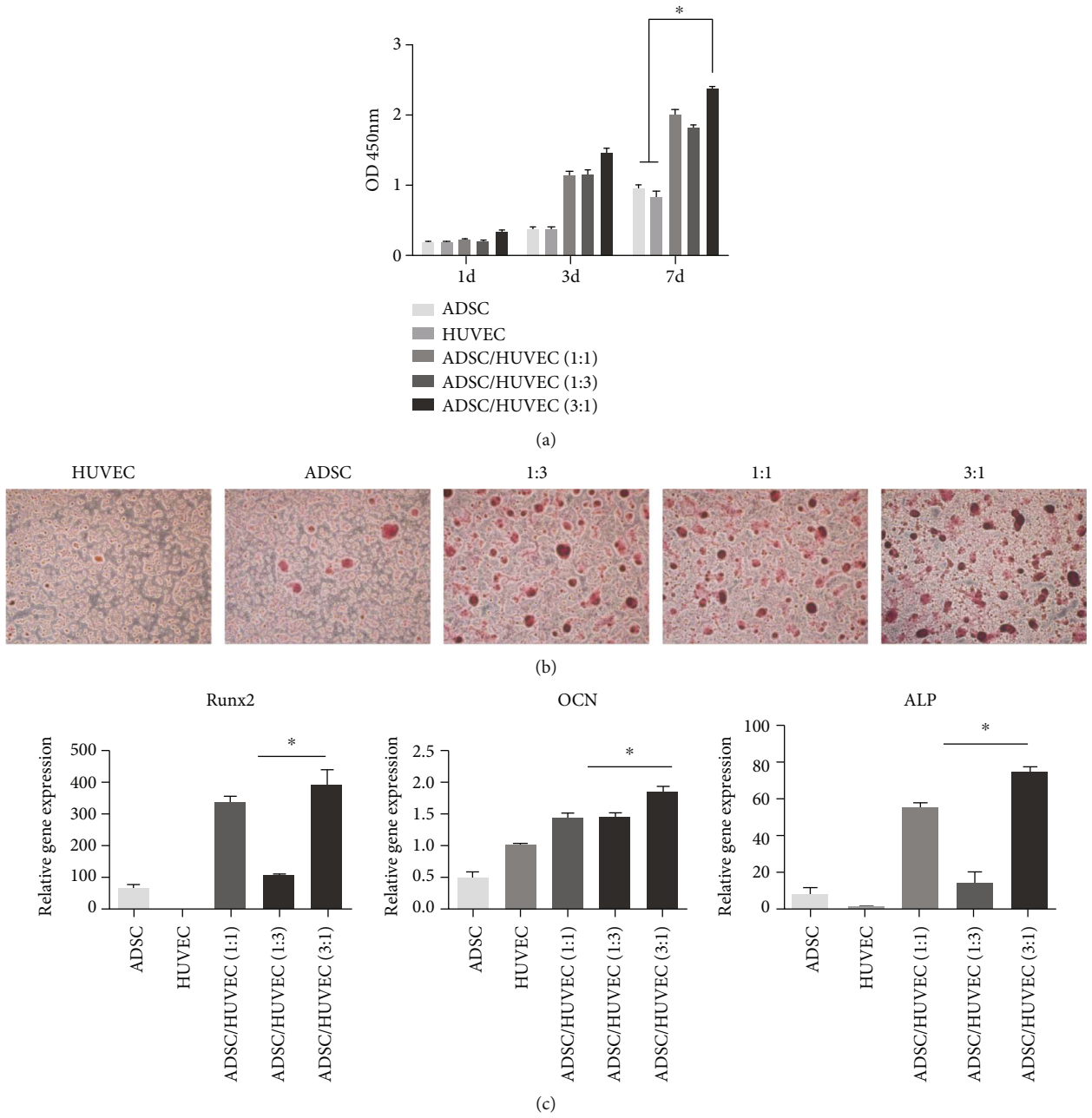


Figure 1: *In vitro* osteogenesis and angiogenesis. ASC/HUVEC ratios of 1 : 1, 1 : 3, and 3 : 1 were achieved by culturing $1 \times 10^5$, $0.3 \times 10^5$, and $3.0 \times 10^5$ ADSCs, respectively, with $10^5$ HUVECs. (a) The CCK-8 test of cell viability after coculture for 1, 3, and 7 days. (b) Alizarin Red S staining after 14 days. All values are shown as percentages compared with control. (c) mRNA expression of osteogenic-specific genes (*ALP*, *OCN*, and *RUNX2*) in each group at 10 days. mRNA expression, quantified using real-time quantitative PCR, was normalized to $\beta$-actin as a reference gene. $^*p < 0.05$. Error bars represent the standard deviation ($n = 3$).

*2.8. Statistical Analysis.* Descriptive statistics were used to determine group means and standard deviations. Quantitative data were statistically analyzed using Student's *t*-test (SPSS 22.0). A *p* value of <0.05 was considered statistically significant.

## 3. Results

*3.1. In Vitro Osteogenesis.* To determine the effect of coculture on cell growth, ADSCs, HUVECs, or ADSCs plus HUVECs at ratios of 1 : 1, 1 : 3, and 3 : 1 were seeded onto CS-10%P24/nHA scaffolds. Cell proliferation was measured using the CCK-8 assay. The CCK-8 analysis showed that cell number significantly increased in each of the ADSC, HUVEC, and ADSC/HUVEC coculture groups. No matter what the ratio of cells was, the proliferation rate in the ADSC/HUVEC coculture group was significantly higher than that in the ADSC and HUVEC groups. When the ratio of ADSCs to HUVECs was 3 : 1, the proliferation rate was the most significant, and the absorbance on day 7 was about 2.4

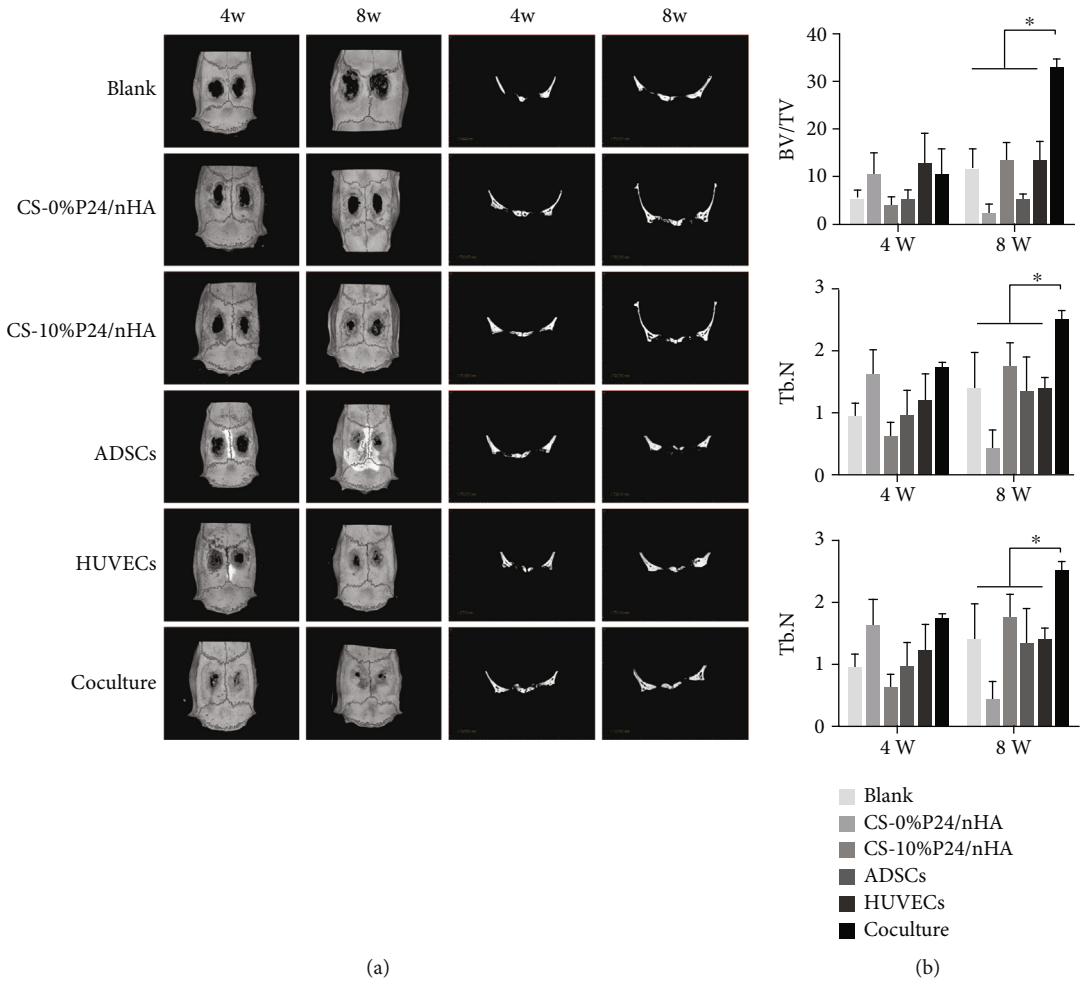


Figure 2: *In vivo* effects of the scaffold plus ADSC/HUVEC coculture on osteoporotic bone formation in critical-sized calvariae defects. Two circular defects, each with a diameter of 3 mm, were created using a trephine bur in mice calvariae. Defects were filled with a CS-0%P24/nHA scaffold, a CS-10%P24/nHA scaffold, or a CS-10%P24/nHA scaffold with HUVECs and/or ADSCs. (a) Reconstructed three-dimensional micro-CT images at 4 and 8 weeks in each group. Micro-CT of whole calvariae in each group, indicating new bone formation at the defect site. (b) Quantitative analysis of mineralized new bone formation at 4 and 8 weeks (BMD, Tb.N, and BV/TV). $^{*}p < 0.05$.

and 2.7 times of that in the ADSC and HUVEC groups (Figure 1(a)).

Alizarin Red S staining was used to evaluate calcium deposition in each group. HUVECs cultured alone appeared light red in color, ADSCs cultured alone appeared as a deeper red color, while cocultured ADSCs/HUVECs appeared as a very deep red color. Although mineralized nodules were observed in all three groups, more distinct nodules were observed in the ADSC/HUVEC coculture group on day 21 (Figure 1(b)).

To evaluate the effect of the CS-P24/nHA scaffold cultured with ADSCs, HUVECs, or ADSCs plus HUVECs on osteogenic differentiation, we performed real-time quantitative PCR to examine osteogenic gene expression. *RUNX2*, *OCN*, and *ALP* were significantly upregulated in the ADSC/HUVEC coculture group (Figure 1(c)). When the ratio of ADSCs to HUVECs was 3 : 1, the expression levels of RUNX2, OCN, and ALP were the highest among all groups.

These results suggested that when ADSCs and HUVECs were cocultured at a ratio of 3 : 1, the degree of cell proliferation and osteogenic differentiation was the most significant. Therefore, in subsequent experiments, 3 : 1 was used as the cell ratio of ADSC and HUVEC coculture.

*3.2. In Vivo Effects of ADSC/HUVEC Coculture on Osteoporotic Bone Formation.* In vivo osteoporotic bone formation was evaluated by micro-CT at 4 and 8 weeks of postimplantation (Figure 2). When CS-10%P24/nHA scaffolds were used to treat critical-sized calvariae defects (control group), most osteoporotic bone defects were not repaired after 8 weeks (Figure 2(a)). Scaffolds with HUVECs alone, ADSC/HUVEC coculture, and ADSCs alone significantly increased the repaired area ($p < 0.05$) compared with the control scaffold (Figure 2(b)). Defects treated with the scaffold plus ADSC/HUVEC coculture had significantly greater BMD ($442.50 \pm 15.00$), Tb.N ($2.52 \pm 0.25$), and BV/TV ($33.00 \pm 3.28$) values compared with the other groups ($p < 0.05$).

Histological findings showed that calvariae defects treated with the scaffold plus ADSC/HUVEC coculture had

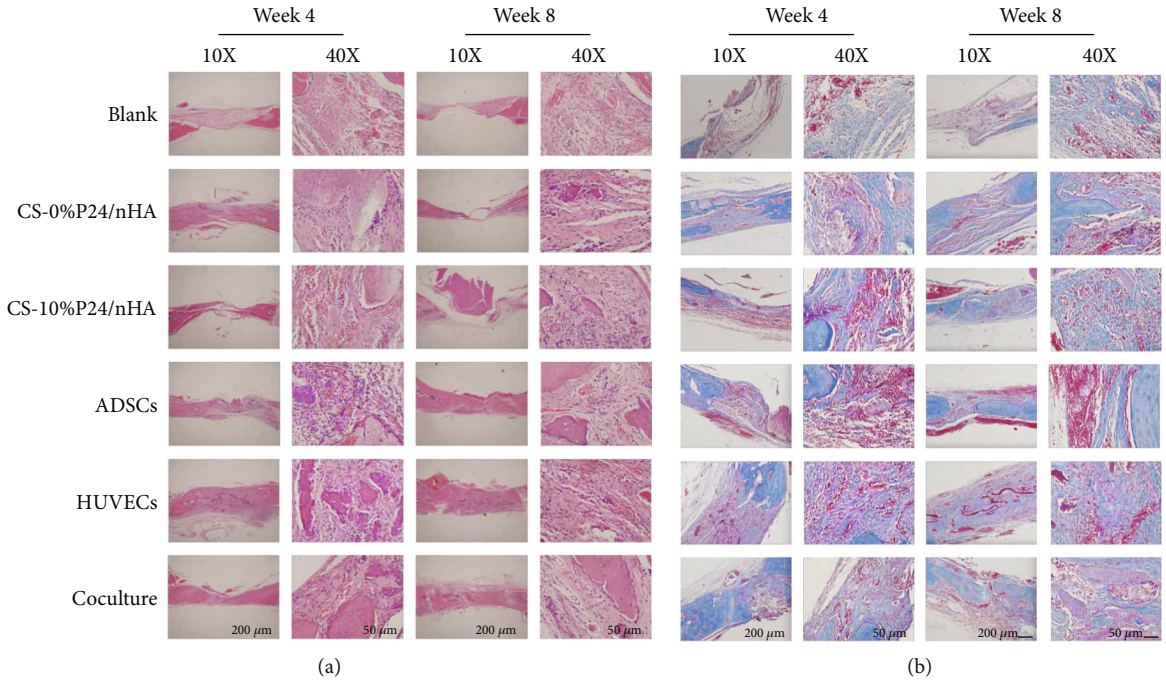


Figure 3: Histology of repaired calvariae 4 and 8 weeks of postimplantation in vivo. (a) Hematoxylin and eosin staining of calvariae defects in the blank, CS-0%P24/nHA, CS-10%P24/nHA, CS-10%P24/nHA plus ADSC, CS-10%P24/nHA plus HUVEC, and CS-10%P24/nHA plus ADSC/HUVEC coculture groups. Red arrows show new blood vessel formation in or around the scaffolds. (b) Masson's trichrome staining of repaired calvariae in each group. Scale bar = 200 $\mu$m and 50 $\mu$m.

a thicker regenerated calvarium and better osseous structure reconstitution compared with those treated with the scaffold, HUVECs, or ADSCs alone (Figure 3). HE staining showed that osteoid cells and microvascular regeneration began to appear in the coculture group 4 weeks after surgery. At 8 weeks postoperatively, the mineralized tissue was filled into the scaffold and new microvessels could be observed (Figure 3(a)). Masson staining showed that fibrotic tissues developed earlier in the coculture group at week 4 and were gradually replaced by new bone tissue at week 8 (Figure 3(b)). These results indicated faster bone regeneration and better osseous structure reconstitution in the coculture group compared to the other groups.

Immunofluorescence and immunohistochemical analyses showed that the area implanted with the scaffold plus ADSC/HUVEC coculture exhibited high expression of OCN and CD31 at 4 and 8 weeks of postimplantation (Figure 4). The mean fluorescence intensity of CD31 and OCN in the coculture group was 2.5 and 2.2 times higher than that in the blank group, respectively (Figure 4(a)). In addition, the number of CD31-positive cells in the coculture group at 4 and 8 weeks was also significantly higher than that in the other groups, which was 4 and 3.5 times of that in the blank group, respectively (Figure 4(b)).

*3.3. Immunohistological Assessment of ADSC/HUVEC Survival In Vivo.* The survival of grafted cells was evaluated by immunohistochemistry using MAB1281. At 4 weeks of postimplantation, immunofluorescence and immunohistochemistry analyses revealed that MAB1281-labeled cells survived within the scaffolds in the group that received the scaffold plus ADSCs and the group that received the scaffold plus ADSC/HUVEC coculture (Figure 5(a)). However, at 8 weeks of postimplantation, only the group with the scaffold plus ADSC/HUVEC coculture showed MAB1281-labeled cells (Figure 5(b)). These results indicate that the scaffold plus ADSC/HUVEC coculture can improve the survival rate of grafted cells.

*3.4. Effect of the Scaffold plus ADSC/HUVEC Coculture on Osteoclastogenesis.* We investigated the effect of the scaffold plus ADSC/HUVEC coculture on osteoclast formation in an osteoporotic environment. TRAP staining revealed that multiple osteoclasts lined the eroded bone surface in the blank group and in the group that received the CS-10%P24/nHA scaffold (Figure 6(a)). The erosion surface was reduced in the group that received the scaffold plus ADSCs and the group that received the scaffold plus HUVECs, and the number of osteoclasts was significantly lower in the group treated with the scaffold plus ADSC/HUVEC coculture ($4.60 \pm 0.57$ cell) (Figure 6(b)). Osteoclast formation was also inhibited in the group that received the scaffold plus ADSC/HUVEC coculture.

## 4. Discussion

It is generally believed that there is a close relationship between angiogenesis and osteogenesis [11, 23–26]. In the process of articular cartilage degeneration, hypertrophic chondrocytes enable microvessels to grow into the growth

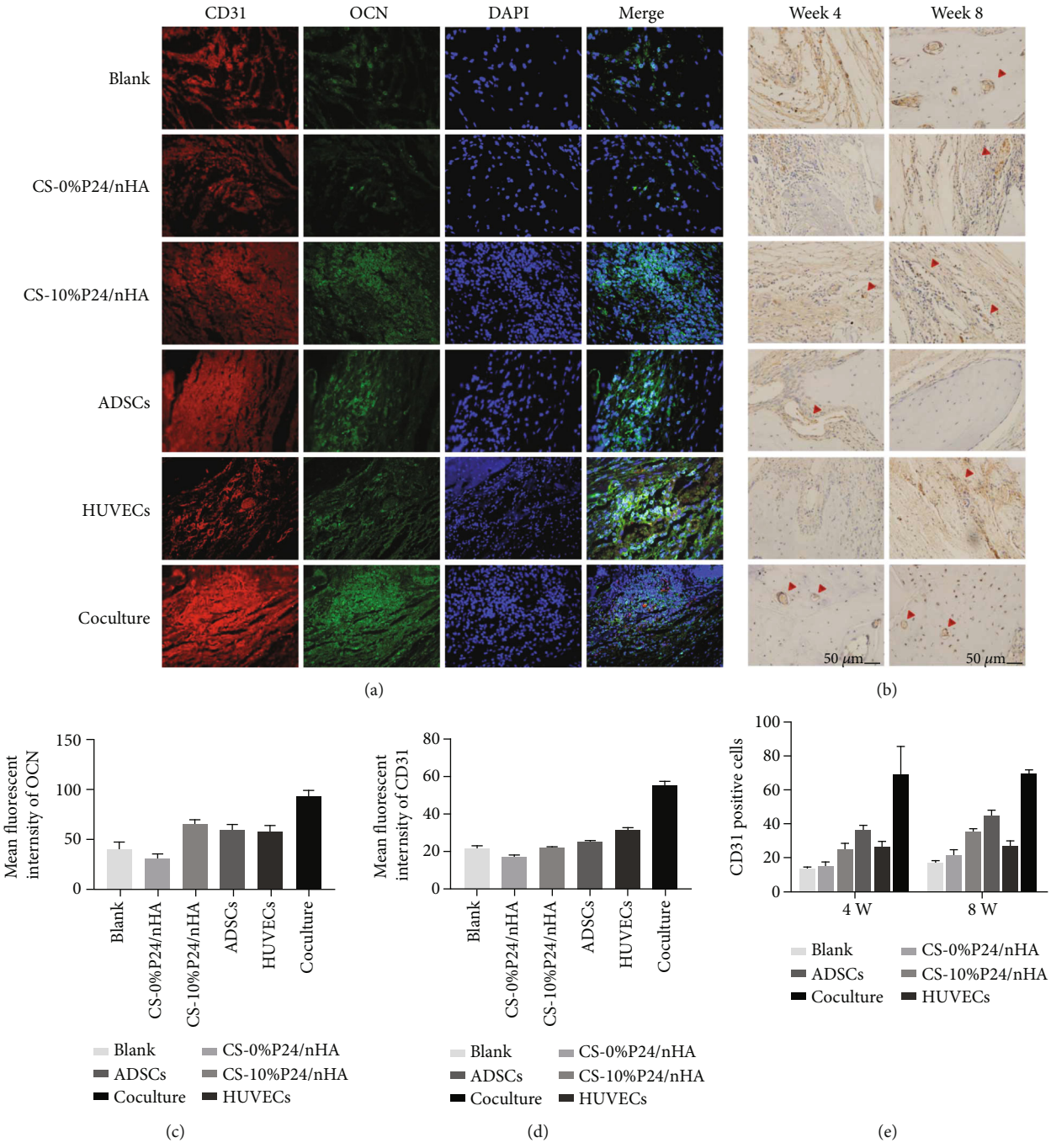


Figure 4: Immunofluorescence and immunohistochemistry. (a) Immunofluorescence of each group 4 weeks after surgery. Cells that appear green represent OCN-positive cells. Areas that appear red represent CD31-positive areas. (b) Immunohistochemistry of 4 and 8 weeks after surgery. Areas that appear dark brown represent CD31-positive areas, which indicate blood vessels (red arrow). The white areas are voids. (c) Mean fluorescent intensity of OCN-positive cells at 4 weeks. (d) Mean fluorescent intensity of CD31-positive cells at 4 weeks. (e) Quantification of CD31-positive cells in each group. Representative magnified images are at ×40 magnification. Scale bar = 50 $\mu$m.

plate by secreting angiogenic factors, such as VEGF, which leads to cartilage absorption and bone formation [27, 28]. During bone repair, microvessels provide a prerequisite for the exchange of oxygen and nutrients for bone regeneration [23]. Lack of blood vessels will delay bone regeneration and can even lead to implant ischemic necrosis, delayed healing, and nonunion [11, 23]. In patients with osteoporosis, it is more difficult to repair the bone defect because of active bone resorption and inhibition of osteogenesis [8, 29]. Therefore, providing adequate vascular support for bone repair is helpful to facilitate bone regeneration, which is of great importance for the treatment of patients with osteoporotic bone defects. As the initiation and maintenance cells of vascular regeneration, endothelial cells play an indispensable role in

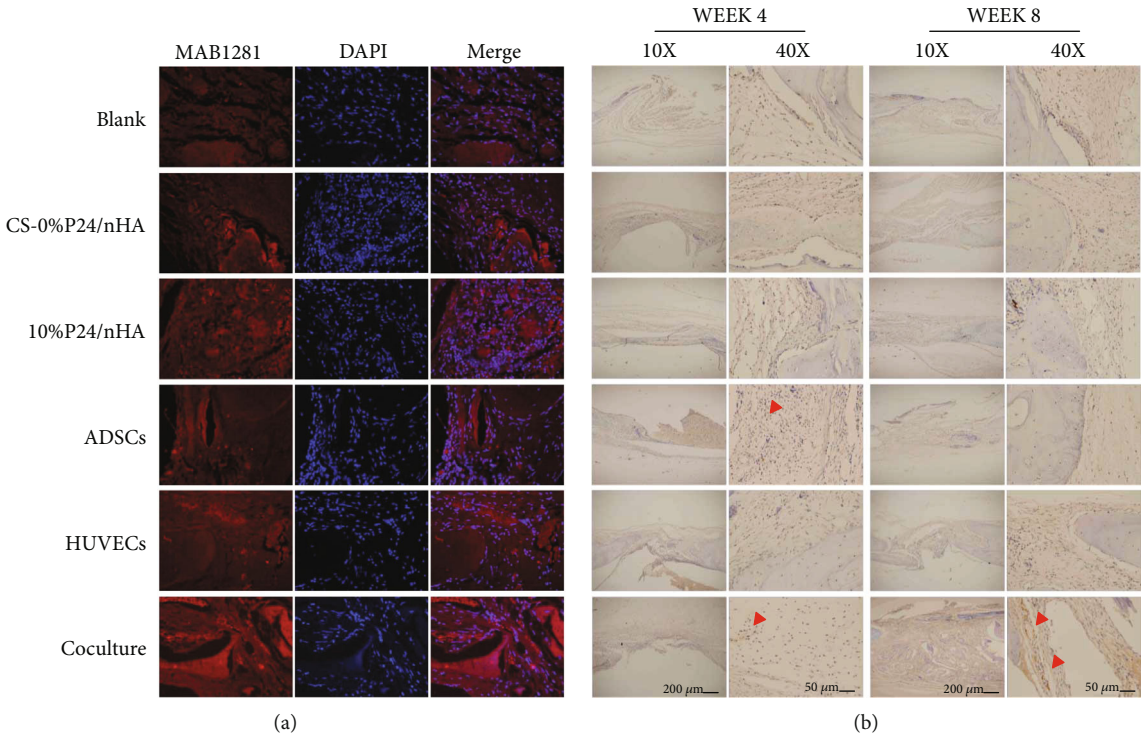


Figure 5: Survival of ADSCs/HUVECs in the scaffold. (a) Immunofluorescence and immunohistochemistry show MAB1281-labeled cells in the scaffold at 4 weeks. Areas that appear dark brown represent MAB1281-labeled areas. (b) Red arrows show MAB1281-labeled cells. Scale bar = 200 $\mu$m and 50 $\mu$m.

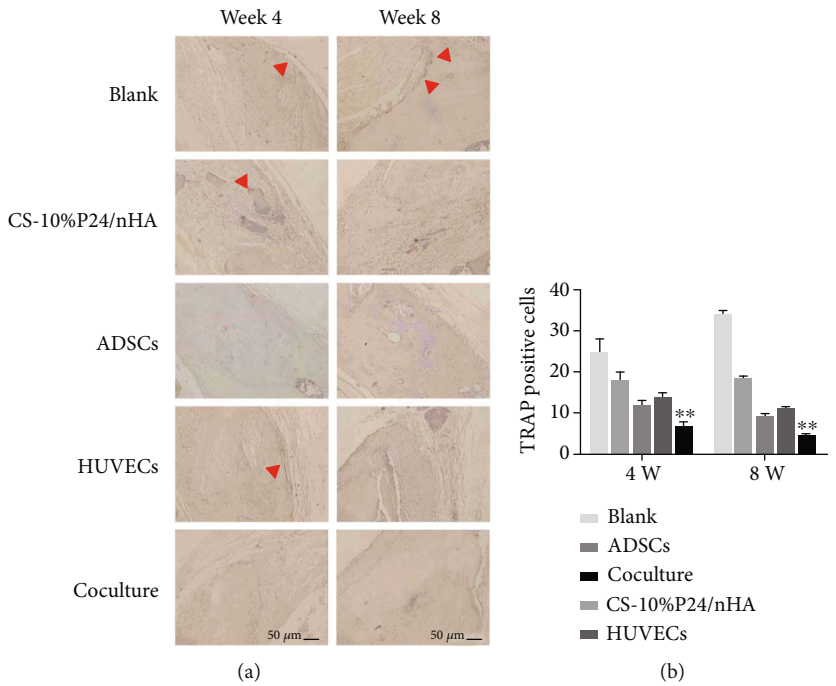


Figure 6: In vivo effects of the scaffold plus ADSC/HUVEC coculture on osteoclast genesis. (a) TRAP staining was performed on three sections per group. (b) Quantification of TRAP-positive cells in each group. Red arrows show TRAP-positive cells. Representative magnified images are at ×40 magnification. Scale bar = 50 $\mu$m.

bone defect repair. Previous studies have observed an interaction between endothelial cells and mesenchymal cells. This interaction promotes proliferation and osteogenic differentiation of mesenchymal cells in vitro [15, 24]. Studies have found that endothelial cells promote MSC differentiation through cell-to-cell contact, which makes cell coculture a

feasible method [30–32]. These findings encourage research into the effects of endothelial cell and mesenchymal cell coculture to promote bone regeneration.

This study is aimed at determining the effect of HUVEC/ADSC coculture on osteogenic differentiation and angiogenesis in CS-P24/nHA scaffolds. We also aimed to explore the optimal proportion of cells needed for coculture and the effect of coculture on osteoporotic bone defect repair. After human ADSC extraction, ADSCs were inoculated with HUVECs on CS-P24/nHA scaffolds to form a coculture system. Compared with separately cultured ADSCs and HUVECs, coculture of HUVECs and ADSCs can significantly promote cell proliferation, which is consistent with the results of previous studies [13, 33]. To determine the optimal proportion of cells, we cocultured HUVECs and ADSCs at different ratios. The results show that when ADSCs and HUVECs were cocultured at a ratio of 3 : 1, cell proliferation was significantly promoted. These results indicate that the proportion of cocultured cells affects cell behavior. In most studies, a 3 : 1 ratio of MSCs to HUVECs has achieved good results in promoting cell proliferation and bone regeneration [10, 33–35]. But in a study by Pennings et al., MSCs and HUVECs were cocultured at a ratio of 4 : 1 to promote bone regeneration [36]. Moreover, Carvalho et al. found that the promoting effects of coculture were best at a ratio of 1 : 1 [37]. However, Shah et al. found that a HUVEC to MSC ratio of 5 : 1 significantly promoted angiogenesis, while a HUVEC to MSC ratio of 1 : 5 effectively promoted osteogenesis and mineralization [38]. Given the above discrepancies, we cocultured these two cell types at a ratio of 3 : 1 and detected osteogenic differentiation of ADSCs. PCR showed that coculture at a ratio of 3 : 1 had the most obvious effect on osteogenic differentiation and significantly increased the expression of osteogenesis-related genes, including *RUNX2*, *OCN*, and *ALP*. In our study, 3 : 1 was the most suitable ratio for coculture of endothelial cells and stem cells, and this ratio significantly promoted cell proliferation and osteogenic differentiation. Despite these observations, there is no unified standard for the best proportion of cocultured cells. Thus, this area is worthy of further research.

To verify the effect of coculture on osteoporotic bone defect repair, ADSCs and HUVECs were inoculated on CS-P24/nHA scaffolds at a ratio of 3 : 1 and implanted to repair calvariae defects in osteoporotic rats. Micro-CT showed that CS-P24/nHA scaffolds containing cocultured cells were more effective in repairing osteoporotic bone defects. Histological results also showed that coculture effectively promoted bone regeneration. Thicker regenerated skulls and better bone remodeling were observed in the coculture group compared with the single-cell groups. We also observed that the defect was only filled with fibrous tissue in the blank and scaffold groups, which indicated that bone regeneration was significantly less evident. This may be due to inhibition of osteoblast activity in osteoporotic animals, resulting in a poor effect of simple scaffold filling on bone defect repair [29, 39]. Our results proved that the combination of nanoscaffolds and cell coculture can improve the effect of scaffolds on bone defect repair. Coculture of HUVECs and ADSCs in the scaffold can provide seed cells for bone repair and promote vascular regeneration by endothelial cells, especially in the context of osteoporotic bone defect repair. However, the CS-TBA nanocomposite scaffold not only provided an appropriate external environment for HUVECs and ADSCs but also promoted the proliferation and differentiation of cells by releasing P24 and mechanical stress [40, 41]. The combination of nanomaterial and cell coculture improves the therapeutic effect, and this combination method is helpful to explore more improved methods of nanomaterials.

In addition to promoting bone regeneration, inhibiting bone resorption is important for osteoporotic bone defect repair [4, 5]. Therefore, we use TRAP staining to further explore the effect of coculture scaffolds on the activity of osteoclasts in bone defects. The results show that the number of osteoclasts at the defect site was reduced in the group that received the scaffold plus ADSC/HUVEC coculture. The results show that coculture does not only promote bone regeneration but that it also inhibits bone resorption, which is essential for osteoporotic bone defect repair. Other studies have shown that coculture of endothelial cells and mesenchymal cells can inhibit osteoclast activity [26, 42, 43]. However, some studies suggest that cocultured microvessels promote osteoclast proliferation and activity [44]. In our study, cell coculture inhibited osteoclast activity at the defect site, which may be due to the activity of HUVECs. Alternatively, other cell-to-cell interactions may have played a role, which should be clarified in the future.

## 5. Conclusion

This study demonstrated that coculture of HUVECs and ADSCs in CS-P24/nHA nanocomposite scaffolds can promote cell proliferation and osteogenic differentiation. When ADSCs and HUVECs were cocultured at a ratio of 3 : 1, their effect on proliferation and osteogenic differentiation was the most obvious. Using a rodent model of osteoporotic bone defect, we further confirmed that coculture of HUVECs and ADSCs with the CS-P24/nHA nanocomposite scaffold promoted bone defect repair and inhibited osteoclast activity at the defect site. Our research shows that the CS-P24/nHA nanocomposite scaffold plus ADSC/HUVEC coculture can effectively repair osteoporotic bone defects, which has broad application and development prospects in the field of orthopedics.

## Data Availability

The generated or analyzed data used to support the findings of this study are included within the article.

## Conflicts of Interest

The authors have no conflicts of interest to declare.

## Acknowledgments

This work was supported by the National Natural Science Foundation of China (grant numbers: 81371931, 81974323, and 81301240), the Natural Science Foundation of Guangdong Province, China (grant numbers: 2014A030313352,

and 2014A030313310), the Shenzhen Strategic Emerging Industries Project (grant number: CXZZ20130517095548798), the Guangzhou Science and Technology Program Project (grant number: 201804010082), and the Special Funds for the Cultivation of Guangdong College Students' Scientific and Technological Innovation (grant number: pdjh2016b0097).

## References

[1] A. Sterodimas, J. de Faria, B. Nicaretta, and I. Pitanguy, "Tissue engineering with adipose-derived stem cells (ADSCs): current and future applications," *Journal of Plastic, Reconstructive & Aesthetic Surgery*, vol. 63, pp. 1886–1892, 2010.

[2] F. Salamanna, A. Gambardella, D. Contartese, A. Visani, and M. Fini, "Nano-based biomaterials as drug delivery systems against osteoporosis: a systematic review of preclinical and clinical evidence," *Nanomaterials*, vol. 11, no. 2, 2021.

[3] R. Kocijan, K. Klaushofer, and B. M. Misof, "Osteoporosis Therapeutics 2020," *Handbook of Experimental Pharmacology*, vol. 262, pp. 397–422, 2020.

[4] M. Lorentzon, "Treating osteoporosis to prevent fractures: current concepts and future developments," *Journal of Internal Medicine*, vol. 285, no. 4, pp. 381–394, 2019.

[5] L. Aghebati-Maleki, S. Dolati, R. Zandi et al., "Prospect of mesenchymal stem cells in therapy of osteoporosis: a review," *Journal of Cellular Physiology*, vol. 234, no. 6, pp. 8570–8578, 2019.

[6] C. Zhang and C. Song, "Combination therapy of PTH and antiresorptive drugs on osteoporosis: a review of treatment alternatives," *Frontiers in Pharmacology*, vol. 11, article 607017, 2020.

[7] A. Saadat, S. Karbasi, A. Ghader, and M. Khodaei, "Characterization of biodegradable P3HB/HA nanocomposite scaffold for bone tissue engineering," *Procedia Materials Science*, vol. 11, pp. 217–223, 2015.

[8] Z. Zou, W. Liu, L. Cao et al., "Advances in the occurrence and biotherapy of osteoporosis," *Biochemical Society Transactions*, vol. 48, no. 4, pp. 1623–1636, 2020.

[9] A. Qadir, S. Liang, Z. Wu, Z. Chen, L. Hu, and A. Qian, "Senile osteoporosis: the involvement of differentiation and senescence of bone marrow stromal cells," *International Journal of Molecular Sciences*, vol. 21, no. 1, 2020.

[10] D. N. Heo, M. Hospodiuk, and I. T. Ozbolat, "Synergistic interplay between human MSCs and HUVECs in 3D spheroids laden in collagen/fibrin hydrogels for bone tissue engineering," *Acta Biomaterialia*, vol. 95, pp. 348–356, 2019.

[11] L. Krishnan, N. J. Willett, and R. E. Guldberg, "Vascularization strategies for bone regeneration," *Annals of Biomedical Engineering*, vol. 42, no. 2, pp. 432–444, 2014.

[12] C. Seebach, D. Henrich, K. Wilhelm, J. H. Barker, and I. Marzi, "Endothelial progenitor cells improve directly and indirectly early vascularization of mesenchymal stem cell-driven bone regeneration in a critical bone defect in rats," *Cell Transplantation*, vol. 21, no. 8, pp. 1667–1677, 2012.

[13] I. Kocherova, A. Bryja, P. Mozdziak, A. Angelova Volponi, M. Dyszkiewicz-Konwińska, H. Piotrowska-Kempisty et al., "Human umbilical vein endothelial cells (HUVECs) co-culture with osteogenic cells: from molecular communication to engineering prevascularised bone grafts," *Journal of Clinical Medicine*, vol. 8, 2019.

[14] J. Zhang, K. G. Neoh, and E. T. Kang, "Electrical stimulation of adipose-derived mesenchymal stem cells and endothelial cells co-cultured in a conductive scaffold for potential orthopaedic applications," *Journal of Tissue Engineering and Regenerative Medicine*, vol. 12, no. 4, pp. 878–889, 2018.

[15] S. M. Goerke, J. Obermeyer, J. Plaha, G. B. Stark, and G. Finkenzeller, "Endothelial progenitor cells from peripheral blood support bone regeneration by provoking an angiogenic response," *Microvascular Research*, vol. 98, pp. 40–47, 2015.

[16] W. Chen, X. Liu, Q. Chen et al., "Angiogenic and osteogenic regeneration in rats via calcium phosphate scaffold and endothelial cell co-culture with human bone marrow mesenchymal stem cells (MSCs), human umbilical cord MSCs, human induced pluripotent stem cell-derived MSCs and human embryonic stem cell-derived MSCs," *Journal of Tissue Engineering and Regenerative Medicine*, vol. 12, no. 1, pp. 191–203, 2018.

[17] K. Kafedjiiski, F. Föger, M. Werle, and A. Bernkop-Schnürch, "Synthesis and in vitro evaluation of a novel chitosan-glutathione conjugate," *Pharmaceutical Research*, vol. 22, no. 9, pp. 1480–1488, 2005.

[18] A. Matsuda, H. Kobayashi, S. Itoh, K. Kataoka, and J. Tanaka, "Immobilization of laminin peptide in molecularly aligned chitosan by covalent bonding," *Biomaterials*, vol. 26, no. 15, pp. 2273–2279, 2005.

[19] Y. Chen, X. Liu, R. Liu et al., "Zero-order controlled release of BMP2-derived peptide P24 from the chitosan scaffold by chemical grafting modification technique for promotion of osteogenesisinvitro and enhancement of bone repairin vivo," *Theranostics*, vol. 7, no. 5, pp. 1072–1087, 2017.

[20] Y. J. Seol, Y. J. Park, S. C. Lee et al., "Enhanced osteogenic promotion around dental implants with synthetic binding motif mimicking bone morphogenetic protein (BMP)-2," *Journal of Biomedical Materials Research. Part A*, vol. 77, no. 3, pp. 599–607, 2006.

[21] J. Li, J. Hong, Q. Zheng et al., "Repair of rat cranial bone defects with nHAC/PLLA and BMP-2-related peptide or rhBMP-2," *Journal of Orthopaedic Research*, vol. 29, no. 11, pp. 1745–1752, 2011.

[22] J. Rehman, D. Traktuev, J. Li et al., "Secretion of angiogenic and antiapoptotic factors by human adipose stromal cells," *Circulation*, vol. 109, no. 10, pp. 1292–1298, 2004.

[23] L. F. Fröhlich, "MicroRNAs at the interface between osteogenesis and angiogenesis as targets for bone regeneration," *Cells*, vol. 8, no. 2, p. 121, 2019.

[24] Y. Jia, Y. Zhu, S. Qiu, J. Xu, and Y. Chai, "Exosomes secreted by endothelial progenitor cells accelerate bone regeneration during distraction osteogenesis by stimulating angiogenesis," *Stem Cell Research & Therapy*, vol. 10, no. 1, p. 12, 2019.

[25] R. Shi, Y. Huang, C. Ma, C. Wu, and W. Tian, "Current advances for bone regeneration based on tissue engineering strategies," *Frontiers in Medicine*, vol. 13, no. 2, pp. 160–188, 2019.

[26] Y. Yin, Q. Tang, M. Xie, L. Hu, and L. Chen, "Insights into the mechanism of vascular endothelial cells on bone biology," *Bioscience Reports*, vol. 41, no. 1, 2021.

[27] L. Shang, Y. Xu, C. Shao, C. Ma, and Y. Feng, "Anti-vascular endothelial growth factor (VEGF) antibody ameliorates cartilage degradation in a rat model of chronic sports arthritic injury," *Medical Science Monitor*, vol. 24, pp. 4073–4079, 2018.

[28] X. Zhang, R. Crawford, and Y. Xiao, "Inhibition of vascular endothelial growth factor with shRNA in chondrocytes ameliorates osteoarthritis," *Journal of Molecular Medicine (Berlin, Germany)*, vol. 94, no. 7, pp. 787–798, 2016.

[29] U. Föger-Samwald, P. Dovjak, U. Azizi-Semrad, K. Kerschan-Schindl, and P. Pietschmann, "Osteoporosis: pathophysiology and therapeutic options," *EXCLI Journal*, vol. 19, pp. 1017–1037, 2020.

[30] M. Grellier, L. Bordenave, and J. Amédée, "Cell-to-cell communication between osteogenic and endothelial lineages: implications for tissue engineering," *Trends in Biotechnology*, vol. 27, pp. 562–571, 2009.

[31] B. Guillotin, R. Bareille, C. Bourget, L. Bordenave, and J. Amédée, "Interaction between human umbilical vein endothelial cells and human osteoprogenitors triggers pleiotropic effect that may support osteoblastic function," *Bone*, vol. 42, no. 6, pp. 1080–1091, 2008.

[32] D. Steiner, F. Lampert, G. B. Stark, and G. Finkenzeller, "Effects of endothelial cells on proliferation and survival of human mesenchymal stem cells and primary osteoblasts," *Journal of Orthopaedic Research*, vol. 30, pp. 1682–1689, 2012.

[33] X. Liu, W. Chen, C. Zhang et al., "Co-seeding human endothelial cells with human-induced pluripotent stem cell-derived mesenchymal stem cells on calcium phosphate scaffold enhances osteogenesis and vascularization in rats," *Tissue Engineering*, vol. 23, no. 11-12, Part A, pp. 546–555, 2017.

[34] W. L. Fu, Z. Xiang, F. G. Huang et al., "Coculture of peripheral blood-derived mesenchymal stem cells and endothelial progenitor cells on strontium-doped calcium polyphosphate scaffolds to generate vascularized engineered bone," *Tissue Engineering*, vol. 21, no. 5-6, Part A, pp. 948–959, 2015.

[35] Y. Xue, Z. Xing, A. I. Bolstad, T. E. Van Dyke, and K. Mustafa, "Co-culture of human bone marrow stromal cells with endothelial cells alters gene expression profiles," *The International Journal of Artificial Organs*, vol. 36, no. 9, pp. 650–662, 2013.

[36] I. Pennings, L. A. van Dijk, J. van Huuksloot et al., "Effect of donor variation on osteogenesis and vasculogenesis in hydrogel cocultures," *Journal of Tissue Engineering and Regenerative Medicine*, vol. 13, no. 3, pp. 433–445, 2019.

[37] M. S. Carvalho, J. C. Silva, R. N. Udangawa et al., "Co-culture cell-derived extracellular matrix loaded electrospun microfibrous scaffolds for bone tissue engineering," *Materials Science & Engineering. C, Materials for Biological Applications*, vol. 99, pp. 479–490, 2019.

[38] A. R. Shah, J. C. Wenke, and C. M. Agrawal, "Manipulation of human primary endothelial cell and osteoblast coculture ratios to augment vasculogenesis and mineralization," *Annals of Plastic Surgery*, vol. 77, no. 1, pp. 122–128, 2016.

[39] F. Xu, W. Li, X. Yang, L. Na, L. Chen, and G. Liu, "The roles of epigenetics regulation in bone metabolism and osteoporosis," *Frontiers in Cell and Developmental Biology*, vol. 8, article 619301, 2020.

[40] L. Wang, S. Wu, G. Cao, Y. Fan, N. Dunne, and X. Li, "Biomechanical studies on biomaterial degradation and co-cultured cells: mechanisms, potential applications, challenges and prospects," *Journal of Materials Chemistry B*, vol. 7, pp. 7439–7459, 2019.

[41] L. Wang, C. Wang, S. Wu, Y. Fan, and X. Li, "Influence of the mechanical properties of biomaterials on degradability, cell behaviors and signaling pathways: current progress and challenges," *Biomaterials Science*, vol. 8, pp. 2714–2733, 2020.

[42] S. K. Ramasamy, A. P. Kusumbe, M. Schiller et al., "Blood flow controls bone vascular function and osteogenesis," *Nature Communications*, vol. 7, no. 1, article 13601, 2016.

[43] S. G. Romeo, K. M. Alawi, J. Rodrigues, A. Singh, A. P. Kusumbe, and S. K. Ramasamy, "Endothelial proteolytic activity and interaction with non-resorbing osteoclasts mediate bone elongation," *Nature Cell Biology*, vol. 21, no. 4, pp. 430–441, 2019.

[44] H. Pang, X. H. Wu, S. L. Fu et al., "Co-culture with endothelial progenitor cells promotes survival, migration, and differentiation of osteoclast precursors," *Biochemical and Biophysical Research Communications*, vol. 430, no. 2, pp. 729–734, 2013.

Hindawi
Journal of Nanomaterials
Volume 2021, Article ID 6696733, 8 pages
https://doi.org/10.1155/2021/6696733

*Research Article*

# The Use of Fullerene C60 to Preserve Testicular Tissue after Cryopreservation

**Nataliia Volkova, Mariia Yukhta, and Anatoliy Goltsev**

*Department of Cryopathophysiology and Immunology, Institute for Problems of Cryobiology and Cryomedicine of the National Academy of Sciences of Ukraine, Pereyaslavskaya Str., 23, Kharkov 61015, Ukraine*

Correspondence should be addressed to Nataliia Volkova; volkovana781@gmail.com

Received 20 January 2021; Revised 22 March 2021; Accepted 31 March 2021; Published 17 April 2021

Academic Editor: Nicholas Dunne



Autologous transplantation of cryopreserved fragments of an immature testis is an actively developing approach to save fertility in patients facing a gonadotoxic therapy. The use of bioavailable fullerene C60 as a powerful antioxidant opens up a new potential for the prevention and correction of ischemic-reperfusion pathological processes in tissues including those associated with freezing-thawing procedure. In this work, we aimed to study the antioxidant status, apoptotic/necrotic processes, and morphological characteristics of cryopreserved fragments of the seminiferous tubules of testis (CrFSTT) of immature rats after incubation in media with different concentrations of fullerene C60 (10, 15, and 20 $\mu$g/mL). Our results indicated that the addition of C60 in a concentration of 15 $\mu$g/mL decreased ROS production, cytochrom C release, and degree of histological damage of spermatogenic epithelium as well as increased the activity of the mitochondria, antioxidant defense system, and cell density in histological sections of CrFSTT compared to the control. Fullerene C60 at investigated concentrations did not impact significantly on apoptosis in cells of CrFSTT but, after incubation with 15 $\mu$g/mL C60, a percentage of living cells was 1.2-fold higher and a value of necrotic ones in this group was 1.6-fold lower than the control samples ($p < 0.05$). Relative amount of cells of the spermatogonia germ layer did not differ between the studied concentrations. The general analysis of obtained data showed that the C60 addition in the concentration of 15 $\mu$g/mL was the most optimal for the rehabilitation of CrFSTT. The results can be used for the development of an effective rehabilitation medium for the cryopreserved testicular tissue.

## 1. Introduction

Currently, an autologous transplantation of cryopreserved fragments of an immature testis is an actively developing approach to restore fertility of adolescent patients facing gonadotoxic therapy [1]. The advantage of this method is a preservation of spermatogenic cell niche, due to the support of cellular contacts and interactions, which contributes to the normal development of germ cells. But there are other, no less difficult tasks: minimization of tissue damage by ice crystals and avoidance of ischemic-reperfusion pathological processes associated with cryopreservation.

Some properties of nanoparticles can be useful in solving these problems. For example, oxidized quasicarbon nitride quantum dots can inhibit ice growth/recrystallization through the density of hydrogen bonds formed with ice [2]. And nanoparticle-mediated trehalose delivery technology helps to overcome the major limitation of ultralow permeability of this disaccharide resulting in favorable postthaw cell survival rates without the need of any organic solvent [3].

But the capabilities of nanoparticles are not limited to freeze-thaw processes, because they can also be used for the rehabilitation of biological objects after cryopreservation. Since oxidative stress is one of the cryodamage factors, the use of carbon nanoparticles as components of rehabilitation media is a promising direction for the cell and tissue regeneration after cryopreservation. So, the idea of our study is to increase the efficiency of cryopreservation of seminiferous tubules using water-soluble fullerene C60 as an antioxidant agent.

Fullerene C60 has unique structural and functional properties, including nanosize, low surface energy, high chemical

stability, spherical shape, weak intermolecular bonding, and high load-bearing capacity [4]. The C60 molecule is able to interact with biological membranes, penetrating into the intracellular space by passive diffusion or endocytosis [5].

Previous biological *in vitro* and *in vivo* screening of unmodified fullerene C60 aqueous colloid solution showed that it does not have acute toxic effects on normal cells at low concentrations, is not immunogenic, is nonallergenic, and is able to neutralize the excess of free radicals [6, 7]. Thus, the use of bioavailable fullerene C60 as a powerful antioxidant opens up a new potential for the prevention and correction of ischemic-reperfusion pathological processes in tissues associated with the freezing-thawing procedure.

Here, we present a study on how different concentrations of fullerene C60 affect the antioxidant status, apoptotic/necrotic processes, and morphological characteristics of cryopreserved fragments of the seminiferous tubules of the testis (CrFSTT) of immature rats.

## 2. Materials and Methods

*2.1. Animals.* All the manipulations were carried out in accordance to the European convention for the protection of vertebrate animals used for experimental and other scientific purposes (Strasbourg, 18.III.1986). The protocols were approved by the Bioethics Committee of Institute for Problems of Cryobiology and Cryomedicine of the NAS of Ukraine (permit no. 2016-05).

Outbreed white sexually immature male rats (aged 7-8 weeks, $n = 50$) were used in the study. Humane euthanasia by $CO_2$ asphyxiation was performed to obtain testes of experimental animals right before the study. Excised testes were rinsed in L-15 medium (Leibovitz) (prod. no. L0300500, BioWest, Nuaille, France). Tunica albuginea was removed using sterile medical instruments, and the testes were then rinsed again. Fragments of the seminiferous tubules of the testis weighing $75 \pm 5$ mg were isolated mechanically and cryopreserved.

*2.2. Cryopreservation.* Cryoprotective medium based on a fibrin gel with the addition of glycerol (prod. no. G5516, Sigma-Aldrich, St. Louis, USA) at the final concentration of 0.7 M was made *ex tempore*. Fibrin gel was received from the fresh blood of animals, which was obtained from a cardiac vein and centrifuged for 12 min at a rate of 1000 g. The tissue fragments were transferred into 2 mL TPP® cryotubes (prod. no. Z760951, Sigma-Aldrich, St. Louis, USA), where they were exposed to the cryoprotective medium for 30 min at 4°C [8]. Then, cryotubes with samples were cooled in vapors of liquid nitrogen for 40 min down to –70°C and transferred to liquid nitrogen (–196°C) [9]. Cryotubes were stored in a cryobank for a month and then were warmed up in a water bath at 40°C until a liquid phase appearance. After thawing, cryoprotectants were removed from the samples by a three-step change of the solution to the L-15 medium.

*2.3. Manipulations with Fullerene C60.* Fullerene-$C_{60}$ (99.9%) was purchased from Sigma-Aldrich, St. Louis, USA (prod. no. 572500). It consisted of agglomerates of spherical or fibrous primary particles. To obtain an aqueous suspension of fullerene C60, a method based on the transfer of this carbon nanostructure from toluene to water followed by sonication was used [10]. The result was a typical colloid solution of C60.

The thawed CrFSTT were incubated at 22°C for 30 min in the L-15 medium with the addition of fullerene C60 at final concentrations of 10, 15, and 20 $\mu$g/mL. The samples incubated in the L-15 medium without C60 served as a control.

The scheme of experiment is shown in Figure 1.

*2.4. Analysis of Total Antioxidant Status (TAS).* The samples of CrFSTT were homogenized, filtered, and centrifugated (1000 g for 10 min). TAS activity was estimated quantitatively by the method of UV spectrophotometry (ERBA CHEM 7, Erba Lachema s.r.o., Brno, Czech Republic) using test kits (prod. no. NX2332, Randox Laboratories Ltd., Crumlin, UK) according to the manufacturer's instructions and normalized to 1 mg of protein (prod. no. TP8336, Randox Laboratories Ltd., Crumlin, UK).

*2.5. Flowcytometry Analysis.* The cell suspension was obtained from CrFSTT by enzymatic disaggregation: the samples were incubated with 0.25% trypsin (37°C for 30 min), filtered, and centrifugated (1000 g for 10 min).

Intracellular reactive oxygen species (ROS) was estimated quantitatively using a fluorometric test kit (prod. no. MAK-142, Sigma-Aldrich, St. Louis, USA). In brief, the cells of CrFSTT (0.5 mL) at a concentration of $1 \times 10^6$ cells/mL were suspended with 1 $\mu$L of ROS detection reagent stock solution and incubated under 5% $CO_2$ at 37°C for one hour.

The apoptotic/necrotic processes in cells of CrFSTT were studied using Annexin-V-FITC (Annexin V) (prod. no. 556419 BD Pharmingen™, San Jose, USA) and 7-aminoactinomycin D (7AAD) (prod. no. 559925, BD Pharmingen™, San Jose, USA) dyes. The cells of CrFSTT (0.5 mL) at a concentration of $1 \times 10^6$ cells/mL were suspended with 5 $\mu$L of Annexin V and 5 $\mu$L of 7AAD. The samples were incubated at 22°C for 20 min.

The functional state of the mitochondria was investigated using a mitochondrial membrane potential detection kit JC-1 (prod. no. 551302, BD Pharmingen™, San Jose, USA). Incubation of the cells with the JC-1 working solution (0.5 mL/sample) for 15 min at 37°C in a $CO_2$ incubator was performed. Then, cells were washed twice.

The number of cells positively stained for cytochrome C was determined using the test system Cyt.C (prod. no. 560263, BD Pharmingen™, San Jose, USA). The cells of CrFSTT (0.5 mL) at a concentration of $1 \times 10^6$ cells/mL suspended with 5 $\mu$L of Cyt.C and incubated at 22°C for 20 min.

All investigations were performed according to the manufacturer's instructions. BD FACSCalibur™ (Becton Dickinson, San Jose, USA) was used for these tests. Data were analyzed using WinMDI v.2.8.

*2.6. Histomorphology.* The samples of CrFSTT for histological examination were fixed in 10% formalin solution (prod. no. HT501128, Sigma-Aldrich, St. Louis, USA). Sections

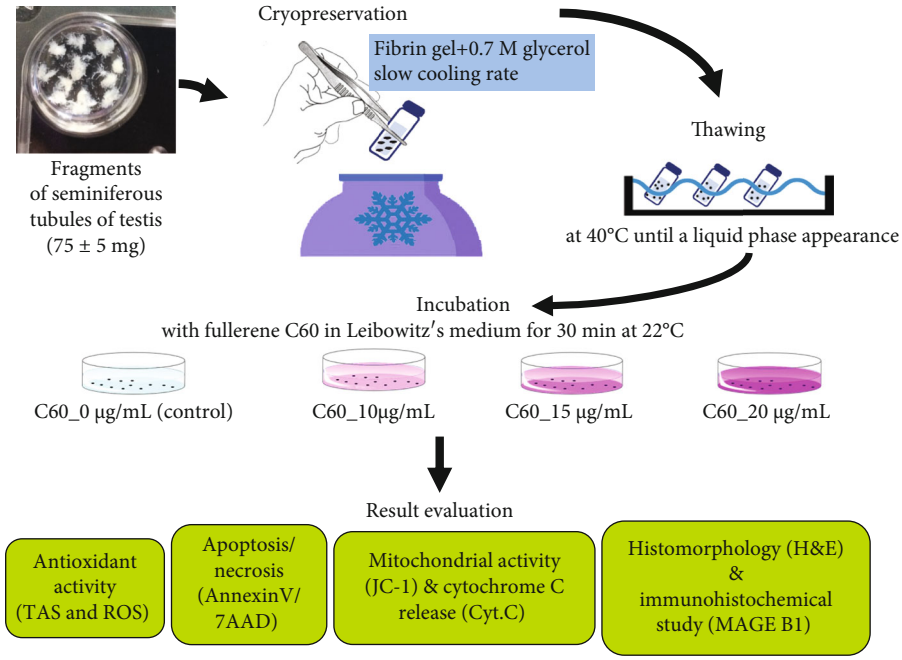


Figure 1: Experimental scheme.

were cut from paraffin-embedded blocks (7 $\mu$m thick), stained with hematoxylin and eosin, and studied using Zeiss Axio Observer Z1 inverted microscope (Carl Zeiss Microscopy GmbH, Jena, Germany). Obtained images were processed using ZEISS ZEN 2 (blue edition) (Carl Zeiss Microscopy GmbH, Jena, Germany). Histomorphology was carried out maintaining blinding by involving the third person who did not take part in the experiment. The integrity and the structural changes of spermatogenic epithelium in the fragments of the semeniferous tubules of the testis sections were evaluated semiquantitatively. They were scored as follows: (i) retraction of spermatogenic epithelium cells scored as 0 if absent, as 1 if slight, and as 2 if more obvious; (ii) nuclei condensation was scored as 0 if absent or present in only 1 nucleus, as 1 if 40% of nuclei were condensed, and as 2 if 40% were pyknotic; (iii) detachment of cells from the basement membrane was scored as 0 if absent, as 1 if partial, and as 2 if total or observed on 75% of the circumference; and (iiii) gap formation and shrinkage were scored as 0 if absent, as 1 if slight, and as 2 if more obvious. Therefore, the total score for each section of the seminiferous tubules was between 0 and 8. It was determined in 30 seminiferous tubules with the calculation of the average value for each observation. The minimal total score (0-1) corresponded to the intact structure of the spermatogenic epithelium. A score more than 1 to 3 points inclusively was accepted as mild damage of spermatogenic epithelium, more than 3 to 6 points inclusively as moderately expressed ones, and in the case of more than 6 points, changes were considered pronounced. An average cell density of the spermatogenic epithelium (a number of nuclei per area unit) was also evaluated.

*2.7. Immunohistochemical Study.* Immunohistochemical staining of deparaffinized sections of CrFSTT was performed using polyclonal antibodies to Melanoma Antigen Family B1 (MAGE-B1, prod. no. PA5-51532, 1 : 500, Invitrogen™, New York, USA) according to the protocol recommended for the peroxidase detection system Ultra Vision Quantro HRP DAB (prod. no. TL-060-QHD, Thermo Fisher Scientific, Fremont, USA). We counted MAGE-B1$^+$ cells using ZEISS ZEN 2 (blue edition) (Carl Zeiss Microscopy GmbH, Jena, Germany) and determined their relative amount as the ratio of the number of stained cells to the total number of cells in the tubule section, which was taken as 100%. For the negative control, MAGE-B1 was replaced by a mouse immunoglobulin G isotype control (prod. no. 02-6502; Invitrogen™, New York, USA).

*2.8. Statistical Analysis.* Kruskal-Wallis ANOVA test and multiple comparisons $p$ values were applied to compare the difference between the groups using Statistica 8 (StatSoft Inc., Tulsa, USA) software. Histological scores were compared using a Mann–Whitney $U$-test.

## 3. Results and Discussion

*3.1. Effect of Fullerene C60 on TAS and ROS Generation in the CrFSTT.* The obtained results showed a 1.5- and 1.7-fold increase ($p < 0.05$) of TAS activity and decreased content of ROS+ cells in CrFSTT by 1.2 and 1.3 times ($p < 0.05$), respectively, after C60 addition at concentrations of 10 and 15 $\mu$g/mL versus control (Figures 2(a) and 2(b)). The use of 20 $\mu$g/mL fullerene C60 did not lead to changes in studied parameters relative to the control and as a result had a significant difference with the previous two concentrations. Thus, the addition of C60 (10 and 15 $\mu$g/mL) to the incubation medium decreased the ROS generation and increase TAS activity in the CrFSTT.

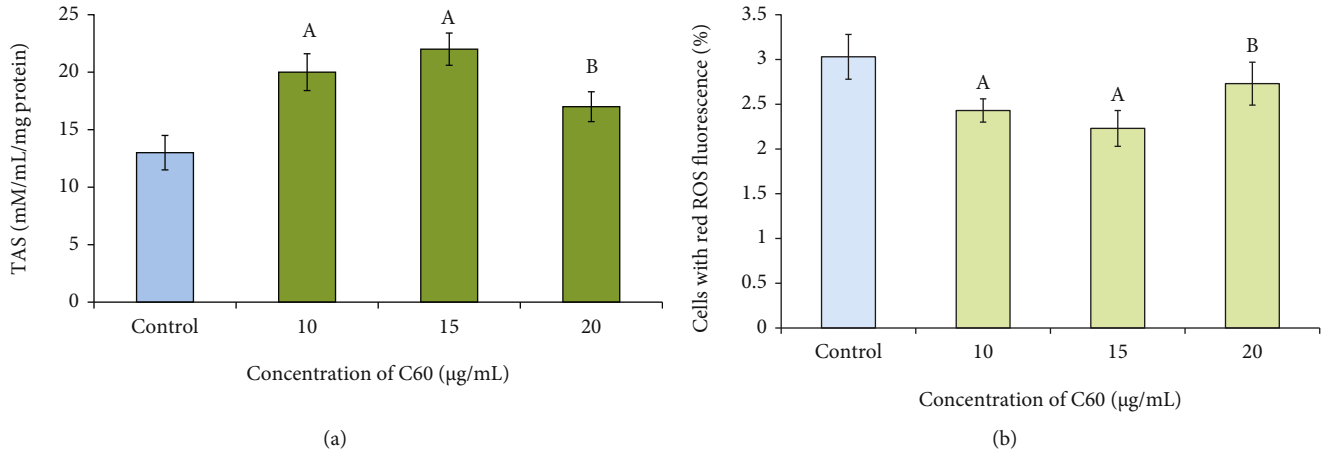


Figure 2: The effect of incubation in the media with C60 addition on TAS activity (a) and content of ROS$^+$ cells (b) in CrFSTT. Notes: $^A$difference is significant versus the control ($p < 0.05$); $^B$difference is significant versus C60_15 $\mu$g/mL ($p < 0.05$).

It is known that oxidative stress occurs in response to damage, when the antioxidant activity and absorption capacity of a biological object cannot neutralize free radicals caused by a harmful effect. ROS are involved in different pathophysiological processes in the testis; as a result, oxidative stress causes a testicular dysfunction due to inhibition of steroidogenesis and vasomotion [11]. The main antioxidant enzymes that neutralize the ROS in semen and various parts of the male reproductive system are superoxide dismutase, glutathione peroxidase, and catalase. But, many others so-called "indirect" antioxidant enzymes are also associated with the mechanism of antioxidative protection because they promote the biosynthesis/recycling of thiols or contribute to excretion of oxidized metabolites [12]. At the same time, the increase of TAS activity after the use of C60 at concentrations of 10 and 15 $\mu$g/mL is apparently associated with the direct antioxidant action of fullerenes. Due to the presence on the surface of a system of $\pi$-conjugated double bonds between hexa- and pentagonal structures, fullerenes collect and bind free radicals to each other, while they themselves remain unchanged [13]. Thus, the addition of 10 and 15 $\mu$g/mL C60 to the rehabilitation medium helps to neutralize oxidative stress in CrFSTT triggered by cryopreservation without significant difference between these two concentrations.

*3.2. Effect of C60 on Apoptotic and Necrotic Processes in CrFSTT of Rats.* The results obtained by flow cytometry (Table 1) suggested that C60 at all investigated concentrations did not cause the development of necrosis/apoptosis in cells. Conversely, C60 addition at the concentration of 15 $\mu$g/mL led to the 1.2-fold increase ($p < 0.05$) of percentage of live cells (Annexin V$^-$/7AAD$^-$) and to the 1.6-fold decrease ($p < 0.05$) in the number of necrotic cells (AnnexinV$^+$/7AAD$^+$ and Annexin V$^-$/7AAD$^+$) compared to the control samples.

The processes for initiating apoptosis are identical for most of the cells. Wherein changes of plasma membrane are observed, phosphatidyl serine goes from the cytoplasmatic part of the bilayer to the outer one, leading to the activation of caspase cascade, chromatin condensation, dysfunction of the mitochondria, and ultimately stopping ATP synthesis. Thus, programmed cell death can be caused by receptor-mediated physiological stimuli due to genetic disorders, physical or chemical triggers, and other changes in cells [14].

The next stage of the study was the quantitative evaluation of the mitochondrial activity and cytochrome C release in cells of CrFSTT after incubation with C60. The results obtained by flow cytometry (Figures 3(a) and 3(b)) showed that C60 addition in concentrations of 10 and 20 $\mu$g/mL did not affect investigated indexes. The use of C60 in concentration of 15 $\mu$g/mL led to a 1.15-fold increase ($p < 0.05$) in the content of JC$^+$ cells (orange fluorescence) and to a 1.3-fold decrease ($p < 0.05$) in the number of Cyt.C$^+$ cells compared to the control samples.

The analysis of the results showed a decrease in the release of cytochrome C into the cytosol and a high mitochondrial activity in the CrFSTT cells, which had the highest viability index by staining with Annexin V and 7AAD (Table 1, C60_15 $\mu$g/mL). As known, the mitochondria play a major role in cellular partitioning of death-regulating signals; the loss of mitochondrial membrane potential is an early event in several types of apoptosis. The high transmembrane potential of healthy cells loaded with JC-1 allows for the formation and sequestration of JC aggregates in the mitochondrion that is detected by a peak in red/orange fluorescence (585 nm) [15]. The various key events in apoptotic processes focus on the mitochondria, including the release of caspase activators (such as cytochrome C), changes in electron transport, loss of mitochondrial transmembrane potential, and activation of lipid peroxidation processes in cells. The various signals that converge in the mitochondria to trigger or inhibit these events and their subsequent effects determine several major pathways of physiological cell death [16, 17].

*3.3. Effect of Fullerene C60 on Histomorphological Parameters of CrFSTT of Rats.* The histological structure in control samples of CrFSTT of rats was characterized by moderate damage according to the semiquantitative scale (Figure 4(a)).

Table 1: Cytofluorimetric analysis of cells from CrFSTT after incubation with C60, staining with Annexin V and 7AAD, % of cells.

| Sample/region | Annexin $V^-/7AAD^-$ (live) | Annexin $V^+/7AAD^-$ (apoptosis) | Annexin$V^+/7AAD^+$+Annexin$V^-/7AAD^+$ (necrosis) |
|---|---|---|---|
| Control | 69.31 ± 1.27 | 6.02 ± 0.77 | 24.67 ± 1.12 |
| C60_10 $\mu$g/mL | 74.91 ± 2.35 | 5.92 ± 0.54 | 19.17 ± 1.02 |
| C60_15 $\mu$g/mL | 79.86 ± 1.24[a] | 4.28 ± 1.18 | 15.86 ± 0.95[a] |
| C60_20 $\mu$g/mL | 65.25 ± 1.01[b] | 6.60 ± 1.12 | 28.15 ± 1.08[b] |

Notes: [a]difference is significant versus the control ($p < 0.05$); [b]difference is significant versus C60_15 $\mu$g/mL ($p < 0.05$).

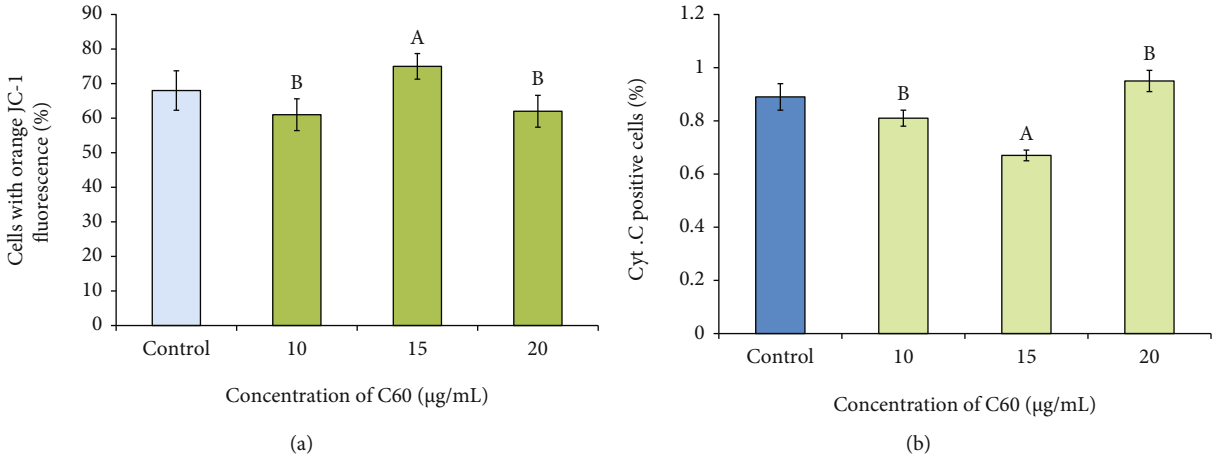


Figure 3: Mitochondrial activity (a) and level of cytochrome C release (b) in cells of CrFSTT after incubation with C60. Notes: [A]difference is significant versus the control ($p < 0.05$); [B]difference is significant versus C60_15 $\mu$g/mL ($p < 0.05$).

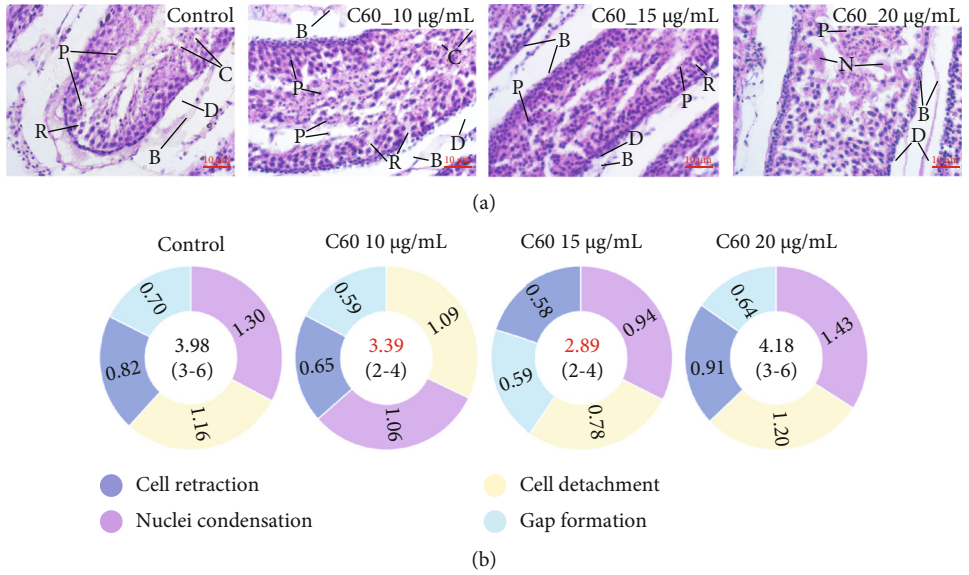


Figure 4: CrFSTT of immature rats after incubation in the media with fullerene C60. (a) Light microscopy; staining with hematoxylin and eosin. Notes: B: basement membrane; C: cavities; D: desquamation of epithelium; N: necrosis; R: retraction of cells; P: pyknosis. (b) Morphological damage scoring of the spermatogenic epithelium. An average value of the total score is shown in the center of each diagram. Boundary values of the total points are specified in the round brackets. Values significantly different from control are highlighted in red ($p < 0.05$).

Basically, there was unexpressed cell retraction and insignificant spherical cavities in the epithelial layer and its partial desquamation. The basement membrane at the desquamation sites appeared thickened and swollen. In some of the germinogenic cells, especially in the adluminal compartment, pyknosis of the nuclei was noted. Incubation of

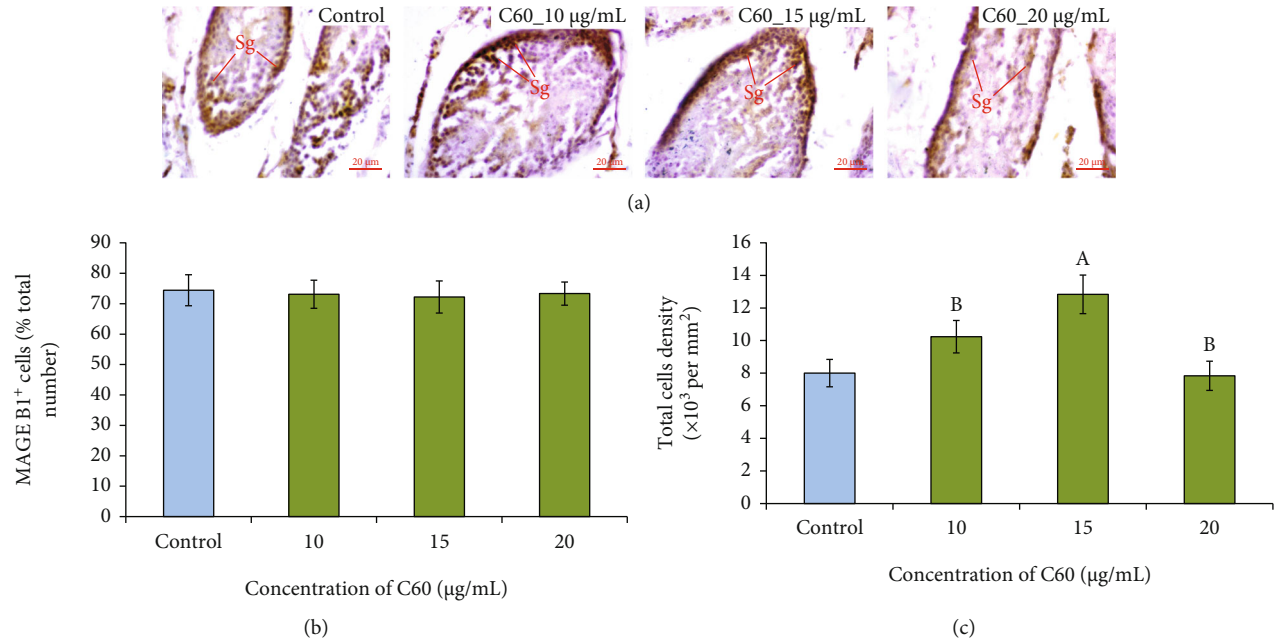


FIGURE 5: CrFSTT of immature rats after incubation in the media with fullerene C60. (a) Immunohistochemical staining for MAGE-B1, light microscopy. Notes: Sg: spermatogenic cells positively stained by MAGE-B1 (brown color); (b) relative amount of MAGE-B1$^+$ cells; (c) average cell density of spermatogenic epithelium. Notes: $^A$difference is significant versus the control ($p < 0.05$); $^B$difference is significant versus C60_15 $\mu$g/mL ($p < 0.05$).

CrFSTT in the media with the addition of C60 at the concentrations of 10 and 15 $\mu$g/mL had a generally positive effect on the histostructure compared to the control.

The desquamation of the spermatogenic epithelium and swelling of the basement membrane were almost absent; the frequency of pyknosis of cell nuclei decreased with a more pronounced effect in the case of 15 $\mu$g/mL C60 addition (Figure 4(b)). The degree of the spermatogenic epithelium damage in this group decreased to 2.89 points, which corresponds to mild changes. The samples of CrFSTT incubated with C60 at a concentration of 20 $\mu$g/mL had a similar to control histological structure; only small foci of necrosis were observed in the central parts of the seminiferous tubules.

Cells positively stained for MAGE-B1 were located in a dense layer on the inner surface of the spermatogenic epithelium and had a rounded shape with a dense cytoplasm and a rounded nucleus (Figure 5(a)).

In histological sections of CrFSTT, it was possible to distinguish a population of typical spermatogenic cells which were positively stained by MAGE-B1. Stratification and disruption of the structural architecture of the tubules were observed; as a result of which the spermatogonia germ layer (MAGE-B1$^+$) was shifted to the center. Relative amount of MAGE-B1$^+$ cells in CrFSTT did not change between the investigated media and ranged within 70-80% (Figure 5(b)). Thus, incubation with fullerene C60 did not have a selective effect on the population of MAGE-B1$^+$ cells in the spermatogenic epithelium ($p < 0.05$).

According to the results of measuring of the average density of spermatogenic epithelial cells, it can be concluded that the addition of fullerene C60 to the rehabilitation medium for CrFSTT was effective at a concentration of 15 $\mu$g/mL, significantly increasing this parameter relative to the control (by 1.6 times ($p < 0.05$)) and other investigated concentrations (10 and 20 $\mu$g/mL) (Figure 5(c)).

So, the histological examination showed a decrease of spermatogenic epithelium damage down to the mild degree and an increase of the average cell density of spermatogenic epithelium after incubation with 15 $\mu$g/mL C60. At the same time, it is important that the relationship between the spermatogenic epithelium and basement membrane was preserved because the last one in the testis serves as a reservoir of uniquely important cytokines to regulate junction dynamics that are associated with germ cell cycle progression and movement [18].

The use of modern cryopreservation technologies allows obtaining a stock of reproductive cells and tissues with their subsequent long-term storage at low temperatures, which allows them to be free transported and defrosted immediately before therapeutic use [19]. Determining the optimal conditions for cryopreservation of testicular tissue fragments is crucial for further restoration of fertility. It is known that freezing-thawing leads to a decrease in antioxidant protection of biological systems that causes the damage of the cell membrane integrity and activation of apoptosis and necrosis [20]. Free radicals initiate the processes of lipid peroxidation and inhibit mitochondrial enzymes of the respiratory chain, ATPase activity, etc. [21]. Interaction of highly reactive hydroxyl radicals with polyunsaturated fatty acids causes significant damage to cells and tissues, which in turn leads to increased permeability of cell membranes [22].

Thus, this research was aimed at comprehensively studying the effect of different concentrations of fullerene C60 on the antioxidant capacity, apoptotic/necrotic processes, and

morphological characteristics of CrFSTT of immature rats. One of the important conditions for manifestation of the biological effect of fullerene C60 is their interaction with cell membranes. The C60 molecule is characterized by the hydrophobic properties and affinity to the biological membranes. Fullerenes can affect cellular membranes both through adsorption on the surface and through incorporation into the lipid bilayer [23]. The authors [24] reported that C60 in the concentration of $10^{-5}$ M is able to penetrate the bilayer lipid membrane (phosphatidylcholine-cholesterol (1 : 1)) locally increasing its conductivity. In addition, the authors [25] showed that molecules of fullerene C60 are connected predominantly with the mitochondria inside the cell. And this is very important because the mitochondria are very susceptible to oxidative damage due to large amounts of pathogenic mutant mtDNA can accumulate in the testis resulting mitochondrial respiratory dysfunction in spermatogenic cells that ultimately induces meiotic arrest and abnormalities in sperm morphology [26].

## 4. Conclusions

Our results demonstrated that 10 and 15 $\mu$g/mL C60 similarly affected TAS activity and ROS generation, but the use of fullerene C60 at concentration of 15 $\mu$g/mL led also to an increase in the activity of mitochondria, to a decrease in cytochrom C release, and to an increase in the cell density in histological section. Furthermore, all studied concentrations of fullerene C60 did not lead to significant changes in the level of processes of apoptosis in cells from CrFSTT of rats. At the same time, it should be noted that the percentage of living cells after incubation with 15 $\mu$g/mL C60 was higher and a value of necrotic ones was lower than in the control samples. In our study, the fullerene C60 regardless of concentration had no effect on the relative amount of MAGE-B1$^+$ cells in CrFSTT of rats but at a concentration of 15 $\mu$g/mL reduced the degree of histological damage of spermatogenic epithelium. So, the general analysis of obtained data showed that the fullerene C60 can be used for rehabilitation of CrFSTT and it is the most optimal in the concentration of 15 $\mu$g/mL. The results can be used for the development of an effective rehabilitation medium for CrFSTT using C60. These findings relate to the applied nanotechnology in its extension to reproductive medicine.

## Data Availability

The data used to support the findings of this study are included within the article.

## Conflicts of Interest

The authors declare that they have no competing interests.

## Authors' Contributions

Anatoliy Goltsev and Nataliia Volkova contributed to the study design. Nataliia Volkova and Mariia Yukhta performed the experiments, analyzed the data, and wrote the manuscript. All authors read and approved the final manuscript.

## Acknowledgments

This work was supported by the program of the National Academy of Sciences of Ukraine "Support for the development of priority areas of scientific research" (code 6541230), contract number 2.2.6.130.

## References

[1] F. del Vento, M. Vermeulen, F. de Michele et al., "Tissue engineering to improve immature testicular tissue and cell transplantation outcomes: one step closer to fertility restoration for prepubertal boys exposed to gonadotoxic treatments," *International Journal of Molecular Sciences*, vol. 19, no. 1, p. 286, 2018.

[2] G. Bai, Z. Song, H. Geng et al., "Oxidized quasi-carbon nitride quantum dots inhibit ice growth," *Advanced Materials*, vol. 29, no. 28, p. 1606843, 2017.

[3] W. Rao, H. Huang, H. Wang et al., "Nanoparticle-mediated intracellular delivery enables cryopreservation of human adipose-derived stem cells using trehalose as the sole cryoprotectant," *ACS Applied Materials & Interfaces*, vol. 7, no. 8, pp. 5017–5028, 2015.

[4] U. Ritter, Y. I. Prylutskyy, M. P. Evstigneev, N. A. Davidenko, and V. V. Cherepanov, "Structural features of highly stable reproducible C 60 fullerene aqueous colloid solution probed by various techniques," *Fullerenes, Nanotubes, and Carbon Nanostructures*, vol. 23, no. 6, pp. 530–534, 2014.

[5] S. Emelyantsev, E. Prazdnova, V. Chistyakov, and I. Alperovich, "Biological effects of C60 fullerene revealed with bacterial biosensor-toxic or rather antioxidant?," *Biosensors*, vol. 9, no. 2, p. 81, 2019.

[6] S. Y. Zay, D. A. Zavodovskyi, K. I. Bogutska, D. N. Nozdrenko, and Y. I. Prylutskyy, "Prospects of C60 fullerene application as a mean of prevention and correction of ischemic-reperfusion injury in the skeletal muscle tissue," *Fiziolohichnyĭ zhurnal*, vol. 62, no. 3, pp. 66–77, 2016.

[7] D. M. Nozdrenko, D. O. Zavodovskyi, T. Y. Matvienko et al., "C60 fullerene as promising therapeutic agent for the prevention and correction of skeletal muscle functioning at ischemic injury," *Nanoscale Research Letters*, vol. 12, no. 1, p. 115, 2017.

[8] N. Volkova, M. Yukhta, and A. Goltsev, "Biopolymer gels as a basis of cryoprotective medium for testicular tissue of rats," *Cell and Tissue Banking*, vol. 19, no. 4, pp. 819–826, 2018.

[9] N. O. Volkova, M. S. Yukhta, L. G. Chernyshenko, L. V. Stepanyuk, L. V. Sokil, and A. M. Goltsev, "Cryopreservation of rat seminiferous tubules using biopolymers and slow noncontrolled rate cooling," *Problems of Cryobiology and Cryomedicine*, vol. 28, no. 4, pp. 278–292, 2018.

[10] P. Scharff, U. Ritter, O. P. Matyshevska et al., "Therapeutic reactive oxygen generation," *Tumori Journal*, vol. 94, no. 2, pp. 278–283, 2008.

[11] T. T. Turner and J. J. Lysiak, "Oxidative stress: a common factor in testicular dysfunction," *Journal of Andrology*, vol. 29, no. 5, pp. 488–498, 2008.

[12] R. Wu, J. Feng, Y. Yang et al., "Significance of serum total oxidant/antioxidant status in patients with colorectal cancer," *PLoS One*, vol. 12, no. 1, article e0170003, 2017.

[13] O. O. Gonchar, A. V. Maznychenko, N. V. Bulgakova et al., "C60 Fullerene Prevents Restraint Stress-Induced Oxidative Disorders in Rat Tissues: Possible Involvement of the Nrf2/ARE-Antioxidant Pathway," *Oxidative Medicine and Cellular Longevity*, vol. 2018, Article ID 2518676, 17 pages, 2018.

[14] N. A. Volkova, M. S. Yukhta, E. V. Pavlovich, and A. N. Goltsev, "Change in functional state of bone marrow-derived mesenchymal stem cells after incubation with silver nanoparticles," in *Nanophotonics, Nanooptics, Nanobiotechnology, and Their Applications*, O. Fesenko and L. Yatsenko, Eds., pp. 273–282, Springer Nature, Cham, Switzerland, 2019.

[15] A. Cossarizza, M. Baccaranicontri, G. Kalashnikova, and C. Franceschi, "A New Method for the Cytofluorometric Analysis of Mitochondrial Membrane Potential Using the J-Aggregate Forming Lipophilic Cation 5,5′,6,6′-Tetrachloro-1,1′,3,3′-tetraethylbenzimidazolcarbocyanine Iodide (JC-1)," *Biochemical and Biophysical Research Communications*, vol. 197, no. 1, pp. 40–45, 1993.

[16] R. A. Stuart, D. W. Nicholson, and W. Neupert, "Early steps in mitochondrial protein import: receptor functions can be substituted by the membrane insertion activity of apocytochrome c," *Cell*, vol. 60, no. 1, pp. 31–43, 1990.

[17] D. Sinha, "The complexities of human mitochondrial inner-membrane protein translocases in the maintenance of organeller function," *Proceedings of the Indian National Science Academy*, vol. 83, no. 4, pp. 877–891, 2017.

[18] M. K. Siu and C. Y. Cheng, "Extracellular matrix: recent advances on its role in junction dynamics in the seminiferous epithelium during spermatogenesis," *Biology of Reproduction*, vol. 71, no. 2, pp. 375–391, 2004.

[19] Y. Song, R. Sharp, F. Lu, and M. Hassan, "The future potential of cryopreservation for assisted reproduction," *Cryobiology*, vol. 60, no. 3, pp. S60–S65, 2010.

[20] T. Finkel and N. J. Holbrook, "Oxidants, oxidative stress and the biology of ageing," *Nature*, vol. 408, no. 6809, pp. 239–247, 2000.

[21] M. Hermes-Lima and T. Zenteno-Savın, "Animal response to drastic changes in oxygen availability and physiological oxidative stress," *Comparative Biochemistry and Physiology Part C: Toxicology & Pharmacology.*, vol. 133, no. 4, pp. 537–556, 2002.

[22] R. Pamplona, "Membrane phospholipids, lipoxidative damage and molecular integrity: a causal role in aging and longevity," *Biochimica et Biophysica Acta*, vol. 1777, no. 10, pp. 1249–1262, 2008.

[23] A. Bianco, T. Da Ros, M. Prato, and C. Toniolo, "Fullerene-based amino acids and peptides," *Journal of Peptide Science*, vol. 7, no. 4, pp. 208–219, 2001.

[24] S. V. Prylutska, O. P. Matyshevska, I. I. Grynyuk, Y. I. Prylutskyy, U. Ritter, and P. Scharff, "Biological effects of C60 fullerenes in vitro and in a model system," *Molecular Crystals and Liquid Crystals*, vol. 468, no. 1, pp. 265/[617]–274/[626], 2007.

[25] S. Foley, C. Crowley, M. Smaihi et al., "Cellular localisation of a water-soluble fullerene derivative," *Biochemical and Biophysical Research Communications*, vol. 294, no. 1, pp. 116–119, 2002.

[26] S. Rajender, P. Rahul, and A. A. Mahdi, "Mitochondria, spermatogenesis and male infertility," *Mitochondrion*, vol. 10, no. 5, pp. 419–428, 2010.